

Distribution Agreement

In presenting this thesis or dissertation as a partial fulfillment of the requirements for an advanced degree from Emory University, I hereby grant to Emory University and its agents the non-exclusive license to archive, make accessible, and display my thesis or dissertation in whole or in part in all forms of media, now or hereafter known, including display on the world wide web. I understand that I may select some access restrictions as part of the online submission of this thesis or dissertation. I retain all ownership rights to the copyright of the thesis or dissertation. I also retain the right to use in future works (such as articles or books) all or part of this thesis or dissertation.

Signature:

Keith Szulwach

Date

MeCP2 Mediated Regulation of Small Noncoding RNA

By

Keith E Szulwach, B.S., SUNY Geneseo, 2003

Graduate Division of Biological and Biomedical Science

Genetics and Molecular Biology

Peng Jin, Ph.D., Advisor

Jeremy Boss, PhD., Committee Member

Anthony Chan, Ph.D., Committee Member

Joseph Cubells, MD, Ph.D., Committee Member

Stephen Warren, PhD., FACMG, Committee Member

Accepted:

Lisa A. Tedesco, Ph.D. Dean of the James T. Laney School of Graduate Studies

_____ Date

MeCP2 Mediated Regulation of Small Noncoding RNA

By

Keith E Szulwach, B.S., SUNY Geneseo, 2003

Advisor: Peng Jin, PhD

An abstract of

A Dissertation submitted to the Faculty of the

James T. Laney School of Graduate Studies of Emory University

In partial fulfillment of the requirements for the degree of

Doctor of Philosophy

Graduate Division of Biological and Biomedical Science

Genetics and Molecular Biology

2010

Abstract

MeCP2 Mediated Regulation of Small Noncoding RNA

By Keith Szulwach

A core issue toward understanding the molecular etiology of Rett Syndrome is determining how mutations in *MECP2*, which encodes a DNA methyl-CpG binding protein, ultimately cause altered transcriptional output. I have worked toward identifying transcripts displaying altered expression in MeCP2 deficient adult neural stem cells (aNSCs), focusing on small noncoding RNA. The diverse regulatory roles that small noncoding RNA, including microRNA (miRNA), have on impacting gene expression suggests the importance of understanding their function in Rett Syndrome. As such, the central hypothesis of this work is that MeCP2 mediated regulation of a subset of small noncoding regulatory RNA in the context of neurodevelopment contributes to the pathogenesis of Rett Syndrome. Based on this, the specific subset of miRNA exhibiting altered expression in MeCP2 deficient aNSCs were identified. Functional characterization of one such miRNA, miR-137, was carried out in aNSCs at different neurodevelopmental stages, ultimately revealing the complexity in gene regulatory networks influenced by MeCP2 mediated regulation of miRNA. The effect of MeCP2 on the expression of small noncoding RNA was further evaluated using a more high-throughput Sequence by Synthesis approach. These experiments identified a unique and previously unannotated set of ~18nt RNA that associated specifically with transcription start sites. These small RNA reflected promoter proximal regulation of transcription at stimulus responsive genes. Since MeCP2 influences activity dependent transcription in neurons, the subset of genes differentially expressing small RNA at TSSs was identified in order to find MeCP2 targets more likely to be stimulus dependent. At one such gene, *Pcdh10*, MeCP2 was found to bind proximal to the TSS, a result suggesting MeCP2 may directly influence promoter proximal stalling of RNA Polymerase II dependent transcription at targeted genes in aNSCs. Together, these findings demonstrate the misexpression of specific small noncoding RNA in MeCP2 deficient aNSCs and reveal diversity in the types of gene regulatory pathways that may contribute to the pathogenesis of Rett Syndrome.

MeCP2 Mediated Regulation of Small Noncoding RNA

By

Keith E Szulwach, B.S., SUNY Geneseo, 2003

Advisor: Peng Jin, PhD

A Dissertation submitted to the Faculty of the
James T. Laney School of Graduate Studies of Emory University

In partial fulfillment of the requirements for the degree of

Doctor of Philosophy

Graduate Division of Biological and Biomedical Science

Genetics and Molecular Biology

2010

Table of Contents

Chapter 1: Introduction

Part I: Molecular Genetics of Rett Syndrome and MeCP2

Pages 1-5

Part II: Noncoding RNA and RNA Interference Related Pathways in Mental Retardation

Pages 5-10

Part III: Adult Neurogenesis and its Modulation by Noncoding RNA and Epigenetic Gene Regulatory Processes

Pages 10-14

Chapter 2: Identification and characterization of microRNA regulated by MeCP2 in adult neural stem cells

Abstract – pgs 14-15

Introduction – pgs 15-17

Results – pgs 18-29

Discussion – pgs 29-34

Materials and Methods – pgs 34-53

Figure Legends – pgs 54-64

Chapter 4: MicroRNA miR-137 regulates neuronal maturation by targeting ubiquitin ligase Mind Bomb-1

Abstract – pg 65

Introduction – pgs 66-67

Results – pgs 67-76

Discussion – pgs 77-80

Materials and Methods – pgs 80-94

Figure Legends – pgs 94-98

Chapter 4: Identification of unannotated small RNA regulated by MeCP2 – Transcription start site associated RNAs reveal poised genes with altered expression in MeCP2 deficient neural stem cells

Abstract – pg 99

Introduction – pgs 100-102

Results – pgs 103-107

Discussion – pgs 107-109

Materials and Methods – pgs 109-115

Figure Legends – pgs 116-120

Chapter 5: Discussion and Future Directions

Pages 121-126

References

Pages 127-136

List of Figures and Tables

Chapter 2:

Figure 1. Identification of miRNAs with altered expression in *Mecp2*-deficient adult NSCs. Pg 19

Figure 2. Expression of miR-137 is epigenetically regulated by MeCP2. Pg 22

Figure 3. Transcriptional regulation of miR-137 involves co-regulation by Sox2. Pg 25

Figure 4. miR-137 modulates the proliferation and differentiation of adult NSCs in vitro. Pg 28

Figure 5. miR-137 modulates the proliferation and differentiation of adult NSCs in vivo. Pg 31

Figure 6. Ezh2 is a functional target of miR-137. Pg 33

Figure 7. miR-137 regulates the expression of Ezh2 post-transcriptionally and results in an overall reduction in H3K27-TriMe. Pg 35

Figure S1. miR-137 and primary/precursor miR-137 expression in aNSCs. Pg 61

Figure S2. Determination of the epigenetic state of the miR-137 genomic locus using additional histone ChIP assays. Pg 62

Figure S3. Efficient delivery of control and miR-137 short-hairpin RNA constructs by lentivirus. Pg 63

Figure S4. Verification of a functional interaction between miR-137 and Ezh2. Pg 64

Figure S5. miR-137 has distinct effects on the expression of CDK6 in different cell types. Pg 65

Supplemental Table I. aNSC miRNA Profile. Pg 66-75

Supplemental Table II. Candidate miR-137 Target List. Pg 76

Chapter 3:

Figure 1. miR-137 is enriched in neurons and is expressed in the dentate gyrus and molecular layer of the hippocampus. Pg 81

Figure 2. miR-137 regulates dendritic development and phenotypic maturation of new neurons in vivo. Pg 83

Figure 3. Overexpression of miR-137 leads to altered neuronal maturation of new neurons in vivo. Pg 86

Figure 4. miR-137 is important for dendritic development in vitro. Pg 89

Figure 5. Mib-1 is a functional target of miR-137. Pg 91

Figure 6. Mib-1 could rescue the neuronal maturation deficits associated with miR-137 overexpression in vitro. Pg 93

Figure 6. Mib-1 could rescue the neuronal maturation deficits associated with miR-137 overexpression in vitro. Pg 111

Chapter 4:

Table 1. Summary and annotation of aNSC small RNA obtained from WT and *Mecp2*^{-/y} aNSCs by SBS. Pg 116

Figure 1. Size distributions of small RNA in WT and *Mecp2*^{-/y} aNSCs. Pg 117

Figure 2. Association of unannotated small RNA with RefSeq TSSs. Pg 118

Figure 3. Differential expression analysis of TSS associated small RNA in WT and *Mecp2*^{-/y} aNSCs. Pg 121

Figure 4. Expression of TSS associated small RNA and full-length transcripts at *Pcdh10* and *DivPcdh10*. Pg 122

Figure 5. RNAPII occupancy and direct interaction of MeCP2 proximal to *Pcdh10*. Pg 123

Supp Fig 1. The TSS associated chromatin state at *Pcdh10* in WT and *MeCP2*^{-/y} aNSCs. Pg 133

Supp Fig 2. TSS associated small RNA expression at *c-Fos* in WT and *MeCP2*^{-/y} aNSCs. Pg 134

Supp Fig 3. TSS associated small RNA expression at *c-Myc* in WT and *MeCP2*^{-/y} aNSCs. Pg 135

Supp Fig 4. TSS associated small RNA expression at *Jun* in WT and *MeCP2*^{-/y} aNSCs. Pg 135

Supp Fig 5. TSS associated small RNA expression at *Homer1* in WT and *MeCP2*^{-/y} aNSCs. Pg 136

Supp Fig 6. TSS associated small RNA expression at *Bdnf* in WT and *MeCP2*^{-/y} aNSCs. Pg 136

Supplemental Table I. RefSeq transcripts differentially expressing transcription start site associated small RNA. Pg 137-143

Acknowledgments:

The work presented in Chapter 2 is published in *The Journal of Cell Biology* according to the following reference. Authors contributing to this work are included within this reference:

Szulwach, KE., Li, X., Smrt, RD., Li, Y., Luo, Y., Lin, L., Santistevan, N., Li, W., Zhao, X., Jin, P. Cross-talk between microRNA and epigenetic regulation in adult neural stem cells. (2010) *Journal of Cell Biology*. Vol. 189, No. 1, 127-141.

At the time this dissertation was submitted, the work presented in Chapter 3 was accepted for publication in the journal *Stem Cell* and was in press. Authors contributing to this work are included within the following reference:

Smrt, RD., Szulwach KE., Pfeiffer, RL., Li, X., Guo, W., Pathania, M., Luo, Y., Peng, J., Wilson, MC., Bordey, A., Jin, P., Zhao, X. MicroRNA-137 regulates neuronal maturation by targeting ubiquitin ligase Mind Bomb-1. (2010) In Press, *Stem Cells*.

The work presented in Chapter 4 was the subject of a manuscript that was in preparation at the time this dissertation was submitted. I would like to acknowledge the contributing authors as listed below:

Szulwach, KE., Li, X., Shetty, AC., Zwick ME., Jin, P. Poised genes with altered expression in MeCP2 deficient neural stem cells. (2010) In preparation.

Chapter 1: Introduction

Part I: Molecular Genetics of Rett Syndrome

Rett Syndrome (RTT) is classically characterized as a neurodevelopmental disease caused by *de novo* mutations in the X-linked *MECP2* gene (Amir, Van den Veyver et al. 1999). RTT is among the most common forms of mental retardation affecting females, having an incidence of approximately 1/10,000 to 1/15,000 live births, with 100% penetrance. Although occurring much less frequently than in females, milder mutations in *MECP2* are also known to cause RTT in males. Patients generally display normal development through 6-18 months of age before exhibiting a characteristic period of regression in the form a decelerated head growth, loss of speech and motor skills, pseudo-stabilization, and eventually severe mental retardation and motor defects (Bienvenu and Chelly 2006; Chahrour and Zoghbi 2007). Conventional non-synonymous mutations in MeCP2 cause the majority of identified RTT cases, however, duplications in the gene are also associated with neurological disease and phenotypes overlapping with RTT (Meins, Lehmann et al. 2005; Van Esch, Bauters et al. 2005; Friez, Jones et al. 2006; Lugtenberg, de Brouwer et al. 2006). These observations highlight the importance of maintaining proper MeCP2 expression in normal central nervous system function.

MECP2 encodes a DNA CpG methyl binding protein with the ability to mediate epigenetic states of transcription via binding methylated CpG dinucleotides (Lewis,

Meehan et al. 1992; Nan, Campoy et al. 1997; Nan, Ng et al. 1998). The gene is known to produce 4 coding exons and two alternative splice variants (*MECP2- α* encoding MeCP2-e1, and *MECP2- β* encoding MeCP2-e2) that differ by inclusion/exclusion of a portion of exon 2 (Kriaucionis and Bird 2004; Mnatzakanian, Lohi et al. 2004; Dragich, Kim et al. 2007). It is member of larger methyl-CpG binding protein family containing a methyl binding domain (MBD), transcription repression domain (TRD), a C-terminal domain, and two nuclear localization signals (NLS) (Hendrich and Bird 1998). Binding of methyl CpG dinucleotides by MeCP2 is linked to chromatin based regulation through association with various chromatin remodeling complexes, including HDACs 1&2, Sin3a, Swi/Snf(Brahma), Suv39H1, coREST, DNMT1, and ATRX (Jones, Veenstra et al. 1998; Nan, Ng et al. 1998; Kimura and Shiota 2003; Ballas, Grunseich et al. 2005; Nan, Hou et al. 2007). MeCP2 also interacts with various co-repressors and transcription factors including c-ski, N-cor, LANA, TFIIB and PU.1 (Kaludov and Wolffe 2000; Kokura, Kaul et al. 2001). However, the precise mechanism(s) by which MeCP2 interacts with various chromatin remodeling complexes and/or various combinations of transcription factors to influence transcription remains incomplete.

In both humans and mice the expression of MeCP2 increases as neurons mature, and is eventually highly enriched in neurons (Shahbazian, Antalffy et al. 2002; Balmer, Goldstine et al. 2003; Cohen, Matarazzo et al. 2003; Kishi and Macklis 2004). The

correlation between MeCP2 expression patterns during development of the brain and the onset of RTT phenotypes has led to the hypothesis that MeCP2 mediated transcriptional regulation is involved in postnatal neuronal morphogenesis and activity dependent synaptic plasticity (Moretti and Zoghbi 2006). Indeed, MeCP2 has been linked to activity dependent transcriptional regulation in neurons, a process known to influence synaptic plasticity (Chen, Chang et al. 2003; Martinowich, Hattori et al. 2003; Zhou, Hong et al. 2006; Tao, Hu et al. 2009). At a subset of target genes, phosphorylation of MeCP2 upon membrane depolarization results in release of MeCP2 and altered mRNA expression. Interestingly, MeCP2 has been reported as both an activator and repressor of transcription, consistent with a role in establishing and/or maintaining epigenetic chromatin states that direct transcription (Chahrour, Jung et al. 2008). Such a role has been further supported by observations indicating that MeCP2 is expressed at near histone octamer levels in neurons and globally influences neuronal histone H3 acetylation (Skene, Illingworth et al.). However, the identification of downstream targets of MeCP2 has remained a central challenge in understanding the molecular etiology of RTT.

Mouse models harboring mutations in *MeCP2* have so far proven particularly useful models toward advancing an understanding of the disease. This has largely been due to the mimicry of human phenotypes. Knockout models considered to be null encompass targeted deletions of exon 3, parts of exons 3 and 4, or exons 3 and 4 (Summarized in (Chahrour and Zoghbi 2007)). When the loss of MeCP2 was restricted to only neuronal lineages, phenotypes indistinguishable from mice null

for *MeCP2* in all tissues were observed, indicating that expression of mutant *MeCP2* specifically in neurons is sufficient to cause RTT-like phenotypes (Guy, Hendrich et al. 2001). A *MeCP2* truncation allele, *MeCP2³⁰⁸* has been of particular interest due to its milder phenotype yet ability to recapitulate key aspects of RTT (Shahbazian, Young et al. 2002). This particular allele removes the approximate C-terminal one third of the protein, leaving the methyl-DNA binding domain (MBD), transcriptional repressor domain (TRD), and nuclear localization signal. Deletions of this portion of the protein have also been found in human patients with classic Rett syndrome phenotypes. Furthermore, the truncated allele allows for survival of male mice, thus eliminating complications arising from unpredictable X-inactivation in female mice. Importantly, male mice carrying mutations in *MeCP2* have been shown to have symptoms closely related to those seen in humans. These have included hippocampus-dependant impairment in spatial memory, contextual fear memory, and social memory. In addition, *MeCP2* mutant mice display reduced synaptic density cross-sectional length in asymmetric synapses in the CA1 area of the hippocampus. Schaffer collateral synapses display enhanced basal synaptic transmission, decreased paired pulse facilitation, and impaired long-term potentiation (Shahbazian, Young et al. 2002). These observations have established *MeCP2* mutant mice as an essential tool in studying RTT.

Perhaps the most striking results yielded from mouse studies have involved models whereby *MeCP2* expression has been re-established in initially null mice. Using this approach, phenotypic reversibility in both young and mature animals was

demonstrated (Guy, Gan et al. 2007). This remarkable rescue of RTT like phenotypes in mice has led to the suggestion that RTT may indeed be a treatable or reversible disease in humans.

Part II: Noncoding RNA and RNA Interference Related Pathways in Mental Retardation

High-throughput, genome-wide interrogations of transcribed RNA have yielded compelling evidence for pervasive and complex transcription throughout the large majority of mammalian genomes. Nevertheless, a significant portion of this transcribed RNA appears to be non-protein coding and is currently uncharacterized. In-depth analysis of 1% of the human genome (30 Mb) performed by the Encyclopedia of DNA Elements project revealed that 92.6% of the interrogated bases could be detected as primary transcripts and that, among these, many novel non-protein-coding transcripts could be identified (Birney, Stamatoyannopoulos et al. 2007). Likewise observations have been found in mice. Similarly, another study found that the majority (64%) of polyadenylated (poly-A+) transcripts ≥ 200 nucleotides (nt) in length lay outside annotated protein-coding regions (Kapranov, Cheng et al. 2007). These and other genome-wide analyses have led to the identification of tens of thousands of noncoding RNA transcripts expressed from the human genome, most of which have yet to be functionally characterized. Along with the revelation that noncoding RNAs are surprisingly abundant, there has been a surge in molecular and genetic data showing important and diverse regulatory roles

for noncoding RNA. In the context of this work I have considered the contribution of MeCP2 mediated regulation of noncoding RNA, and specifically, small noncoding RNAs 14-35nt in length, including microRNA (miRNA).

To date, many concerted efforts to identify MeCP2 target transcripts have focused on protein-coding mRNA transcripts. These approaches have revealed a number of direct MeCP2 target genes in specific cell and tissue types (summarized in (Chahrour and Zoghbi 2007)). However, as pathogenic target transcripts have yet to be convincingly identified, expansion of the discussion on MeCP2 target transcripts to include noncoding RNAs is warranted. Here, I highlight previous observations surrounding the involvement of noncoding RNAs in MeCP2 function to provide context for the presented studies on small noncoding regulatory RNA.

miRNA are perhaps the best studied of the small noncoding RNAs. Originally discovered as heterochronic regulators of development in *C. elegans* (Lee, Feinbaum et al. 1993; Reinhart, Slack et al. 2000), miRNA are now recognized as evolutionally conserved master regulators of developmental timing, spatial control of cell fate and proliferation, and apoptosis. miRNAs are generally classified as ~19-24nt small RNA able to repress translation or cause degradation of mRNA with partially complementary 3'-UTR sequence. Genetically, a loss of function mutation in a miRNA can be equivalent to a gain of function mutation in an mRNA target. miRNA are usually transcribed by RNA polymerase II in the form primary miRNA (pri-miRNA) transcripts that range from a few hundred base pairs in length to several

kilobases. Pri-miRNA transcripts are subsequently processed within the nucleus to ~60-70nt precursor miRNAs (pre-miRNAs) by the microprocessor complex which contains the RNase-III type enzyme Drosha and its partner DGCR8/Pasha. Pre-miRNAs are then exported from the nucleus in a Ran-GTP dependant process requiring Exportin-5. Cytoplasmic pre-miRNAs are next cleaved by another RNase-III type complex containing Dicer and TRBP. Mature ~19-24nt miRNA are then bound by Argonaute proteins during loading of an RNA induce silencing complex (RISC) that is able to direct translational repression or degradation of mRNA targets (Du and Zamore 2005). Argonaute proteins, as well as the homologous Miwi protein, have been shown to associate with the RNA binding protein FMRP, which itself is associated with translational repression (Jin, Zarnescu et al. 2004; Grivna, Pyhtila et al. 2006). Loss of FMRP is the cause of Fragile X syndrome, a common form of inherited mental retardation that exhibits some phenotypes similar to Rett syndrome. Additionally, many of the PAZ (Piwi-Argonaute-Zwille) family proteins are known factors regulating stem cell self-renewal. It is becoming increasingly recognized that many members of the miRNA, or RNA interference (RNAi), pathway are important regulators of potency, proliferation, and lineage specification of stem cells.

Regulation of miRNA expression could provide an alternative means by which MeCP2-mediated epigenetic regulation could ultimately influence protein expression and phenotype. Rather than directly influencing the expression of mRNA protein-coding transcripts, MeCP2 may also regulate the transcription of noncoding

RNA elements, such as miRNA. Thus, in the absence of MeCP2, some miRNAs might display increased expression, which may result in a negative effect on the translation of mRNAs targeted by that particular miRNA.

In fact MeCP2 has been reported as regulating expression of an imprinted miRNA in mouse. Examination of an imprinted locus on mouse chromosome 9, in which genes are known to be imprinted and expressed specifically in brain, revealed that MeCP2 binds upstream and regulates the paternal expression of miR-184 located within 55 kb of the imprinted locus. Moreover, the induction of miR-184 expression in depolarized cultured neurons is concomitant with a loss of MeCP2 binding upstream of the miR-184 locus. These data indicate that the regulation of miR-184 expression by MeCP2 is activity dependent. It was noted, however, that in whole brain tissue derived from MeCP2-deficient mice, there is a slight decrease in miR-184 expression compared with wild type (Nomura, Kimura et al. 2008).

MeCP2's interaction with the histone lysine methyltransferase SUV39H1 occurs as part of a corepressor complex specific for neuronal genes called repressor-element-1-silencing transcription factor (REST) repressor complex or RCOR1 (Bienvenu and Chelly 2006; Moretti and Zoghbi 2006). In fact, REST has even been shown to directly bind regions proximal to a family of miRNAs including mir-9, mir-124a, and mir-132. Reduced expression of REST during neuronal differentiation of mouse P19 embryonal carcinoma cells using retinoic acid has been shown to correlate with increased expression of mir-124a and decreased expression of non-neuronal

mRNAs (Conaco, Otto et al. 2006). However, neither epigenetic regulation nor the effect of loss of functional MeCP2 has been examined for the mir-124a genomic locus.

The cAMP response element-binding (CREB) protein is known to be a critical transcription factor regulating neuronal plasticity and activity-dependent refinement of dendritic branching, both of which are defective processes in RTT patients. Initial identification of CREB protein targets identified a miRNA (miR-132) that was predicted to posttranscriptionally regulate MeCP2. In postnatally cultured rat neurons, miR-132 did in fact directly repress the expression of MeCP2. However, by blocking miR-132-mediated regulation of MeCP2, thereby increasing MeCP2 levels, it was found that the expression of brain-derived neurotrophic factor (BDNF) increased (Klein, Liroy et al. 2007). These results were contradictory to two previous studies describing the activity-dependent release of MeCP2 from the BDNF locus in embryonic cultured neurons, which indicated that MeCP2 was acting as a negative regulator of BDNF (Chen, Chang et al. 2003; Martinowich, Hattori et al. 2003). Because BDNF is both a known target of MeCP2 and an activator of CREB, together, these findings led to the hypothesis that miR-132 functions within a feedback loop involving homeostatic regulation of MeCP2 expression through BDNF-activated CREB. Homeostatic regulation of MeCP2 by miR-132 may therefore indicate a mechanism by which MeCP2 levels are normally maintained within the narrow range required for proper neuronal development and synaptic maturation in the postnatal brain and highlight the importance of miRNA in these processes (Klein,

Lioy et al. 2007).

The influence of MeCP2 at imprinted loci may also be of significance in RTT and other mental retardation syndromes. In fact, a common feature among imprinted loci is the presence of noncoding RNA and antisense transcription, including expression of diverse types of small noncoding RNA. Although much of the data surrounding MeCP2-mediated transcriptional control at imprinted loci have been controversial, with many groups obtaining conflicting results, few have examined the expression of noncoding RNA derived from these loci. The imprinted loci implicated in RTT have been reviewed in detail (LaSalle 2007). From these data, it remains possible that MeCP2 mediates allele-specific expression of noncoding RNAs from imprinted loci by directing or establishing a chromatin state in the imprinted region, which in turn affects the transcription of nearby protein-coding genes. In fact, MeCP2 has been proposed to function in establishing 'chromatin loops' that allow for proper expression of the included transcripts (LaSalle 2007), and it is an intriguing hypothesis that small noncoding RNA may play a role in the formation or maintenance of such chromatin structures.

Part III: Adult Neurogenesis and its Modulation by Noncoding RNA and Epigenetic Gene Regulatory Processes

Neural stem cells are defined as cells that can 1) generate all types of neural cells, including neurons, astrocytes, and oligodendrocytes 2) have some capacity for self-

renewal, and 3) give rise to cells other than themselves via asymmetric division (Gage 2000). Neurogenesis is defined the process by which neural progenitor proliferate, specify cell fate, mature, and functionally integrate into neural circuits. Neural stem cells are present in all mammalian organisms, and it is now well established that neurogenesis occurs postnatally and throughout adulthood in all mammals so far examined (Altman and Das 1965; Altman and Das 1967; Caviness 1973; Gueneau, Privat et al. 1982; Kuhn, Dickinson-Anson et al. 1996; Gould, Tanapat et al. 1998; Gage 2000). Primarily, adult neurogenesis is confined to the subventricular zone (SVZ) of the lateral ventricles and the subgranular zone (SGZ) of the dentate gyrus (DG) within the hippocampal formation. Progenitor cells within the SVZ migrate through the rostral migratory stream eventually becoming granular neurons and periglomerular neurons in the olfactory bulb. Progenitor cells of the SGZ are able to migrate into the granule layer, differentiate, extend axons, and express neuronal markers (Kaplan and Hinds 1977; Kaplan and Bell 1984; Stanfield and Trice 1988; Cameron, Woolley et al. 1993). Ablation of hippocampal adult neurogenesis has been found to impair hippocampal-dependent learning and memory tasks in rodents (Shors, Miesegaes et al. 2001; Snyder, Hong et al. 2005), suggesting a critical role for adult hippocampal neurogenesis in some types of learning and memory. As previously mentioned, male mice carrying mutations in *MeCP2* also display defects in hippocampal-dependent learning and memory (Asaka, Jugloff et al. 2006; Moretti and Zoghbi 2006; Pelka, Watson et al. 2006). It may reasonable, therefore, to assess the role of SGZ aNSCs and small RNA regulating development of such aNSCs in the molecular etiology of Rett syndrome.

Adult neurogenesis is intricately modulated through combinations of non-exclusive cell intrinsic and extrinsic mechanisms. One common intrinsic mechanism by which aNSCs, and stem cells in general, are thought to retain potency is through epigenetic regulation. Epigenetic regulation is defined as a heritable change in gene expression, whether meiotically or mitotically, that is not caused by change in DNA sequence, but does cause an altered phenotype (Egger, Liang et al. 2004). Differences in the function of genetic elements without changes in the actual genetic or underlying DNA sequence of those elements allows for cells to differentiate and take on distinct roles, linking cellular genotype with phenotype. In mammalian systems, the molecular mechanisms contributing to epigenetic regulation of genomic information are quite varied and are still not completely understood. Such mechanisms include but may not necessarily be limited to those directly influencing DNA accessibility and gene expression in the context of chromatin, like covalent and non-covalent chemical modifications of DNA and histones. Other mechanisms, including those indirectly influencing the information flow from DNA to protein, like alternative splicing and poly-adenylation of mRNA transcripts, post-translational modifications of proteins, and posttranscriptional regulation of transcribed RNA may also be considered epigenetic under strict definitions.

Two landmark studies in embryonic stem cells, of both humans and mice, have identified core transcriptional networks involved in stem cell maintenance and lineage specification as well as produced further evidence for epigenetic regulation

of miRNA important to the proper maintenance and differentiation of stem cells (Boyer, Lee et al. 2005; Boyer, Plath et al. 2006; Lee, Jenner et al. 2006). These studies identified binding sites for the key transcriptional and epigenetic regulators Oct4, Sox2, Nanog, and Polycomb proteins. Sox2 in particular has been shown to play a critical role in neuronal development. In both studies, the above transcriptional and epigenetic regulators were found to directly interact with a group of miRNAs in embryonic stem cells (Boyer, Lee et al. 2005; Boyer, Plath et al. 2006; Lee, Jenner et al. 2006). Here I have identified and functionally characterized specific miRNA with increased expression in *MeCP2*^{-/-} aNSCs that are also putative targets for regulation by Oct4, Sox2, Nanog, and Polycomb proteins. Interactions between these key regulators of stem cell maintenance and lineage specification, as well as with MeCP2, and particular miRNA, indicates important roles for these miRNA in the related processes and molecular etiology of mental disorders.

Together, the diverse regulatory roles exhibited by small noncoding RNA, including miRNA, represent key steps influencing the expression of genes. Regulatory roles for small noncoding RNA derived from diverse transcripts continue to be uncovered and associated with disease causing processes. As mutations in *MECP2* cause the neurodevelopmental disease RTT, it has become critical to identify transcripts regulated by this DNA methyl-CpG-binding protein, including small noncoding RNA. This work has used a combination of independent approaches to identifying these small RNA transcripts and described the gene regulatory pathways associated with each in aNSCs.

Chapter 2: Identification and characterization of miRNA regulated by MeCP2 in adult neural stem cells

Abstract

Both microRNAs (miRNAs) and epigenetic regulation have important functions in stem cell biology, although the interactions between these two pathways are not well understood. Here we show that MeCP2, a DNA methyl-CpG binding protein, can epigenetically regulate specific miRNAs in adult neural stem cells (aNSCs). MeCP2-mediated epigenetic regulation of one such miRNA, miR-137, involves co-regulation by Sox2, a core transcription factor in stem cells. miR-137 modulates the proliferation and differentiation of aNSCs in vitro and in vivo. Overexpression of miR-137 promotes the proliferation of aNSCs, whereas a reduction of miR-137 enhances aNSC differentiation. We further show that miR-137 post-transcriptionally represses the expression of Ezh2, a histone methyltransferase and Polycomb group (PcG) protein. The miR-137-mediated repression of Ezh2 feeds back to chromatin, resulting in a global decrease in histone H3 trimethyl lysine 27. Coexpression of Ezh2 can rescue phenotypes associated with miR-137 overexpression. These results demonstrate that crosstalk between miRNA and epigenetic regulation contributes to the modulation of adult neurogenesis.

Introduction

Neurogenesis in adult mammalian brains occurs throughout life. This process has been observed at two locations under normal conditions: the subventricular zone (SVZ) of the lateral ventricles and the subgranular zone (SGZ) of the dentate gyrus in the hippocampus (Zhao, Deng et al. 2008). The cellular basis for adult neurogenesis is adult neural stem cells (aNSCs), which exhibit the two essential properties of stem cells: self-renewal and multipotency. Adult neurogenesis is defined as the process of generating new neurons from NSCs, which consists of the proliferation and fate determination of aNSCs, the migration and survival of young neurons, and the maturation and integration of newly produced neurons (Ming and Song 2005; Zhao, Deng et al. 2008). Adult neurogenesis is regulated at many levels by both extrinsic factors, such as physiological and pathological conditions, and intrinsic factors, such as genetic and epigenetic programs. The maintenance and differentiation of stem cells are tightly controlled by intricate molecular networks (Li, Barkho et al. 2008). Uncovering these regulatory mechanisms is crucial to understanding the functions and plasticity of adult brains.

Epigenetic regulation, including DNA methylation and histone modification, is known to play significant roles in the modulation of stem cell proliferation and differentiation, including in NSCs (Abel and Zukin 2008; Zhao, Deng et al. 2008). Recent genome-wide analyses have demonstrated a clear role for DNA methylation and chromatin remodeling, particularly by the Polycomb group (PcG) proteins, in

defining the properties and regulating the functions of stem cells (Bernstein, Meissner et al. 2007). The importance of epigenetic regulation in brain development and neurological disorders has been well documented (Shahbazian and Zoghbi 2002; Abel and Zukin 2008). For example, de novo mutations in *MECP2* give rise to neurodevelopmental disorders, including Rett syndrome (Amir, Van den Veyver et al. 1999; Chahrour and Zoghbi 2007). MeCP2 belongs to a family of DNA methyl-CpG-binding proteins (MBDs) that translate DNA methylation into gene expression regulation (Bird 2002). Two members of the MBD family of proteins, MBD1 and MeCP2, influence either the proliferation and differentiation of aNSCs, or the maturation of young neurons (Zhao, Ueba et al. 2003; Kishi and Macklis 2004; Smrt, Eaves-Egenes et al. 2007). Nonetheless, how these epigenetic factors regulate adult neurogenesis is unclear due to the difficulty in identifying downstream targets via classical gene expression analyses (Bienvenu and Chelly 2006).

microRNAs (miRNAs) are small, non-coding RNAs that regulate gene expression and development by post-transcriptionally targeting RNA-induced silencing complex (RISC) to cognate messenger RNA (Bartel 2004). The loss of components of the miRNA pathway, including Dicer and DGCR8, can alter the proliferation and differentiation of stem cells (Bernstein, Kim et al. 2003; Wang, Medvid et al. 2007). Furthermore, specific miRNAs are known to play important roles in modulating the proliferation and differentiation of many types of stem cells (Ivey, Muth et al. 2008; Yi, Poy et al. 2008).

Here we show that MeCP2 could epigenetically regulate specific miRNAs in mouse aNSCs. The absence of MeCP2 binding to the genomic region proximal to one such miRNA, miR-137, correlates with an altered chromatin state that is reflective of miR-137 expression. In addition, we demonstrate that the MeCP2-mediated effect on miR-137 expression could be through a mechanism involving Sox2, a core transcription factor regulating stem cell self-renewal (Zappone, Galli et al. 2000; Avilion, Nicolis et al. 2003; Ferri, Cavallaro et al. 2004). Furthermore, we found miR-137 influences aNSC proliferation and differentiation both in vitro and in vivo. Lastly, we identified Ezh2, a histone H3 lysine 27 methyltransferase and a member of the PcG protein family, as one of the post-transcriptionally regulated targets of miR-137, and the miR-137-mediated repression of Ezh2 subsequently caused a global decrease in trimethyl H3-lysine 27 (H3-K27-Tri-Me). Functionally, coexpression of Ezh2 rescued the phenotypes associated with miR-137 overexpression. These results demonstrate that crosstalk between epigenetic regulation and the miRNA pathway could play important roles in the modulation of adult neurogenesis. Furthermore, our data suggest that the loss of functional MeCP2 could alter the expression of specific miRNAs, potentially contributing to the molecular pathogenesis of Rett syndrome.

Results

Identification of miRNAs with altered expression in MeCP2-deficient aNSCs

In order to identify miRNAs potentially regulated at the epigenetic level and determine whether MeCP2 could influence the expression of miRNAs in the context of adult neurogenesis, we profiled the expression of 218 miRNAs in primary aNSCs derived from wild-type (WT) and *Mecp2*-deficient mice (Chen, Akbarian et al. 2001) using multiplex reverse transcription and miRNA-specific TaqMan assays (Fig. 1, and Table SI). Nearly all cultured NSCs were positive for the NSC markers Nestin and Sox2, suggesting a relative homogeneity of these primary aNSCs.

These aNSCs incorporate the thymidine analog bromodeoxyuridine (BrdU) under proliferating conditions and produce both β -III tubulin (TuJ1)-positive neuronal cells and glial fibrillary acidic protein (GFAP)-positive glial cells under differentiating conditions, demonstrating that they possess the same essential properties as aNSCs (Fig. 1). We identified a subset of miRNAs that consistently displayed altered expression in the absence of *Mecp2*, relative to WT aNSCs (Fig. 1C, 1D, and Table SI). When considering 95% confidence intervals on mean relative quantities, we identified four miRNAs with expression decreased by ≥ 2.5 -fold and three miRNAs with a ≥ 2.5 -fold increase in *Mecp2*^{-/-} aNSCs (Fig. 1D). These results suggest that the loss of functional MeCP2 leads to the dysregulation of a subset of specific miRNAs in the context of neurogenesis.

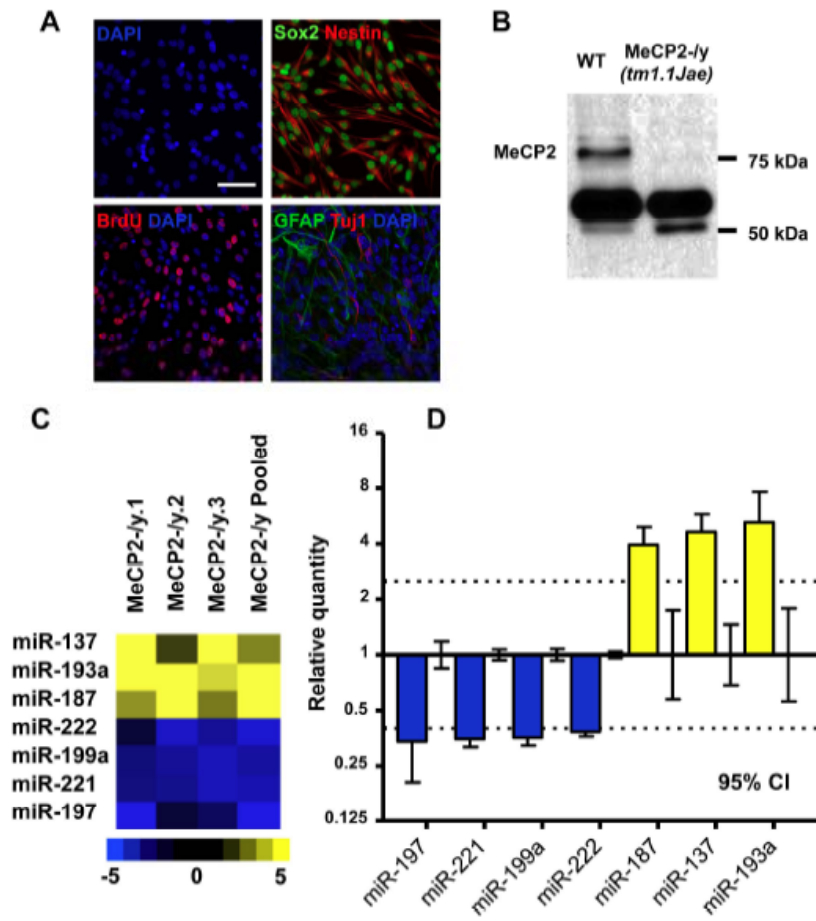


Figure 1. Identification of miRNAs with altered expression in *Mecp2*-deficient adult NSCs. A.

Adult NSCs cultured under proliferating conditions express Sox2 (nuclear, green) and Nestin (cytoplasmic, red) and incorporate BrdU (nuclear, red). Adult NSCs used in this study were multipotent and, when subjected to differentiation, expressed neuron-specific TuJ1 (red) and astrocyte-specific GFAP (green, DAPI in blue), Scale bar = 0.5 μ m. **B.** Western blot showing expression of MeCP2 in WT aNSCs and the absence of MeCP2 in *Mecp2*-/*y* aNSCs (Abcam ab2828 antibody). **C.** Heatmap of miRNA with a ≥ 2.5 -fold change in expression in proliferating *Mecp2*-/*y* aNSCs. Quantities relative to WT aNSCs from each of 4 independent miRNA profiling experiments are shown. Relative quantity scale is shown below for reference. **D.** Relative quantity of

miRNA with ≥ 2.5 -fold change in expression shown for *Mecp2*-/*y* proliferating aNSCs, calibrated to WT proliferating aNSCs (WT relative quantity = 1, mean relative quantity from 3 WT/*Mecp2*-/*y* pairs plus 1 pooled sample per genotype is plotted with error represented as a 95% CI).

To assess the potential for epigenetic regulation of these altered miRNAs, we first evaluated the genomic context of each miRNA, including CpG content and phylogenetic conservation, two hallmarks of functional non-protein-coding regulatory elements. The region immediately upstream of one conserved single copy miRNA, miR-137, is highly conserved, contains multiple CpG-rich regions, and has a consensus binding site for Sox2, an Sry-related HMG-box transcription factor that plays important roles in stem cell function and adult neurogenesis (Fig. 3A, 3B, 3C) (Jaenisch and Young 2008; Zhao, Deng et al. 2008).

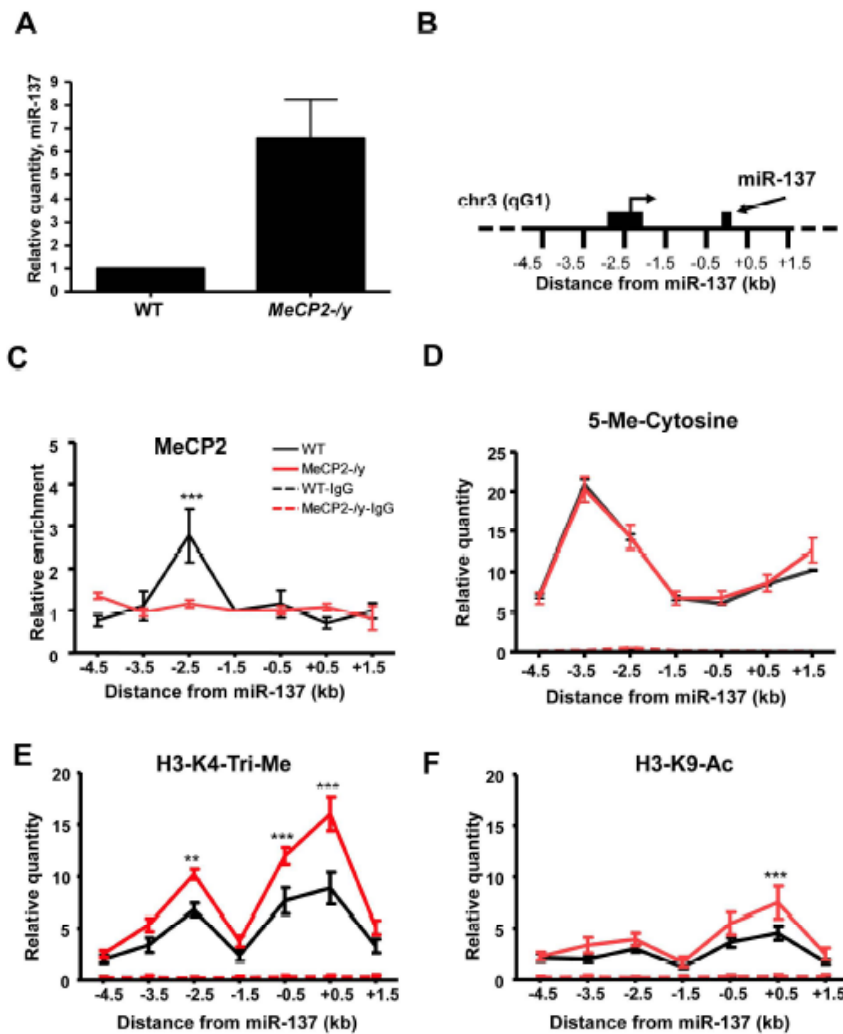
Elevated expression of miR-137 in the absence of MeCP2 was verified using independent assays (Fig. 2A). Overall, miR-137 was 6.5-fold higher in proliferating *Mecp2*^{-/y} aNSCs (Fig. 2A). Furthermore, pri-/pre-miR-137 expression was significantly increased in the absence of MeCP2, indicating that expression of miR-137 was in fact influenced at the level of transcription (Fig. S1C).

The expression of miR-137 has been found to increase during neuronal differentiation, suggesting that the proper temporal expression of miR-137 may indeed influence aNSC proliferation and/or differentiation (Silber, Lim et al. 2008). Consistent with these findings, we observed a significant increase in miR-137 expression upon differentiation of both WT and *Mecp2*^{-/y} aNSCs (Fig. S1A). However, upon aNSC differentiation, we saw no significant difference in the relative increase in miR-137 expression between genotypes (Fig. S1B). These results indicate that the absence of *Mecp2* influences miR-137 expression prior to aNSC differentiation and that miR-137 may be prematurely expressed in *Mecp2*^{-/y} aNSCs. We note that the absence of a MeCP2 mediated influence on miR-137 expression during differentiation also suggests a role for additional regulatory factors in the induction of miR-137 during this process. However, in proliferating aNSCs, precocious expression of miR-137 in the absence of MeCP2 would expose targeted mRNAs to aberrant regulation and potentially result in altered aNSC proliferation and/or differentiation. Based on these observations, we first proceeded to test the

possibility of MeCP2-mediated epigenetic regulation of miR-137 in aNSCs, as well as the involvement of Sox2 in such regulation.

Expression of miR-137 is epigenetically regulated by MeCP2

To test whether MeCP2 interacts directly with genomic regions proximal to miR-137, we performed MeCP2-specific chromatin immunoprecipitation (ChIP) followed by real-time quantitative PCR across a 7-kb region surrounding miR-137, which included most of the highly conserved sequences upstream. Immunoprecipitation of chromatin chemically crosslinked to DNA in WT aNSCs with a MeCP2-specific antibody demonstrated that a region 2.5 kb upstream of miR-137 was enriched ~3-fold relative to *Mecp2*^{-/-} aNSCs (Fig. 2B and 2C). Between 2 kb and 4 kb upstream of miR-137 we also observed significant levels of 5'-methyl-cytosine (5'-Me-C), as detected by immunoprecipitation of DNA with a 5'-Me-C-specific antibody (MeDIP), indicating the presence of methyl CpG dinucleotides to which MeCP2 could bind (Fig. 2D) (Weber, Davies et al. 2005). However, we detected no discernable difference in DNA methylation between different genotypes.



Bonferroni post-test, *** $p < 0.001$). **D.** IP of 5'-Me-C (MeDIP) showing enrichment of methylated cytosines between 4.5 and 1.5 kb upstream of miR-137 with which MeCP2 may normally bind ($n = 3$, mean \pm SEM). **E.** H3-K4-Tri-Me-specific ChIP indicates increased enrichment of sequences 2.5 kb upstream of miR-137, as well as sequences in a 1-kb region directly surrounding miR-137 in *Mecp2*^{-/-} aNSCs. **F.** H3-K9-Ac-specific ChIP with increased enrichment of sequences in the 1 kb surrounding miR-137 in *Mecp2*^{-/-} aNSCs. (All histone ChIP experiments; $n = 3$, mean \pm SEM, ** $p < 0.01$, *** $p < 0.001$, two-way ANOVA, Bonferroni post-test, quantities calculated from an input DNA-generated standard curve.) Quantities in IgG-only nonspecific IP control experiments in E-G are near 0.

Given the role of MeCP2 in epigenetic regulation and its direct association with regions proximal to miR-137, we chose to examine the effect that loss of MeCP2 has on the chromatin state of the miR-137 locus by performing histone-specific ChIP assays in WT and *Mecp2*^{-/-} aNSCs. We found that the absence of MeCP2 correlated

Figure 2. Expression of miR-137 is epigenetically regulated by MeCP2. **A.** Verification of increased expression of miR-137 in *Mecp2*^{-/-} proliferating aNSCs using independent real-time PCR ($n = 6$, mean relative quantity \pm SEM, $p = 0.022$). **B.** Schematic of the 7 kilobases (kb) proximal to miR-137 on chromosome 3qG1 that were assayed in ChIP experiments. The region 2.5 kb upstream is indicated, along with a previously identified transcriptional start site that lies 2.2 kb upstream of miR-137 (Shiraki, Kondo et al. 2003; Carninci, Kasukawa et al. 2005). **C.** MeCP2-specific chromatin immunoprecipitation indicates the enrichment of DNA 2.5 kb upstream of the miR-137 genomic locus in WT aNSCs, but not *Mecp2*^{-/-} aNSCs. Relative enrichment is calculated relative to IgG-only nonspecific control and normalized to the directly adjacent 1.5-kb upstream region ($n = 3$, mean \pm SEM, two-way ANOVA,

with increased trimethyl histone H3 lysine 4 (H3-K4-Tri-Me) in the same 2.5-kb region upstream of miR-137 with which MeCP2 interacted in WT NSCs, as well as in the 1 kb directly surrounding miR-137 (Fig. 2E). Additionally, we observed increased acetylated histone H3 lysine 9 (H3-K9-Ac) in the 1-kb region directly surrounding miR-137 (Fig. 2F). Both H3-K4-Tri-Me and H3-K9-Ac associate with actively transcribed DNA, correlating with the increased expression observed for miR-137 in the absence of MeCP2. In particular, the enrichment of H3K4-Tri-Me across this region strongly indicates that it is indeed a region of transcription initiation. Enrichment of H3-K4-Mono-Me and H3-K9-Tri-Me was minimal and indistinguishable between genotypes (Fig. S2A and S2B). Although H3-K27-Tri-Me was enriched in the 2 kb directly surrounding miR-137, we saw no significant difference between WT and *Mecp2*^{-/-} aNSCs (Fig. S2C).

Additionally, we found that upon differentiation of WT aNSCs, there was a marked increase in H3-K4-Tri-Me and H3-K9-Ac proximal to miR-137 (Fig. S2D and S2E), while H3-K27-Tri-Me levels decreased slightly (Fig. S2F). Therefore, chromatin marks generally associated with active transcription appear to arise prematurely in the absence of MeCP2. Together, these data indicate the precocious establishment of a chromatin state correlating with increased miR-137 expression in the absence of MeCP2 and support a role for MeCP2 in mediating the proper epigenetic regulation of miR-137 specifically in proliferating aNSCs.

We noted that the 2.5-kb upstream region also contains a putative binding site for Sox2, a critical factor regulating stem cell self-renewal (Fig. 3A). Since stem cell self-renewal is process intricately linked with epigenetic regulation, we hypothesized that Sox2 may act in conjunction with MeCP2 to regulate miR-137 expression. Such regulation by Sox2 would also be supportive of a putative regulatory role for miR-137 in aNSCs. Therefore, we performed additional CHIP assays and found that the same region bound by MeCP2 was enriched ~3.3-fold in a Sox2-specific CHIP assay (Fig. 3D). This result correlated with previously observed Sox2-binding at the miR-137 genomic locus in embryonic stem (ES) cells (Boyer, Lee et al. 2005). Interestingly, the enrichment of Sox2-binding to this genomic region was lost in *Mecp2*^{-/-} aNSCs (Fig. 3D). These results indicate that both MeCP2 and Sox2 bind directly to the 5'-regulatory region of miR-137 in aNSCs. Consistent with such a mechanism, we also found that MeCP2 and Sox2 could be coimmunoprecipitated and that their association is DNA-independent (Fig. 3E). Thus, concurrent binding of MeCP2 and Sox2 within the 2.5-kb region upstream of miR-137 could be required for proper transcriptional regulation of miR-137 in aNSCs.

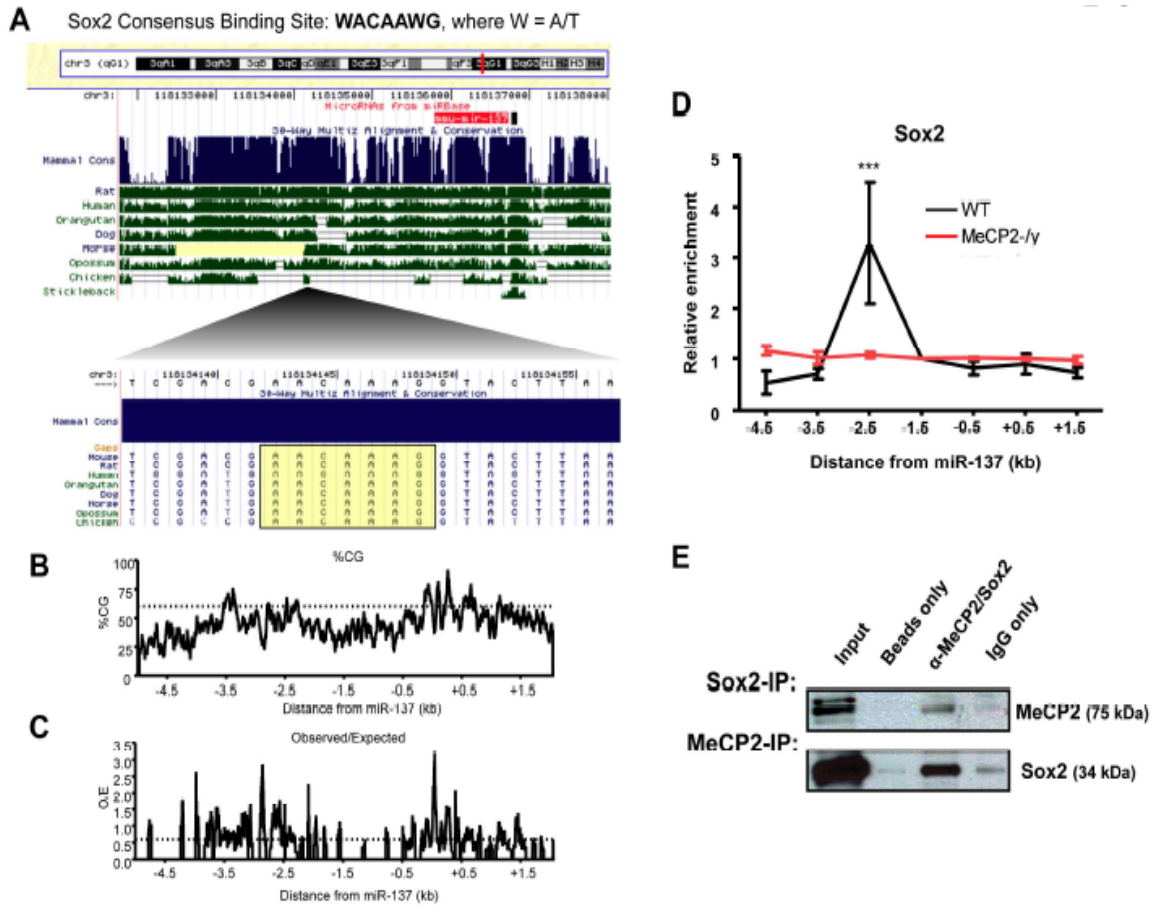


Figure 3. Transcriptional regulation of miR-137 involves co-regulation by Sox2. **A.** Schematic showing the miR-137 genomic locus and the location of a conserved Sox2 consensus-binding site within the 2.5-kb upstream region of miR-137 with which MeCP2 was also found interact by ChIP. **B&C.** Genomic structure and CpG content surrounding the miR-137 genomic locus. **B.** Percentage of CG content across a 7-kb region surrounding miR-137, with a threshold indicated at 60%. **C.** Ratio of observed CpG dinucleotides to the number of CpGs expected with a normal distribution across the same 7-kb region surrounding miR-137. A threshold is indicated at a ratio of 0.6. Data for both plots were generated using EMBOSS CpG plot with a 100-nt window size and a 1-nt window shift increment (Larsen, Gundersen et al. 1992). **D.** Sequences 2.5 kb upstream of miR-137 enriched in a Sox2-specific ChIP relative to IgG only in WT aNSCs but not *Mecp2*^{-/-} aNSCs, normalized to the directly adjacent 1.5-kb upstream region (n = 3, mean \pm SEM, two-way ANOVA, Bonferroni post-test, ***p < 0.001). **E.** MeCP2 and Sox2 could be co-immunoprecipitated. Either MeCP2 or Sox2 was immunoprecipitated and subject to western blots with anti-Sox2 or anti-MeCP2 antibody, respectively. IP beads only and IP with normal IgG were used as negative controls.

miR-137 modulates the proliferation and differentiation of aNSCs in vitro

Our miRNA expression studies and ChIP assays indicated premature expression of miR-137 that was concurrent with the establishment of a chromatin state reflective of active transcription in the absence of MeCP2. An increase miR-137 expression in proliferating aNSCs would expose the distinct population of cellular mRNAs to

aberrant miR-137 targeting, potentially resulting in abnormal aNSC proliferation and/or differentiation. Therefore, we sought to assess the potential regulatory effects of miR-137 by introducing or blocking miR-137 function specifically in proliferating aNSCs, and then asking what the subsequent effects on proliferation and/or differentiation were. To do this, we first created a lentiviral vector expressing a miR-137 shRNA (sh-miR-137) under a U6 snRNA RNA polymerase III promoter and enhanced green fluorescent protein (eGFP) under a CMV promoter (Li, Barkho et al. 2008). Lentiviruses were used to infect cultured aNSCs with nearly 100% infection efficiency as indicated by GFP expression (Fig. 4 and Fig. S3A). We also verified overexpression of miR-137 independent of changes in several other miRNAs with altered expression in *Mecp2^{-/-}* aNSCs, such that miR-137 would exert its functional effect independently of other miRNAs in aNSCs (Fig. S3F). Quantification of BrdU-positive cells after pulse labeling indicated that miR-137-overexpressing (GFP⁺) aNSCs had 87.4% higher GFP⁺BrdU⁺ cells relative to sh-control lentivirus-infected aNSCs (Fig. 4A and 4C). This effect did not appear to be due to altered cell survival since we did not observe a significant difference in the apoptotic marker activated Caspase-3 when comparing sh-Control and sh-miR-137 treated cells (Fig. S4A). Using a miR-137-specific inhibitor (anti-miR-137), we found that by blocking endogenous miR-137 in proliferating cells, GFP⁺BrdU⁺ cells were reduced by 81% relative to control, nonspecific anti-miR-treated cells (Fig. 4B). Therefore, high levels of miR-137 led to a greater proliferative capability for aNSCs, whereas blocking endogenous miR-137 function reduced proliferation.

To assess the effect of precocious miR-137 expression on subsequent aNSC differentiation, sh-miR-137 or sh-control lentivirus-infected aNSCs were subjected to a differentiation protocol. Neuronal differentiation was assessed by both TuJ1 immunostaining and the promoter activity of a pan-neuronal transcription factor, NeuroD1. Astrocyte differentiation was determined by GFAP immunostaining as well as GFAP promoter activity (Zhao, Ueba et al. 2003; Barkho, Song et al. 2006; Smrt, Eaves-Egenes et al. 2007). Sh-miR-137 lentivirus-infected aNSCs exhibited a 65.0% decrease in neuronal differentiation (Fig. 4D and 4H) and a 51.0% decrease in astrocyte differentiation (Fig. 4F and 4H) relative to sh-control lentivirus-infected aNSCs. Consistent with these observations, transfection of sh-miR-137 or synthetic duplex miR-137 reduced the activities of both GFAP and NeuroD1 promoters (Fig. 4I and 4J). Furthermore, anti-miR-137 treatment had opposite effects compared to miR-137 overexpression on neuronal and astrocyte differentiation. The number of TuJ1-positive cells increased by 2.13-fold, while GFAP-positive cells were 2.32-fold more common relative to nonspecific anti-miR-control treatments (Fig. 4E and Fig. 4G). Similarly, blocking the function of endogenous miR-137 led to enhancement of co-transfected NeuroD1- and GFAP-promoter-luciferase activity assayed at 24-48 hours of differentiation, whereas a nonspecific anti-miR had no effect (Fig. 4I and 4J). These results indicate that the dosage of miR-137 in aNSCs is critical for modulating the proliferation and differentiation of aNSCs. Overexpression of miR-137 promoted the proliferation of aNSCs at the expense of aNSC differentiation, while antagonizing miR-137-enhanced aNSC differentiation and reduced proliferation.

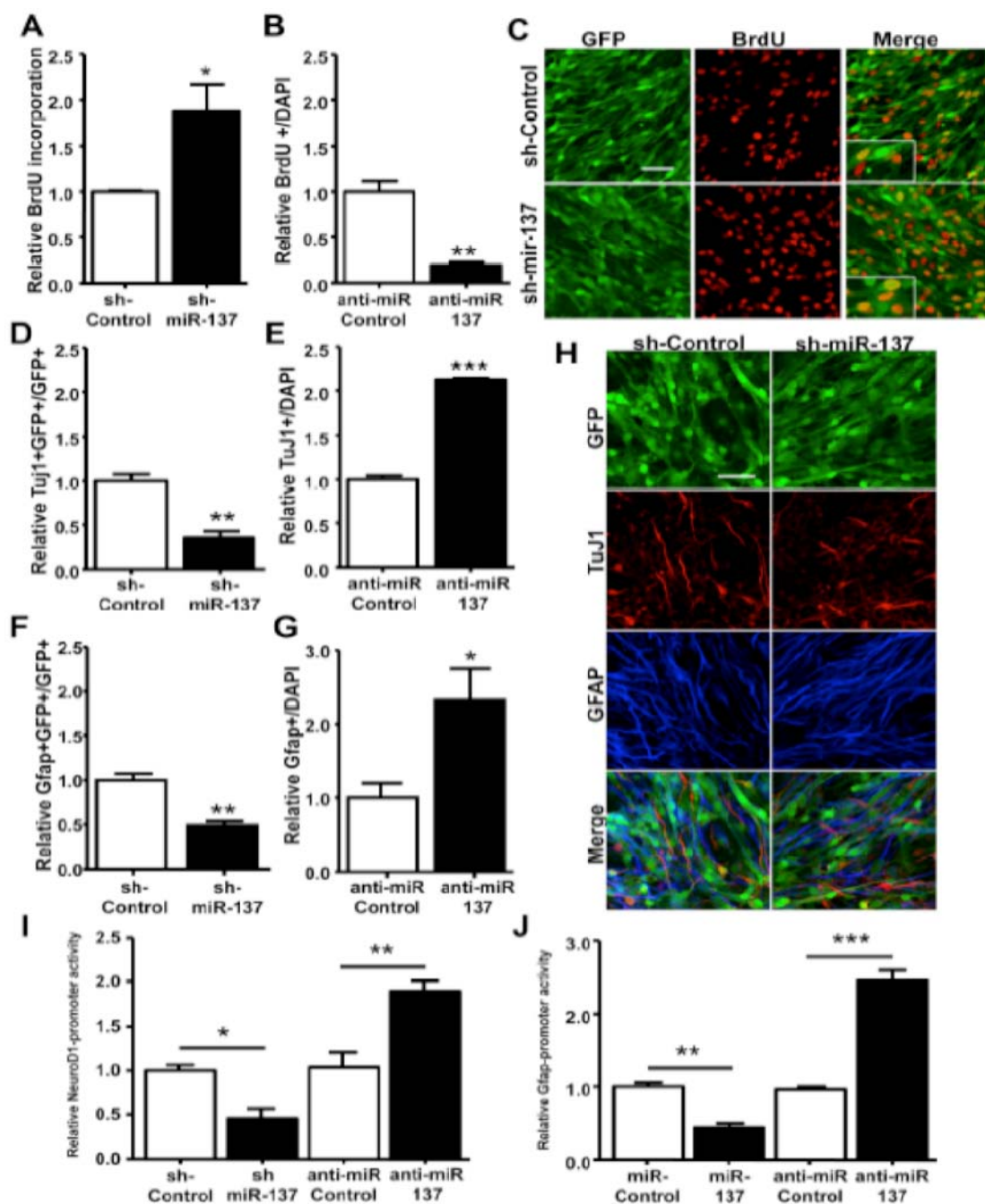


Figure 4. miR-137 modulates the proliferation and differentiation of adult NSCs in vitro. **A.** Cell proliferation was analyzed using BrdU pulse labeling. Quantitative analysis by stereology indicates that miR-137-overexpressing NSCs (GFP positive) produced more BrdU+ cells, indicating increased proliferation, relative to control treated cells (* $p = 0.0403$, unpaired t-test, $n = 3$). **B.** Anti-miR-137 treated aNSCs produced fewer BrdU+ cells relative to anti-miR-Control aNSCs (** $p = 0.0024$, unpaired t-test, $n = 3$). **C.** Representative images of WT aNSCs infected with lentivirus expressing either sh-control or lentivirus expressing sh-miR-137, which were pulse-labeled with BrdU. Scale bar = 50 μ m. **D.** sh-miR-137-infected cells differentiated into fewer neurons compared with sh-control virus-infected cells as determined by the percentage of TuJ1-positive cells among infected, GFP-positive cells (** $p = 0.0037$, unpaired t-test, $n = 3$, sh-control treatment is normalized to 1.0). **E.** Anti-miR-137 treatment reduces production of TuJ1-positive cells during differentiation (** $p < 0.0001$, $n = 3$, anti-miR-Control treatment is normalized to 1.0). **F.** Among infected, GFP-positive cells, sh-miR-137-infected cells differentiated into fewer GFAP-positive cells compared with sh-control virus-

infected cells (**p = 0.0046, unpaired t-test, n = 3, sh-Control treatment is normalized to 1.0). **G.** Anti-miR-137 treatment reduces production of GFAP-positive cells during differentiation (*p = 0.0483, n = 3, anti-miR-Control treatment is normalized to 1.0) **H.** Representative images of lentivirus-infected NSCs that were differentiated into Tuj1-positive neurons (red) and GFAP-positive astrocytes (blue). Scale bar = 50 μ m. **I.** While overexpression of miR-137 leads to a decrease in NeuroD1-promoter activity relative to control treatment and as assessed by a luciferase reporter (**p = 0.0128, unpaired t-test, n \geq 3), anti-miR-137 treatment leads to increased NeuroD1-promoter-luciferase activity (**p = 0.0046, unpaired t-test, n = 3). Control treatments are normalized to 1.0. **J.** Overexpression of miR-137 leads to a decrease in GFAP-promoter activity (**p = 0.0021, unpaired t-test, n = 3), while anti-miR-137 treatment leads to increased GFAP luciferase activity (**p = 0.0007, unpaired t-test, n = 3). Control treatments are normalized to 1.0. Data in all panels is plotted as mean \pm SEM.

miR-137 modulates the proliferation and differentiation of aNSCs in vivo

To assess the function of miR-137 in vivo, we took advantage of the persistent neurogenesis in the dentate gyrus (DG) of the postnatal hippocampus, which recapitulates the neurogenic process during development (van Praag, Schinder et al. 2002; Ge, Goh et al. 2006; Smrt, Eaves-Egenes et al. 2007). Recombinant retroviruses capable of infecting dividing cells have previously been used to label and follow the differentiation of NSCs in postnatal DG (van Praag, Schinder et al. 2002; Ge, Goh et al. 2006; Smrt, Eaves-Egenes et al. 2007). We therefore engineered a retroviral vector that expresses both sh-miR-137 under an U6 promoter and eGFP under a chicken actin promoter (Fig. 5A). The retrovirus expressing sh-miR-137 was stereotaxically grafted into the right side of the DG, and retrovirus-expressing sh-control was grafted into the left side of the DG of the same animal. To assess proliferation of retrovirus-labeled progenitors, mice also received BrdU injections immediately after the surgery. At one week following viral grafting, a time when some of the retrovirus-labeled NSCs were expected to differentiate, we analyzed BrdU incorporation and expression of the early neuronal marker doublecortin (DCX) using triple fluorescence immunohistology and confocal microscopy (van Praag, Schinder et al. 2002; Ge, Goh et al. 2006; Smrt, Eaves-Egenes et al. 2007).

Many retrovirus-labeled aNSCs (GFP⁺) were also positively labeled with BrdU (Fig. 5C), indicating that these infected cells were in fact dividing after surgery. Some of these retrovirus-labeled cells had initiated neuronal differentiation and were, therefore, positive for DCX expression (Fig. 5C). Using Z-stack images of confocal microscopy at 1- μ m resolution, we quantified the percentage of retrovirus-labeled GFP⁺ cells that expressed either DCX or incorporated BrdU. Compared with sh-control retrovirus-infected cells, a lower percentage of sh-miR-137 retrovirus-infected cells expressed DCX (Fig. 5B, DCX⁺ GFP⁺/GFP⁺) and a higher percentage of sh-miR-137 retrovirus-infected cells incorporated BrdU (Fig. 5B, BrdU⁺GFP⁺/GFP⁺), suggesting that miR-137-overexpressing aNSCs proliferated more and exhibited reduced neuronal differentiation capacity in vivo. Therefore, both our in vitro cell culture assay and in vivo single-cell genetic analyses indicate that a high level of miR-137 promoted aNSC proliferation, but repressed neuronal differentiation.

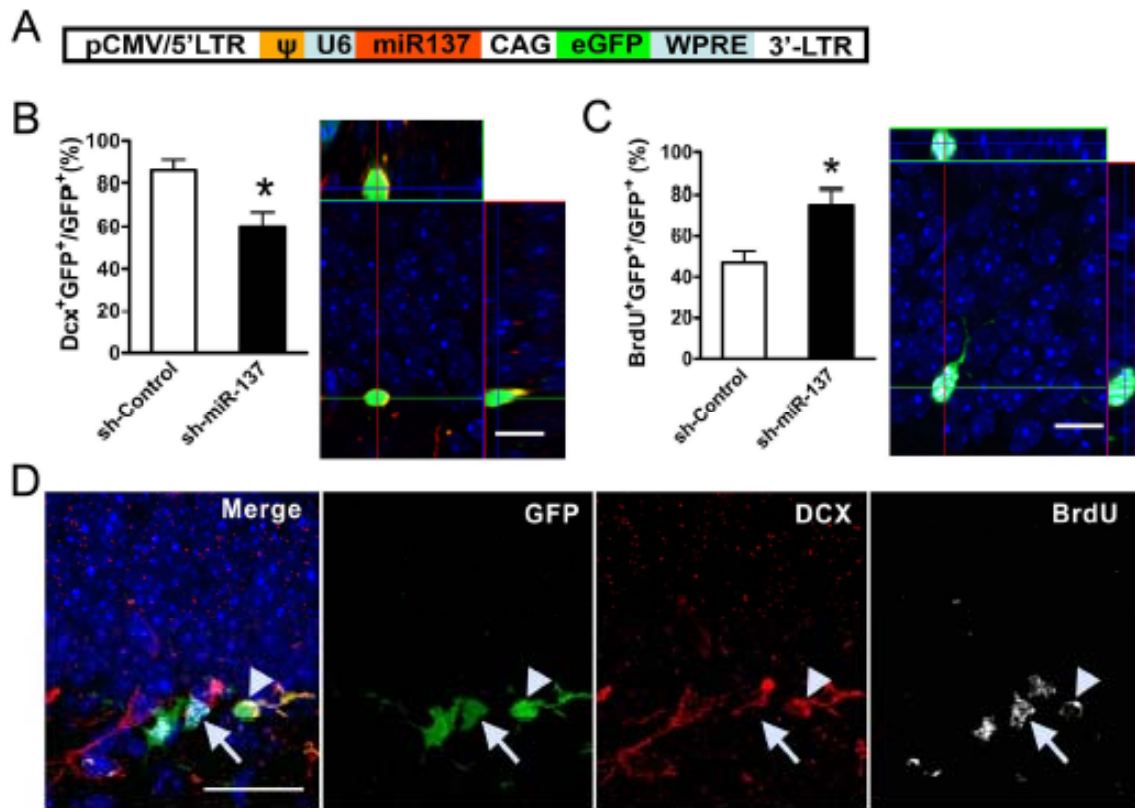


Figure 5. miR-137 modulates the proliferation and differentiation of adult NSCs in vivo. **A.** A schematic diagram of the retroviral vector used for in vivo miRNA expression. **B.** Left panel shows that sh-miR-137-infected cells differentiated into fewer DCX+ early neurons compared with sh-control virus infected cells ($n \geq 3$, $p < 0.05$). Right panel shows a representative confocal 3D Z-stack image used for quantification of DCX+GFP+ cells (Scale bar = 5 mm). **C.** Left panel shows that more sh-miR-137-infected cells proliferated than control virus-infected cells ($n = 3$, $p < 0.05$). Right panel shows a representative 3D Z-stack image used for quantification of BrdU+GFP+ cells (Scale bar = 5 mm). **D.** A representative image of immunohistological analysis of virus-infected endogenous NSCs in the subgranular zone of the dentate gyrus. (Scale bar = 20 mm). Arrowhead indicates a cell that is positive for GFP (green), BrdU (white), and DCX (red), suggesting that this cell was proliferating during the viral grafting period and has differentiated into early neurons within one week after grafting. Arrow points to a cell that is positive for GFP and BrdU, but not for DCX, indicating that this cell did not differentiate.

Ezh2, a histone methyltransferase, is a functional target of miR-137 in aNSCs

To understand the mechanisms by which miR-137 modulates adult neurogenesis, we cross-referenced TargetScan 4.1, PicTar, and miRanda to identify potential miR-137 targets (Lewis, Shih et al. 2003; John, Enright et al. 2004; Krek, Grun et al. 2005). Given the effects of miR-137 on aNSC proliferation and differentiation, 20 candidate miR-137 targets were selected for further analyses on the basis of three

criteria: conservation and context score of target “seed sequences,” and known ontology relevant to neurodevelopment. To test whether miR-137 could indeed target to any of these candidates, we cloned 3'-UTRs directly from aNSC cDNA, ensuring expression of the putative target within aNSCs. We successfully cloned 15 3'-UTRs into a dual luciferase 3'-UTR reporter construct, allowing for the assessment of luciferase expression as dependent on a given 3'-UTR in response to miR-137 (Table SII). With these constructs, we performed a series of reporter assays in cell culture and found that miR-137 overexpression in HEK293T cells could suppress the activity of multiple 3'UTR luciferase reporter genes (Fig. 6A). To determine which gene(s) could be involved in miR-137-mediated modulation of adult neurogenesis, we then performed functional rescue experiments. Based on the observation that overexpression of miR-137 could suppress the activity of transfected NeuroD1-promoter-luciferase reporter at 24 hours of differentiation in WT aNSCs, we asked whether coexpression of any of the genes suppressed by miR-137 in our reporter assays could alleviate the reduction in NeuroD1-luciferase reporter activity. We found that coexpression of Ezh2, but not EphA7, could indeed rescue the decreased NeuroD1-luciferase activity caused by the overexpression of miR-137. Additionally, direct knockdown of Ezh2 using a specific short-hairpin directed against the endogenous Ezh2 mRNA significantly reduced NeuroD1 promoter luciferase activity. This effect was similar to that seen by miR-137 overexpression, suggesting rescue was not simply an artifact of overexpression (Fig. S4C and S4D). Ezh2 overexpression also had no effect miR-137 levels (Fig. 6B and data not shown). To subsequently verify the ability of Ezh2 to rescue the miR-137-

mediated deficit in neuronal differentiation we also assayed the effect of Ezh2 coexpression on the production of TuJ1-positive cells by immunostaining. Indeed, Ezh2 coexpression significantly increased the number of TuJ1-positive cells relative to control treatment (Fig. 6C).

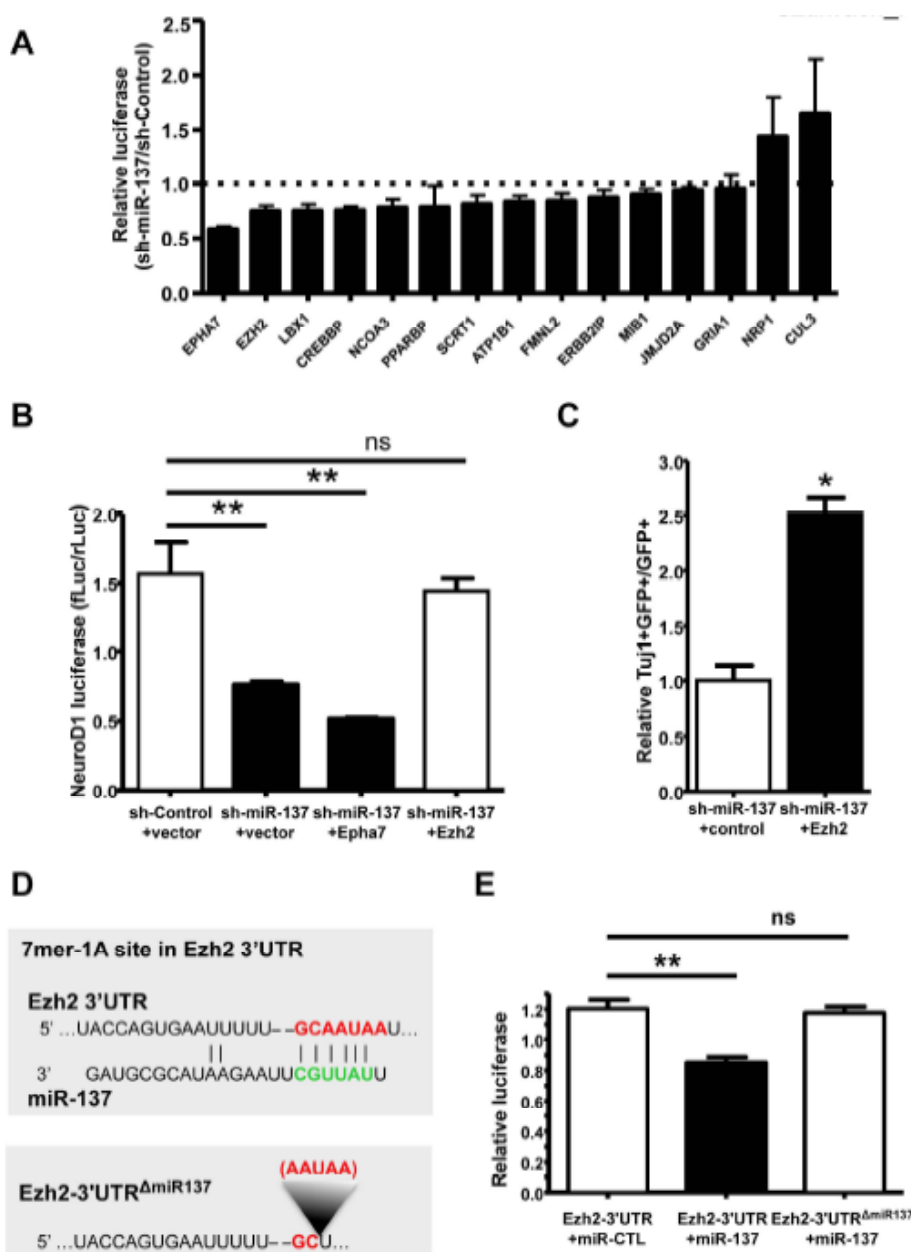


Figure 6. Ezh2 is a functional target of miR-137.

A. Primary screen of predicted miR-137 targets in HEK293FT cells.

3'-UTR-dependent luciferase assays were performed using both sh-control and sh-miR-137 for each of 15 predicted miR-137 targets. For each 3'-UTR, luciferase expression was normalized (hRluc/hLuc+) to 1 for the sh-control control treatment, as indicated by the dotted line. The effect of sh-miR-137 was then calculated relative to sh-control (sh-miR-137/sh-control). For all experiments $n \geq 3$, mean \pm SD.

B. Coexpression of Ezh2 rescued the decreased NeuroD1-luciferase expression caused by the overexpression of miR-137 in aNSCs. NeuroD1 promoter luciferase activity was normalized to co-electroporated E1a-Renilla luciferase activity ($n \geq 3$ for all experiments, one-

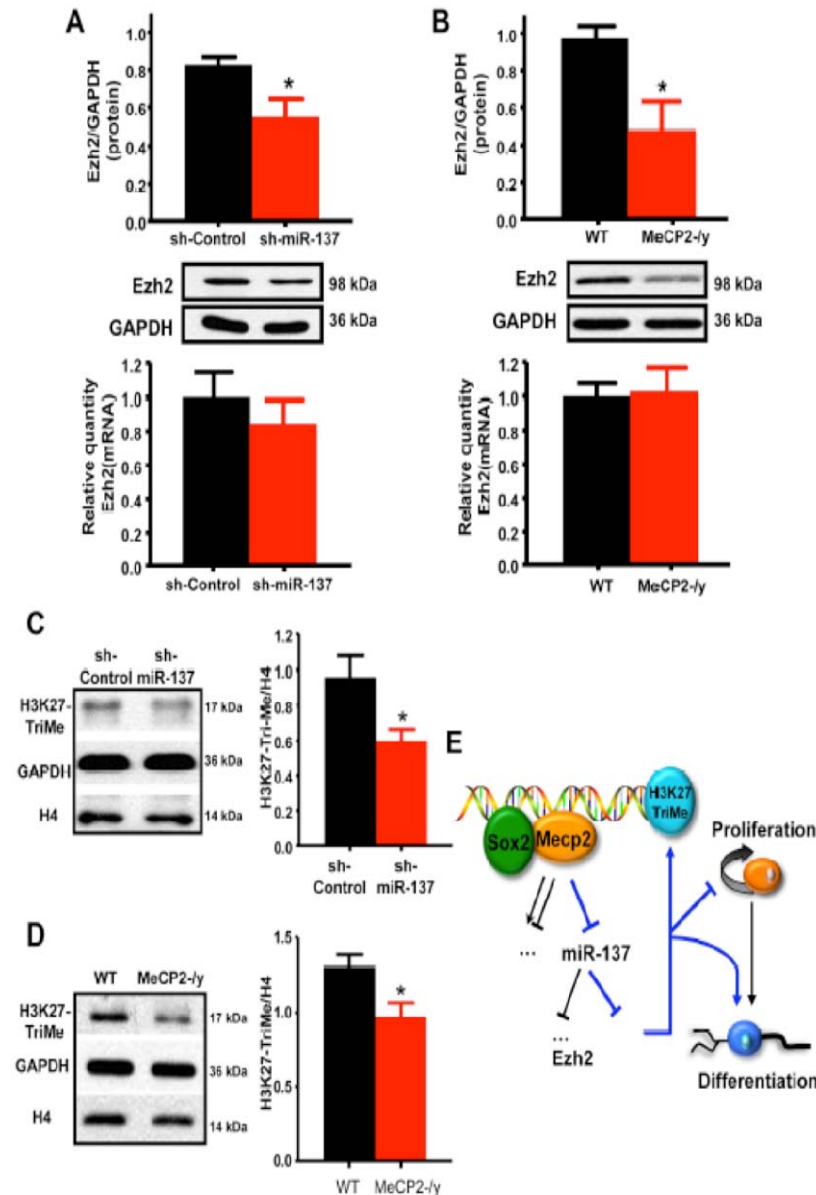
way ANOVA with Bonferroni post-test, ** $p < 0.01$). **C.** Coexpression of Ezh2 rescued the decreased neuronal

differentiation caused by the overexpression of miR-137 in aNSCs, as determined by the percentage of TuJ1-positive cells among infected, GFP-positive cells (* $p = 0.0016$, unpaired t-test, $n = 3$). **D.** The miR-137 7mer-1A target site in the Ezh2 3'-UTR as predicted by TargetScan. **E.** Ezh2-3'-UTR-dependent expression of a luciferase reporter gene was suppressed by miR-137 in HEK293FT cells. MiR-137-mediated suppression of luciferase was specific, as deletion of the miR-137 target site in the Ezh2 3'-UTR abolished repression by miR-137. Renilla luciferase-Ezh2-3'-UTR expression was normalized to firefly luciferase ($n = 6$ for HEK293FT cells, unpaired t-test, $p < 0.05$).

Ezh2 expression was further capable of significantly reducing proliferation as assayed by BrdU incorporation, an effect opposite to that seen with miR-137 overexpression (Fig. S4B). This suggests that Ezh2 coexpression could also rescue the miR-137-mediated increase in aNSC proliferation. Furthermore, targeting of Ezh2 by miR-137 was specific, since mutating the seed sequence targeted by miR-137 within the luciferase-Ezh2-3'UTR reporter alleviated miR-137-mediated suppression (Fig. 6D and 6E).

We went on to examine the effect of miR-137 on endogenous Ezh2 expression and saw a ~35% reduction of endogenous Ezh2 protein in WT aNSCs infected by sh-miR-137-expressing lentivirus (Fig. 7A). However, the reduction in protein did not correlate with a proportional reduction in steady-state mRNA expression, indicating post-transcriptional regulation of Ezh2 mRNA by miR-137 (Fig. 7A). Importantly, Ezh2 protein expression was also reduced in *Mecp2*^{-/-} aNSCs, where expression of miR-137 is increased similarly (Fig. 7B). To further verify the miR-137-mediated repression of Ezh2, we transfected anti-miR-137 into *Mecp2*^{-/-} cells and asked whether blocking miR-137 expression in *Mecp2*^{-/-} aNSCs could restore Ezh2 expression to levels similar to those seen in WT aNSCs. Indeed, Ezh2 protein expression recovered to levels comparable with those seen in WT aNSCs (Fig. S4E).

Together, these data demonstrate that the effect of miR-137 on Ezh2 protein expression is repressive, posttranscriptional, and specific, and they also suggest that



Ezh2 is a functional target of miR-137 in the context of adult neurogenesis.

Figure 7. miR-137 regulates the expression of Ezh2 post-transcriptionally and results in an overall reduction in H3K27-TriMe. **A.** Overexpression of miR-137 in WT aNSCs led to the reduction of endogenous Ezh2 protein expression (top, n = 4, mean ± SEM, p = 0.0366) without a proportional reduction in Ezh2 mRNA (bottom, n = 3, mean with 95% CI). **B.** Loss of MeCP2 in aNSCs led to a similar reduction in endogenous Ezh2 protein expression (top, n = 4, mean ± SEM, p = 0.0417) without a proportional reduction in Ezh2 mRNA (bottom, n = 3, mean with 95% CI). **C.** Overexpression miR-137 resulted in a reduction in H3K27-TriMe relative to histone H4 (p = 0.0379, n ≥ 3, unpaired t-test). **D.** H3K27-TriMe is also reduced relative to histone H4 in *MeCP2-/-* aNSCs (p = 0.0367, n ≥ 3, unpaired t-test). **E.** Model for the crosstalk between MeCP2, miR-137, and Ezh2 in modulating adult

neurogenesis. MeCP2 along with Sox2 mediates the epigenetic regulation of miR-137 in aNSCs, where increased expression of miR-137 promotes aNSC proliferation and inhibits aNSC differentiation, while decreased expression of miR-137 promotes differentiation of aNSCs. One target gene involved in this process is Ezh2. The miR-137-mediated suppression of Ezh2 feeds back to chromatin by decreasing global H3K27-TriMe.

We next asked whether the functional targeting of Ezh2 by miR-137 correlated with an altered epigenetic state, in terms of chromatin, by assaying the effect of miR-137

overexpression on global H3-K27-Tri-Me. In both miR-137–overexpressing cells and *Mecp2*-/*y* cells, the miR-137–mediated decrease in Ezh2 protein correlated with an overall reduction in H3-K27-Tri-Me (Fig. 7C and Fig. 7D). This indicates the integration of epigenetic regulation in aNSCs through MeCP2-mediated control of miR-137, the subsequent repression of Ezh2, and feedback to chromatin in the form of decreased H3-K27-Tri-Me.

Discussion

Epigenetic regulation is proposed to play important roles in neurogenesis. Emerging evidence implicates both chromatin remodeling and epigenetic modifications as critical to the regulation of various aspects of adult neurogenesis (Zhao, Ueba et al. 2003; Lim, Huang et al. 2009; Ma, Jang et al. 2009); however, the identification of downstream targets has proved elusive (Hsieh and Gage 2004; Cheng, Tavazoie et al. 2005; Abel and Zukin 2008). Our results suggest that one such class of targets is miRNAs, including miR-137. We show that miR-137 is an intrinsic modulator of adult neurogenesis. The finding that overexpression and inhibition of miR-137 have distinctly opposite effects on aNSCs suggests that the dosage of miR-137 is critical to the modulation of adult neurogenesis. Previous studies have found that miR-137 could inhibit proliferation and induce differentiation of tumor cells (Kozaki, Imoto et al. 2008; Silber, Lim et al. 2008); CDK6 was identified as the miR-137 target relevant to the proliferation phenotype that was observed (Kozaki, Imoto et al. 2008; Silber, Lim et al. 2008). We have directly assayed CDK6 expression in aNSCs

overexpressing miR-137 (both MeCP2-/*y* aNSCs and sh-miR-137 treated aNSCs) and observed an increase in CDK6 protein, an effect opposite to previous results (Fig. S5). This difference between primary cells and transformed tumor cells is not surprising since expression profiles of miRNAs have been shown to distinguish human tumor cells of different origins from their normal tissue counterparts more effectively than the expression profiles of mRNAs (Jay, Nemunaitis et al. 2007; Barbarotto, Schmittgen et al. 2008). Our data further support the notion that miRNAs may play distinct roles in normal and tumor stem cells by post-transcriptionally regulating different target mRNAs.

We show that the expression of miR-137 is subject to epigenetic regulation mediated by MeCP2. Furthermore, we observe a novel interaction between MeCP2 and Sox2, a core transcriptional regulator in stem cells, in the genomic region proximal to miR-137. In *Mecp2*-/*y* aNSCs we find a chromatin state reflective of premature miR-137 expression that also correlated with a loss of Sox2 binding upstream of miR-137. These results indicate a role for MeCP2 in establishing or maintaining an epigenetic state in the chromatin surrounding miR-137. Such chromatin states may allow for proper transcriptional coordination by Sox2, which has been shown to play important roles in the maintenance of stem cell properties and the regulation of adult neurogenesis (Bylund, Andersson et al. 2003; Graham, Khudyakov et al. 2003; Ellis, Fagan et al. 2004; Ferri, Cavallaro et al. 2004; Taranova, Magness et al. 2006; Suh, Consiglio et al. 2007). Together, these observations

reinforce the importance of controlling miRNA expression in stem cells and reveal epigenetic regulation as one such mechanism by which this could be accomplished.

Our data has clearly demonstrated that the dosage of miR-137 in NSCs is important for NSC function and the transcriptional control by MeCP2 helps to retain the levels of miR-137 at its proper level. Overexpression of miR-137 in the absence of MeCP2 results in an influence of miR-137 on subsequent aNSC proliferation/differentiation that was not expected based on the normal expression profile of miR-137 during aNSC differentiation. This indicates that miR-137 overexpression specifically in proliferating aNSCs has a regulatory affect distinct from that which it may have during differentiation. This may not be surprising in light of our findings that miR-137 dosage is critical toward its regulatory role in aNSCs and the fact that proliferating and differentiated aNSCs are likely to express quantitatively distinct populations of mRNAs that would be subjected to differential miR-137 targeting. As a result, it will be interesting and important to further identify miR-137 targets specific to differentiated aNSCs, or even mature neurons, as compared to those targets regulated in proliferating aNSCs.

We identified Ezh2 as a functional miR-137 target with relevance to adult neurogenesis. Ezh2 is a H3-K27 methyltransferase and component of the Polycomb group (PcG) of protein complexes known to perform important functions in stem cells (O'Carroll, Erhardt et al. 2001; Cao and Zhang 2004; De Haan and Gerrits 2007; Lee, Murdoch et al. 2007). PcG proteins function by forming and maintaining the

bivalent chromatin state of stem cells (Boyer, Plath et al. 2006; Lee, Jenner et al. 2006). This so-called “bivalent chromatin state” allows cell/tissue-specific genes to be “primed” for expression but “held in check” by opposing chromatin modifications (Boyer, Plath et al. 2006; Lee, Jenner et al. 2006). Therefore, a bivalent chromatin state is likely a common mechanism in many types of stem and progenitor cells for maintaining their differentiation potential, with PcG proteins being critical factors in this regulatory mechanism. Not surprisingly, Ezh2 is found to be a critical regulator of neuroprogenitor cell maintenance and differentiation (Shen, Liu et al. 2008; Sher, Rossler et al. 2008; Ezhkova, Pasolli et al. 2009). Our finding that miR-137 regulates the expression of Ezh2 in aNSCs reveals a novel interaction between PcG proteins and miRNAs; hence distinct miRNAs may be involved in establishing and maintaining the bivalent chromatin state of stem cells. This further suggests a potential epigenetic circuitry in the modulation of aNSCs, with a feedback regulatory mechanism mediated by miRNAs (Fig. 7E). In this particular example, precocious overexpression of miR-137 results in a reduction of Ezh2 and an altered epigenetic state of aNSCs in the form of a global decrease in H3-K27-Tri-Me. It is likely that altered H3-K27-Tri-Me at specific key developmental genes contributes to the phenotypes observed with miR-137 overexpression and identification of these loci will be an important question moving forward. These results provide direct evidence for the hypothesis that crosstalk between epigenetic regulation and the miRNA pathway plays an important role in modulating adult neurogenesis, which reflects the complexity of the network regulating proliferation and differentiation of stem cells in general.

The postnatal neurodevelopmental disorder known as Rett syndrome is largely caused by mutations in *MECP2* (Amir, Van den Veyver et al. 1999). Recent studies have also shown that MeCP2 aberrations result in a constellation of neuropsychiatric abnormalities, wherein both loss of function and a gain in MeCP2 dosage lead to similar neurological phenotypes (Chahrour and Zoghbi 2007). One challenge in understanding the etiology of MeCP2-related disorders is that MeCP2 processes multiple function domains, post-translational modifications, and cofactors, which allows the protein to be involved in numerous cellular pathways (Zhou, Hong et al. 2006; Chahrour, Jung et al. 2008; Ballas, Liyo et al. 2009; Tao, Hu et al. 2009). The identification of key downstream targets of MeCP2 is critical for understanding the molecular basis of MeCP2-related neurological disorders. Earlier studies have focused mainly on protein-coding RNAs (Chahrour and Zoghbi 2007). Here we demonstrate that MeCP2 can also regulate the expression of small noncoding RNAs, particularly a subset of miRNAs, which reveals another layer of gene regulation mediated by MeCP2. miRNAs are particularly abundant in the brain and play key roles in neuronal function and plasticity (Cheng, Tavazoie et al. 2005). While our present study focuses on miR-137, our results indicate that there are additional miRNAs that could be regulated by MeCP2. In consideration of previous studies suggesting a role for MeCP2 in regulating neural precursor maturation (Kishi and Macklis, 2004; Smrt et al., 2007) it will be important to further evaluate how the miRNAs regulated by MeCP2 could interact with each other in

neurodevelopmental contexts, thereby contributing to the molecular pathogenesis of Rett syndrome and other MeCP2-related disorders.

Materials and Methods

Isolation and culture of adult NSCs

The *Mecp2* mutant mice (*Mecp2^{tm1.1Jae}*) used in this study were created by deleting exon 3 containing the MBD domain of MeCP2 (Chen, Akbarian et al. 2001). These mice have been bred over 40 generations on an ICR background. They begin to show neurological symptoms between 5 and 8 weeks of age and die at about 10-11 weeks. Mice 7 weeks of age and without severe physical symptoms were used for cell isolation, as were WT littermates. The isolation of adult mouse brain-derived NSCs was performed according to an established protocol with modifications (Zhao, Ueba et al. 2003). Briefly, the forebrain without the olfactory bulb was dissociated mechanically followed by enzymatic digestion based on the MACS Neural Tissue Dissociation Kit (Miltenyi Biotec, #130-092-628). After enzymatic digestion was stopped using DMEM/F-12 containing 10% FBS (Sigma-Aldrich, #F 4135), 2 mM L-glutamine (GIBCO, #25030-081), and 1% Antibiotic-Antimycotic (GIBCO, #15240-062), the cell suspension was filtered through a 70- μ m cell strainer (BD Falcon, #252350, CA), and the single-cell suspension was loaded onto 50% Percoll. The NSCs were separated from other cells by ultracentrifugation at 127k rpm for 30 min at 20°C using a SW41 Rotor (Beckman, CA). The fraction containing NSCs was collected and cultured in DMEM/F-12 medium containing 20 ng/ml basic fibroblast

growth factor (FGF-2, PeproTech, #K1606), 20 ng/ml epidermal growth factor (EGF, PeproTech, #A2306), 1% N2 supplement (GIBCO, #17502-048), 1% Antibiotic-Antimycotic, and 2 mM L-glutamine in a 5% CO₂ incubator at 37°C. We replaced half the medium every 2-3 days.

Relative quantification of mature miRNAs by real-time PCR

Profiling of mature miRNA expression was performed using Applied Biosystems' TaqMan microRNA assays with 48-plex reverse transcription and individual TaqMan microRNA real-time PCR assays according to protocols provided by the vendor (Lao, Xu et al. 2006). Briefly, 8 pools of 48 reverse transcription primers each were used in 20- μ l reactions consisting of: 20 ng total RNA, 1X TaqMan miRNA Reverse Transcription Primer Pool, 0.5 mM of each dNTP, 10.0 U/ μ l MultiScribe Reverse Transcriptase, 1X Reverse Transcription Buffer, 0.25 U/ μ l RNase Inhibitor, and nuclease-free water. The reactions were incubated at 16°C for 30 min, 42°C for 30 min, and 85°C for 5 min. Reactions were diluted 1:10 with nuclease-free water for use in the TaqMan real-time PCR reactions. Individual TaqMan microRNA real-time PCR reactions for profiling experiments were performed on an Applied Biosystems 7900HT SDS in a 384-well format running WT and *MeCP2*^{-/-} pairs in parallel for each cDNA pool generated in the reverse transcription step. PCR reactions were carried out in triplicate for each sample and each miRNA. The 10- μ l reactions consisted of 1X TaqMan Universal Master Mix, No AmpErase UNG, 1X

TaqMan miRNA assay mix, 0.8 μ l of 1:10 diluted cDNA, and nuclease-free water. All TaqMan PCR reactions were prepared and aliquoted using a custom method on a Beckman Coulter Biomek FX automated pipettor. PCR reaction conditions were run under the Standard protocol without the 50°C incubation using version 2.3 of the SDS software, with reactions incubated at 95°C for 10 min, followed by 40 cycles of 95°C for 15 sec, and 60°C for 1 min. Relative quantities (RQ) of miRNA were determined using the $\Delta\Delta$ Ct method (Livak and Schmittgen 2001). RQ values and the associated error were determined using Applied Biosystems SDS v1.2 RQ manager to calculate mean RQ and RQ min/max values based on a 95% confidence interval. All paired samples were incorporated into a single analysis within the SDS v1.2 RQ manager to obtain the reported values. Reverse transcription primer pool-specific endogenous controls were chosen based on miRNA with the least variable expression among all samples tested. All relative quantity calculations were calibrated to WT samples.

Individual reverse transcription and TaqMan microRNA assays were performed on an Applied Biosystems 7500 Fast Instrument. The 15- μ l reverse transcription reactions consisted of 10 ng total RNA isolated with TRIzol (Invitrogen, 15596-026), 5 U MultiScribe Reverse Transcriptase, 0.5 mM each dNTP, 1X Reverse Transcription Buffer, 4 U RNase Inhibitor, and nuclease-free water. Reverse transcription reactions were incubated at 16°C for 30 min, 42°C for 30 min, and 85°C for 5 min, and then stored at 4°C until use in TaqMan assays. The 10- μ l TaqMan

real-time PCR reactions consisted of 1X TaqMan Universal PCR Master Mix, No AmpErase UNG, 1X TaqMan miRNA assay, 1.33 μ l of undiluted cDNA, and nuclease-free water. Each TaqMan assay was done in either triplicate or quadruplicate for each sample tested. Relative quantities were calculated using the $\Delta\Delta$ Ct method with RNU6B TaqMan miRNA control assay as the endogenous control and calibrated to the WT samples (Livak and Schmittgen 2001). Reactions were run with the Standard 7500 default cycling protocol without the 50°C incubation stage using the SDS 7500 Fast Real-Time PCR System Software version 1.3.1, with reactions incubated at 95°C for 10 min, followed by 40 cycles of 95°C for 15 sec, and 60°C for 1 min. Fluorescence readings were taken during the 60°C step.

Primary/precursor miR-137 was detected by polyadenylating total RNA, using an SuperScript III oligo-dT reverse transcription to generate first-strand cDNA and real-time PCR targeting the pri-/pre-miR-137. Polyadenylation and reverse transcription were done according to the manufacturer's protocol using the Ncode miRNA First-Strand cDNA Synthesis Kit (Invitrogen Cat. # MIRC-10), with 1 μ g total RNA isolated with TRIzol as input. Relative quantification was done by real-time PCR using 1:10 diluted cDNA, 1X Power SYBR Green Master Mix, 0.5 μ M forward (5'-GTGACGGGTATTCTTGGGT) and reverse primers (Universal qPCR primer provided with kit), and nuclease-free water. 18S rRNA was used as an endogenous control for all samples. Reactions were run in triplicate on four samples per genotype using an Applied Biosystems SDS 7500 Fast Instrument Standard 7500 default cycling

protocol and SDS 7500 Fast System Software version 1.3.1 without the 50°C incubation.

Chromatin immunoprecipitation

ChIP was performed according to a previously published method (Coffee, Zhang et al. 1999). Briefly, cells grown on 3 to 6 confluent 10-cm cell culture plates were fixed by 1% formaldehyde (Sigma-Aldrich) to culture medium for 10 min at room temperature. After washing with cold PBS, cells were collected with cold PBS, washed, and suspended in 1 ml cold cell lysis buffer (5 mM PIPES, pH 8.0, 85 mM KCl, 0.5% NP40, and 1X Complete Proteinase Inhibitor (Roche)), and incubated on ice for 5 min. Cell lysates were pelleted by centrifugation at 3000 rpm for 5 min, resuspended again in 1 ml of cold cell lysis buffer for 5 min on ice, and then repelleted to collect nuclei. Nuclei were lysed at room temperature with 500 µl of nuclei lysis buffer (50 mM Tris pH 8.1, 10 mM EDTA, 1% SDS, and 1X Complete Protease Inhibitor). Nuclear lysates were sonicated using a Misonix 3000 Sonicator. The size of the sonicated chromatin (average size of ~500-600 bp) was verified by treating 5-µl aliquots with 1 µl 20 mg/ml proteinase A for 20 min at 50°C and running on a 1.5% agarose gel stained with ethidium bromide. For immunoprecipitation reactions we used 50 µl of sonicated chromatin, precleared with salmon sperm/tRNA-blocked protein A agarose for 60 min at 4°C in 950 µl IP dilution buffer (0.01% SDS, 1.1% Triton X-100, 1.2 mM EDTA, 20 mM Tris pH 8.1, 500 mM NaCl). Precleared chromatin was rotated at 4°C overnight with 10 µg of the appropriate antibody.

Antibodies: Normal rabbit IgG (Upstate, Cat# 12-370), rabbit polyclonal to MeCP2 (ChIP Grade, Abcam ab2828), rabbit anti-Sox2 (Chemicon International, AB5603), rabbit polyclonal to H3 (tri-methyl K4) (ChIP Grade, Abcam ab8580), anti-acetyl-histone-H3 (Lys9) (Upstate, Cat. #07-352), anti-monomethyl-histone H3 (Lys4) (Millipore, Cat. #07-436), rabbit polyclonal to H3 (tri-methyl K9) (ChIP Grade, Abcam ab8898), Anti-trimethyl-Histone-H3 (Lys27) (Millipore, Cat#07-449).

Antibodies were pulled down with 60- μ l blocked protein A agarose beads for 1 h at 4°C with rotation. The beads were washed sequentially 2 times each in IP dilution buffer, TSE-500 solution (0.1% SDS, 1% Triton X-100, 2 mM EDTA, 20 mM Tris pH 8.1, 500 mM NaCl), freshly prepared Li/Cl wash solution (100 mM Tris pH 8.1, 300 mM LiCl, 1% NP40, 1% deoxycholic acid), and 1X TE for 10 min at 4°C. Protein-DNA complexes were eluted from the protein A agarose beads twice with 250 μ l of IP elution buffer (50 mM NaHCO₃, 1% SDS) for 15 min at 37°C with rotation. Formaldehyde-induced protein-DNA crosslinking was heat reversed by incubating protein-DNA complex at 65°C overnight. DNA was purified using phenol:chloroform:isoamyl alcohol (25:25:1) isolations and precipitated with 2 volumes 100% ethanol and 10 μ g linear acrylamide at -35°C overnight. Immunoprecipitated and purified DNA fragments were resuspended in nuclease-free water, concentrations were determined by NanoDrop, and each sample was diluted to 1 ng/ μ l. We used 8 ng DNA in 20- μ l SYBR Green real-time PCR reactions consisting of 1X Power SYBR Green Master Mix and 0.5 μ M forward and reverse

primers. Reactions were run on an Applied Biosystems SDS 7500 Fast Instrument using the Standard 7500 default cycling protocol and SDS 7500 Fast System Software version 1.3.1 without the 50°C incubation. Primer sequences spaced at 1-kb intervals spanning from 4.5 kb upstream to 1.5 kb downstream of mmu-miR-137 were designed using Applied Biosystems' Primer Express 3.0 software and were: 4.5 kb upstream: FW-5'-ACATTGCCATATCACTCCTATCAAAT, RV-5'-CCCTCCTCCCACCCATACA; 3.5 kb upstream: FW-5'-TCCCTTCCCAGGGCTTGT, RV-5'-GGAGCCGCTGCTCTCTGA; 2.5 kb upstream: FW-5'-AGCTTAAGGAGGTTTGAATTGAATATG, RV-5'-CTTACGAGAACACCATTTCTACGA; 1.5 kb upstream: FW-5'-GGAATTCATGTTGGTTTTTCTACTTG, RV-5'-CACTTCTCCAGGTAGACCAACTCA; 0.5 kb upstream: FW-5'-AAAGCACTTGTCTGTTGTGTGTTAAGT, RV-5'-TGGCTGTTCTATTTCCAATTCTGA; 0.5 kb downstream: FW-5'-GCCGAGCTGCTCAGCAA, RV-5'-CCCCGCCCTTCCTTAG; 1.5 kb downstream: FW-5'-TGCCTTGAAGAGCAAGCTGAA, RV-5'-AAGGCTGTTTTTCCAGGGTTCT.

DNA relative enrichment was determined by taking the absolute quantity ratios of specific immunoprecipitations to nonspecific immunoprecipitations (normal rabbit IgG only), IP/IgG, and normalizing to a control genomic region was not enriched in specific immunoprecipitations relative to nonspecific immunoprecipitations. Absolute quantification was based upon standard curves generated from 4 10-fold dilutions ranging from 0.08-80 ng input DNA treated in parallel with immunoprecipitated DNA during reverse crosslinking and purification steps. For

histone ChIP experiments, quantity was determined based upon input DNA-generated standard curves and reported directly for both specific and IgG nonspecific immunoprecipitations. All ChIP experiments were from 3 independent chromatin preparations, and all real-time PCR reactions were carried out in triplicate for each sample on each amplicon. All primer sets were subjected to a dissociation curve analysis and produced single peaks on a derivative plot of raw fluorescence.

5'-methyl-cytosine immunoprecipitation (MeDIP)

MeDIP was performed as previously described (Weber, Davies et al. 2005). 4 µg of sheared input DNA isolated during histone-specific ChIP experiments was diluted into 450 µL 1X TE. DNA was denatured for 10 min at 100°C in a dry heat block, and then immediately placed on ice for 5-10 min. 51 µL of 10X IP Buffer (100 mM Na-phosphate pH7.0 made from a 1M stock solution (2M monobasic sodium phosphate, 2M dibasic sodium phosphate at 1:1.564 ratio, and equal volume H₂O), 1.4M NaCl, and 0.5% Triton-X100 was added along with 10 µg 5-methylcytidine antibody (Eurogentec #BI-MECY-0500) or 10 µg of normal mouse IgG (Upstate, Cat. #12-371). IP was done at 4°C with rotation for 2 h. Antibody-DNA complexes were pulled down by adding 40 µL Dynabeads (M-280) Sheep anti-Mouse IgG (DynaL Biotech, Invitrogen, #112.01) directly to the IP reaction at 4°C for 2 h with rotation. Beads were collected with a 1.5-mL microfuge tube holder magnet and washed 3 times in 1X IP Buffer at room temperature, 10 min per wash with rotation. Washed beads

were collected by magnet and resuspended in 250 μ L Proteinase K Digestion Buffer (50 mM Tris, pH8.0, 10 mM EDTA, 0.5% SDS). 3.5 μ L of 20 mg/mL Proteinase K was added and digestion was performed at 50°C for 3 h in an Eppendorf Thermomixer set at 800 rpm. Beads were collected by magnet, and DNA was extracted from the supernatant 1X with phenol and 1X with chloroform. DNA was precipitated with 400 mM NaCl, 15 μ g linear acrylamide, and 2 volumes 100% ethanol at -35°C overnight. Precipitated DNA was resuspended in 11 μ L of nuclease free H₂O, and concentrations were determined by NanoDrop. Samples were diluted to 1 ng/ μ L, and 8 ng was used in a SYBR Green real-time PCR reaction identical to the one used for ChIP experiments, including primer pairs. In the case of the normal mouse IgG nonspecific immunoprecipitations, not enough DNA was immunoprecipitated from each of the three individual MeDIP experiments to assay all 7 genomic regions, and so DNA from all three experiments from both genotypes was pooled and diluted to 1 ng/ μ L. Quantities were determined against a non-immunoenriched input DNA-generated standard curve and reported directly for both specific and IgG nonspecific immunoprecipitations.

Immunoprecipitation

Whole cell lysates were prepared using the Nuclear Complex Co-IP Kit (Active Motif, Cat. #54001) according to the manufacturer's protocol. 1 mg of nuclear lysate was precleared with 60 μ L Anti-Rabbit IgG IP Beads (eBioscience Cat. # 00-8800). 5% of precleared nuclear lysate was used as input in western blot analysis. The remaining nuclear lysate was immunoprecipitated with No antibody (beads alone), 2.5 μ g of

specific antibody, or 2.5 µg Normal Rabbit IgG. IP antibodies used were identical to those used in ChIP experiments, including Normal Rabbit IgG. 80 µL of Anti-Rabbit Ig IP Beads were used to bind IP antibodies. IP incubations and IP washes were done using 1X IP Low Buffer. 50% of immunoprecipitated protein was used for western blot analysis. MeCP2 was detected by western blot using Anti-MeCP2 (Millipore/Upstate Cat. # 07-013) at a dilution of 1:1000. Sox2 was detected by western blot using Anti-Sox2 (Millipore/Chemicon Cat. # AB5603) at a dilution of 1:1000. Rabbit TrueBlot: Horseradish Peroxidase (HRP) anti-rabbit IgG (eBioscience Cat. # 18-8816) was used as the secondary antibody at a dilution of 1:1000. Detection of HRP was performed using ECL Western Blotting Detection Reagents (GE Healthcare Cat #RPN2106).

ShRNA expression constructs

PCR-based generation of the miR-137 shRNA driven by a U6 Pol III promoter was done using a PCR-shagging approach as previously described (Paddison, Caudy et al. 2002) with the following PAGE-purified long oligos:

shRNA miR-137 (sh-miR-137):

5'-TATCGATAAAAAAATTATTGCTTAAGAATACGCGTAGTCT
CTTGAACACTACGCGTATTCTTAAGCAATAAAAACAAGGCTTTT
CTCCAAGGGA-3'

shRNA control (sh-Control):

5'-TATCGATAAAAAAATTCTCCGAACGTGTCACGTTCTCTTG
AAACGTGACACGTTCCGAGAATTAACAAGGCTTTTCTCAA
GGGA-3'

Long oligos were used as reverse primers in combination with a common forward primer complementary to the 5' end of the U6 promoter (5'-AAAGTTAACTAGTGGATCCGACGCCGCATCTC-3') to amplify the entire U6 promoter and shRNA in a single PCR product. Amplification was done using 20 ng of a previously generated U6-shRNA lentiviral construct (a gift from Dr FH Gage of the Salk Institute) with Applied Biosystems AmpliTaq Gold PCR (1X PCR buffer, 2.2 mM MgCl₂, 0.2 mM dNTP mix, 0.2 mM forward primer, 0.2 mM reverse primer, 1.75 U AmpliTaq Gold) at 95°C for 9 min, 40 cycles of 94°C for 1 min and 60°C for 1 min, followed by 60°C for 10 min, and then storage at 4°C. We used 2 µl of PCR product in a TOPO TA cloning reaction with pCR2.1 vector and chemical transformation of TOP-10 competent cells (Invitrogen, K4500-01SC). U6-shRNA expression cassettes were removed from the TOPO vector and transferred to lentiviral and retroviral vectors by HpaI and ClaI restriction digestion followed by ligation. The lentiviral vectors expressing miR-137 or control shRNA were then verified by sequencing.

Production of recombinant lentivirus, differentiation and proliferation of lentivirus-infected NSCs

We produced lentivirus as described previously (Barkho, Song et al. 2006). Briefly, lentiviral transfer vector DNA and packaging plasmid DNA were transfected into cultured 293T cells using calcium phosphate methods. The medium containing lentivirus was collected at 40, 64, and 88 h post-transfection, then pooled, filtered through a 0.2-µm filter, and concentrated using an ultracentrifuge at 19.4k rpm for 2 h at 20°C using a SW27 Rotor (Beckman). The virus was washed once and then

resuspended in 500 μ l phosphate-buffered saline. We routinely obtained $0.5-1 \times 10^9$ infectious viral particles/ml. To study the effects of miR-137 on the proliferation and differentiation of NSCs, $\sim 60 \mu$ l of lentivirus was added to the WT NSCs cultured under proliferating conditions on a 10-cm tissue culture plate. After a 3-day incubation, infected NSCs were either collected for RNA analysis or trypsinized and plated into chamber slides (Nalge Nunc, #154526) at a density of $5-7 \times 10^4$ cells/well for differentiation or proliferation analyses. To assess the effects of miR-137 on cell survival, an anti-caspase 3 (active) antibody (AB3623, Millipore) was used for immunostaining.

In vitro NSC proliferation and differentiation assays were performed as described (Zhao, Ueba et al. 2003; Barkho, Song et al. 2006). To assay proliferation, at 6-8 h post-plating, 5 μ M bromodeoxyuridine (BrdU, Sigma-Aldrich) was added to the cells, incubated for 16 h, fixed with 4% paraformaldehyde for 30 min, and followed by immunohistochemical analysis. To detect BrdU incorporation, cells were pretreated with 1M HCl for 30 min at 37°C followed by washing with borate buffer, pH 8.5, for 30 min, before being subjected to a standard immunohistochemistry protocol. For the differentiation assay, at 24-h post-plating, cells were transferred into differentiation medium, DMEM/F12 (1:1), containing 5 μ M forskolin (Sigma-Aldrich, #F-6886) and 1 μ M retinoic acid (Sigma-Aldrich, #R-2625), and incubated for 4 days, followed by fixation with 4% paraformaldehyde for 30 min and washing with Dulbecco's phosphorylated buffered saline pH 7.4 (DPBS) for 30 min. Immunocytochemistry staining was as described (Zhao, Ueba et al. 2003). Briefly,

cells were first preblocked using DPBS containing 5% normal goat serum (VECTOR, #S-1000) and 0.1% Triton X-100 for 30 min, followed by overnight incubation with primary antibodies: mouse neuron-specific type III-tubulin (Tuj1, 1:4000, Promega, #G712A), rabbit glial fibrillary acidic protein (GFAP, 1:1000, DAKO, #Z-0334), rat anti-BrdU (1:3000, Abcam, ab-6326), chicken anti-GFP (1:500, Invitrogen, #A10262), rabbit anti-GFP (1:1000, Invitrogen, #A11122) or rabbit anti-total Mecp2 antibody (1:1000) previously published (Zhou, Hong et al. 2006). After washing with DPBS, cells were incubated with secondary antibodies that included goat anti-mouse Alexa Fluor 568 (1:500, Invitrogen, #A11031), goat anti-rabbit Alexa Fluor 647 (1:500, Invitrogen, #A21245), goat anti-rat Alexa Fluor 568 (1:500, Invitrogen, #A11077), goat anti-rabbit Alexa Fluor 488 (1:500, Invitrogen, #A11008), and goat anti-chicken Alexa Fluor 488 (1:500, Invitrogen, #A11039), followed by counterstaining with the fluorescent nuclear dye DAPI (Sigma-Aldrich, #B2261). After the cells were mounted with VECTASHIELD (VECTOR, #H-1000), the numbers of double positive cells (GFP⁺Tuj1⁺, GFP⁺GFAP⁺, and GFP⁺BrdU⁺) were quantified using an Olympus BX51 microscope equipped with a MicroFire digital camera (Optronics) and a motorized stage. The quantification was carried out using unbiased stereology with the aid of StereoInvestigator software (MicroBrightField). The data were analyzed using a two-tailed unpaired t-test.

To block the activity of endogenous miR-137, WT NSCs were plated onto coated coverslips in a 24-well plate. Anti-miR-Control or anti-miR-137 were transfected at a final concentration of 0.5 mM with FuGENE HD transfection reagent (Roche).

Twenty-four hours post-transfection, cells were treated with 5 mM of BrdU for 3 h or cultured with differentiation medium for 3 days. *MeCP2*^{-/-} NSCs were plated into 6-well plates and transfected with anti-miR-control or anti-miR-137 at a final concentration of 0.5 mM and collected 24 h later for analysis of Ezh2 expression by western blot.

For Ezh2 rescue studies, WT NSCs were infected with lentivirus expressing sh-control+lentivirus expressing GFP as the control treatment or lentivirus expressing sh-miR-137+lentivirus expressing Ezh2. The infected cells were collected and plated onto coated coverslips for proliferation or differentiation assays.

Electroporation and luciferase assay

miR-137, anti-miR-137, and controls were purchased from Ambion (AM17100, AM17110, AM17000, and AM17010). NeuroD1-luciferase DNA, GFAP-luciferase, and internal control E1 α -Rluc DNA plasmids were described previously (Barkho, Song et al. 2006). Ezh2 and EphA7 expression plasmids were purchased from Open Biosystems. Electroporation of these RNA and DNA into aNSCs was carried out using a Nucleofector electroporator based on the manufacturer's protocol (Amaza, #VPG-1004). Briefly, 2 X 10⁶ cells were trypsinized, resuspended in Nucleofector Solution, mixed with DNA and miRNAs, and electroporated using a preset program for mouse NSCs (#A033). The cells were then plated onto polyornithin/laminin-coated 24-well plates in NSC proliferation medium (see above). At 24-h post-plating, cells were transferred into differentiation medium (see above) for 24 h. The cells were then

collected using cell lysis buffer from a Dual-Luciferase Reporter Assay System kit (Promega, #E1910). Luciferase activity was measured using a Veritas Microplate Luminometer (Turner Biosystems) as described (Barkho, Song et al. 2006). The luciferase counts were then normalized to R-Luc counts to obtain final NeuroD1 or GFAP promoter activities.

Construction of retroviral vector expressing sh-miR-137 and in vivo retroviral grafting

Retroviral vector expressing both miR-137 and eGFP was engineered by deleting the original HpaI and ClaI sites in the CAG-EGFP vector (Zhao, Teng et al. 2006; Smrt, Eaves-Egenes et al. 2007) and inserting new HpaI and ClaI sites 5'-upstream from the CAG promoter. The U6-shRNA cassettes were then inserted between the HpaI and ClaI sites.

Retrovirus production was performed as described previously (Zhao, Teng et al. 2006; Smrt, Eaves-Egenes et al. 2007). Briefly, retroviral transfer vector DNA and packaging plasmid DNA were cotransfected with the packaging plasmids pCMV-gag-pol and pCMV-Vsvg into HEK293T cells using the calcium phosphate method. The medium containing retrovirus was collected at 40, 64, and 88 h post-transfection, then pooled, filtered through a 0.2- μ m filter, and concentrated via ultracentrifugation at 19.4k rpm for 2 h at 20°C (Beckman SW27 Rotor). The virus was washed once with PBS and then resuspended in 150 μ l PBS. We routinely obtain greater than $0.5-1 \times 10^9$ infectious viral particles/ml.

In vivo retroviral grafting was performed as described (Zhao, Teng et al. 2006; Smrt, Eaves-Egenes et al. 2007). Briefly, 7- to 8-week-old C57B/L6 male mice were anesthetized with isofluorane, and virus (1.5 μ l with titer greater than $5 \times 10^5/\mu$ l) was injected stereotaxically into the dorsal ganglia (DG) using the following coordinates relative to bregma: anteroposterior, $-(1/2) \times d$ mm; lateral, ± 1.8 mm (if $d > 1.6$) or otherwise ± 1.7 mm; ventral, -1.9 mm (from dura). For each mouse, the sh-Control virus was injected into the left DG, and the miR-137 virus was injected into the right DG. Mice received 2 BrdU injections per day (50 mg/kg, i.p.) for a total of 7 injections, immediately following viral grafting. One week after viral grafting, mice were deeply anesthetized with pentobarbital and perfused with saline followed by 4% PFA. Brains were dissected out, post-fixed overnight in 4% PFA, and then equilibrated in 30% sucrose. Forty-micrometer brain sections were generated using a sliding microtome and were stored in a -20°C freezer as floating sections in 96-well plates filled with cryoprotectant solution (glycerol, ethylene glycol, and 0.2 M phosphate buffer, pH 7.4, 1:1:2 by volume).

Immunohistochemistry and confocal imaging analysis were carried out as described (Smrt, Eaves-Egenes et al. 2007). Floating brain sections containing eGFP⁺ cells were selected for staining and matched by DG region. Sections were pretreated with 1M HCl, as described in a previous study (Tang, Falls et al. 2007). The primary antibodies used were chicken anti-GFP (Invitrogen, #A10262), rat anti-BrdU (Abcam, ab-6326), and rabbit anti-doublecortin (DCX, Cell Signaling, #4604). The secondary antibodies used were anti-chicken Alexa Fluor 488 (Invitrogen,

#A11039), goat anti-rat Alexa Fluor 647 (Invitrogen, #A21242), and goat anti-rabbit Alexa Fluor 568 (Invitrogen, #A11036). The Z-stack images of GFP-BrdU-DCX staining were taken at 1- μ m resolution using a Nikon TE2000 equipped with a spin disc confocal microscope with an oil-immersion objective lens (40 \times ; NA = 1.3; Zeiss) and MetaMorph quantification software; we then counted the proportion of GFP+DCX+ or GFP+BrdU+ out of total GFP+ cells. For co-localization analysis, roughly 70 GFP+ cells per animal were imaged. The data were analyzed using Student's t-test.

3'-UTR dual luciferase assays of candidate miR-137 target mRNA

3'-UTR sequences of candidate mRNAs were PCR-amplified directly from proliferating aNSC first strand cDNA generated from 5 μ g of TRIZOL-isolated total RNA using oligo-dT SuperScript III reverse transcription according to the manufacturer's protocol (Invitrogen, Cat. #1808-093). These primer sequences are available upon request. All primers were designed incorporating XhoI and NotI restriction sites and 4 bp of extra random sequence to aid in restricting digestion. XhoI- and NotI-digested PCR products were cloned into XhoI- and NotI-digested psiCHECK-2 dual luciferase vector (Promega, Cat# C8021). As a primary screen of candidate miR-137 targets, 293FT cells (3×10^3 cells/well, 96-well plate, grown overnight prior to transfection) were transfected with sh-miR-137 cloned into a pCR2.1 TOPO vector (sh-miR-137 TOPO) and psiCHECK-2-3'UTR using TransFast Transfection Reagent (Promega, Cat#E2431) according to the manufacturer's protocol. As a control, psiCHECK-2 plasmid with no 3'-UTR and U6-neg-shRNA were

cotransfected with U6-mir-137-shRNA TOPO or psiCHECK-2-3'-UTR, respectively. All transfections used a total of 1 µg of plasmid DNA. The ratio of luciferase-3'UTR:shRNA plasmid was 1:2 for all experiments. Luciferase expression was detected using the Dual-Luciferase Reporter 1000 System (Promega, Cat# E1980) per the manufacturer's protocol. 48 h after transfection hRLuc activity was normalized to hLuc+ activity to account for variation in transfection efficiencies, and miR-137-mediated knockdown of hRLuc activity was calculated as the ratio of normalized hRLuc activity in the U6-miR-137-shRNA treatments to normalized hRLuc activity in the U6-neg-shRNA treatments. All luciferase readings were taken from either 3 or 4 individual wells for each psiCHECK-2-3'-UTR construct and control construct tested. Each transfection experiment was repeated at least 3 times.

The miR-137 target site in the Ezh2 3'-UTR was deleted using the QuickChange Site-Directed Mutagenesis Kit (Stratagene, Cat. #2000518) to delete 5 bases (AAUAA) from the 7mer-1a miR-137 seed site in the Ezh2 3'-UTR luciferase reporter. Target site deletion was verified by Sanger sequencing.

To confirm the specificity of miR-137 targeting the Ezh2 3'-UTR, the Ezh2 3'-UTR and Ezh2 3'-UTR^{ΔmiR-137} were transferred by XhoI/NotI double digestion and T4 DNA ligation from psiCHECK2 into a pIS2 renilla luciferase vector modified with the addition of an XhoI restriction site and deletion of the SpeI restriction site. MiR-137-dependent Ezh2 3'-UTR luciferase assays were performed as previously described

using 10 pmol of miR-137 duplex RNA or control miRNA duplex and Promega Dual Luciferase Reporter System and pIS0 firefly luciferase as a control (Yekta, Shih et al. 2004). To test whether Ezh2 knockdown modulates NSCs differentiation, Ezh2 shRNA plasmid was electroporated into WT NSCs along with NeuroD1-luciferase DNA and internal control E1 α -Rluc DNA plasmids. Both Ezh2 mRNA and NeuroD1-luciferase activity were determined after 24-hour differentiation as described above.

Western blot analyses

Protein samples were separated on SDS-PAGE gels and then transferred to PVDF membranes (Millipore). Membranes were processed following the ECL Western Blotting Protocol (GE Healthcare, Cat #RPN2106). Anti-MeCP2 (Abcam, ab2828), Anti-Ezh2 (Cell Signaling #4905), Anti-Tri-Methyl-Histone H3 (Lys27) (C36B11) (Cell Signaling #9733), and Anti-Histone H4 (Abcam ab10158) were used as primary antibodies at a 1:1000 dilution. HRP-labeled secondary antibodies were obtained from Sigma (A0545) and were used at a dilution of 1:5000. For loading controls, membranes were stripped and reprobed with the antibody against GAPDH (Ambion AM4300). All Western blot quantifications were done using ImageJ software from NIH.

Real-time PCR relative quantification of Ezh2 mRNA

500 ng of total RNA isolated by TRIzol (Invitrogen, 15596-026) from lentiviral sh-miR-137 and lentiviral sh-control-infected aNSCs was reverse transcribed using

random hexamers to generate first strand cDNA with SuperScript III (Invitrogen) according to the manufacturer's protocol. 1 μ L cDNA was used directly in 20 μ L SYBR Green real-time PCR reactions that consisted of 1X Power SYBR Green Master Mix, 0.5 μ M forward and reverse primers, and nuclease-free water. 18S rRNA was used as an endogenous control for all samples, with 1 μ L of cDNA diluted 1:10 in nuclease-free water used. Reactions were run on an Applied Biosystems SDS 7500 Fast Instrument using the Standard 7500 default cycling protocol and SDS 7500 Fast System Software version 1.3.1 without the 50°C incubation primers for Ezh2 mRNA and 18S rRNA were designed using Applied Biosystems Primer Express 3.0 software and were: Ezh2, FW-5'- GGTGAAGAGTTGTTTTTTGATTACAGA, RV-5'- TCTCGTTCGATGCCACATA, 18S, FW-5'- CGGCTACCACATCCAAGGAA, RV-5'- CCTGTATTGTTATTTTTCGTCACTACCT. All real-time PCR reactions were performed in triplicate, and relative quantities were calculated using the $\Delta\Delta$ Ct method (95% confidence level) with calibration to sh-control-treated samples. All primer sets were subjected to a dissociation curve analysis and produced single peaks on a derivative plot of raw fluorescence.

Supplemental Figures

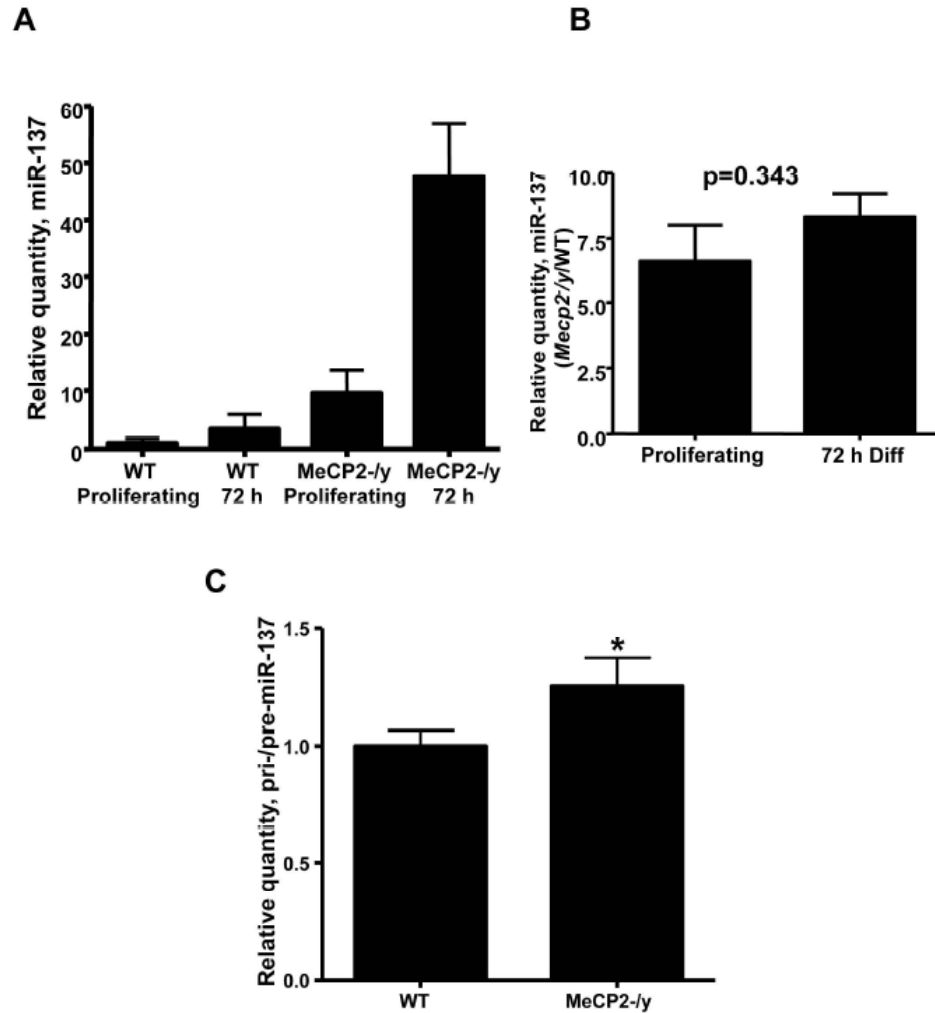


Figure S1. miR-137 and primary/precursor miR-137 expression in aNSCs. **A.** miR-137 expression is significantly increased after 72 h differentiation of both WT and *Mecp2*^{-/y} aNSCs (n ≥3, mean with 95%CI). **B.** The relative increase of miR-137 expression in *Mecp2*^{-/y} cells is no different in proliferating and differentiated aNSCs (n ≥3, mean ± SEM, p = 0.343, unpaired t-test). **C.** Pri-/pre- miR-137 is increased 1.25-fold in *Mecp2*^{-/y} proliferating aNSCs relative to WT proliferating aNSCs (n=4, mean with 95%CI).

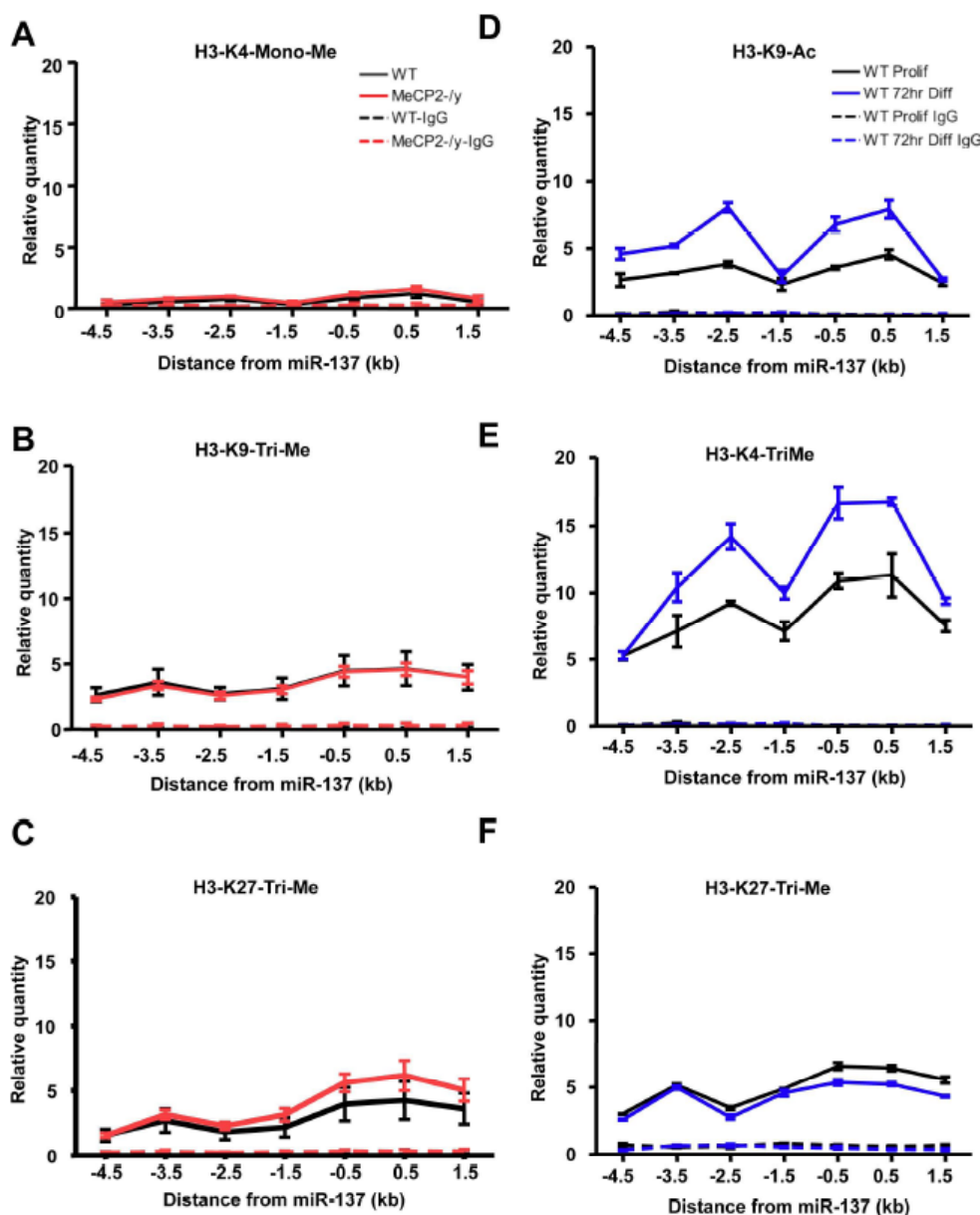


Figure S2. Determination of the epigenetic state of the miR-137 genomic locus using additional histone ChIP assays. **A.** H3-K4-Mono-Me is not enriched at the miR-137 genomic locus in either WT or *Mecp2*^{-/-} cells. **B.** H3-K9-Tri-Me is not enriched at the miR-137 genomic locus in either WT or *Mecp2*^{-/-} cells. **C.** H3-K27-Tri-Me is enriched in the 3 kb surrounding miR-137, but is not significantly different between genotypes. (All histone ChIP experiments; n = 3, mean ± SEM, quantities calculated from an input DNA-generated standard curve. Quantities in IgG-only nonspecific IP control experiments in e-g are near 0). **D.** H3-K4-Tri-Me is enriched at the miR-137 genomic locus upon differentiation (72 h) of WT aNSCs, similar to what is seen in *Mecp2*^{-/-} proliferating cells. **E.** H3-K9-Ac is enriched at the miR-137 genomic locus upon differentiation (72 h) of WT aNSCs, similar to what is seen in *Mecp2*^{-/-} proliferating cells. **F.** H3-K27-Tri-Me is enriched in the 3 kb surrounding miR-137 and is decreased slightly upon differentiation (72 h) of WT aNSCs. (All histone ChIP experiments; mean ± SEM relative quantity, quantities calculated from an input DNA-generated standard curve. Quantities in IgG-only nonspecific IP control experiments in e-g are near 0. Representative experiments are shown).

A Lentiviral vector:

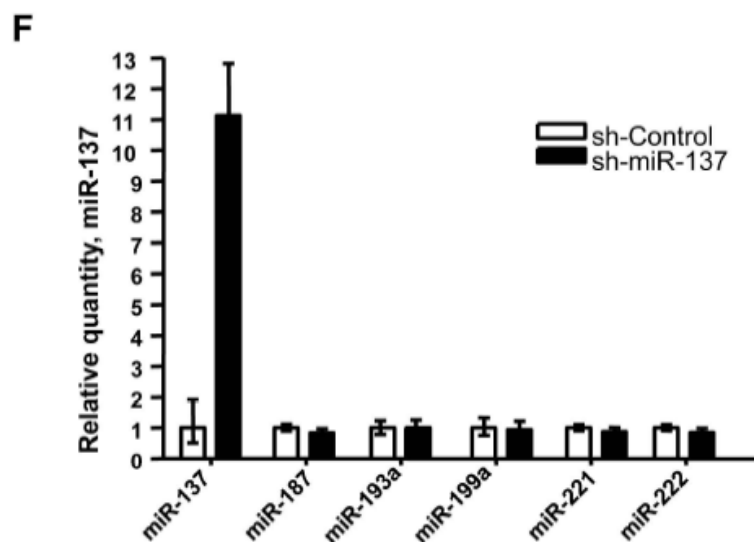
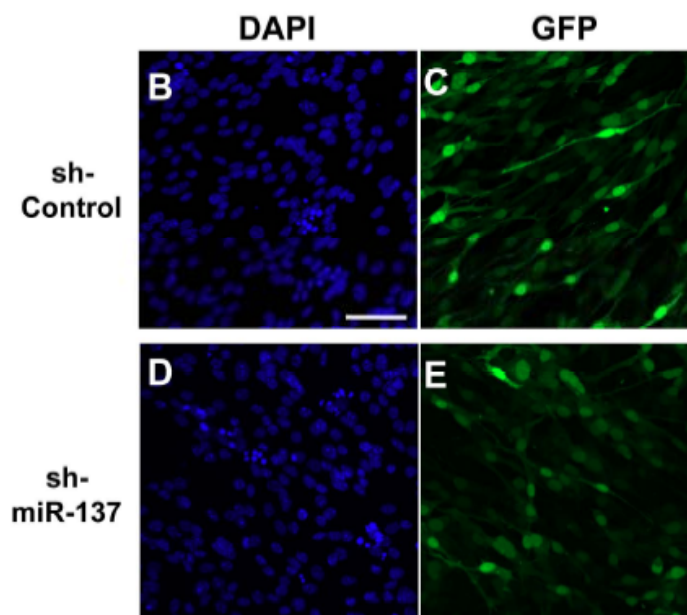
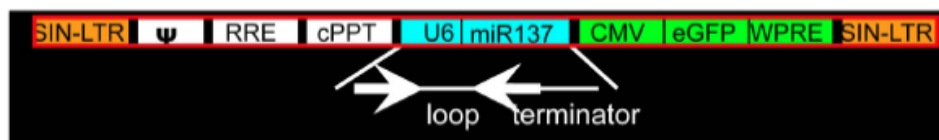


Figure S3. Efficient delivery of control and miR-137 short-hairpin RNA constructs by lentivirus. **A.** Schematic drawing of the third generation lentiviral constructs used in this study. **B-C,** aNSCs infected by lentivirus expressing sh-Control. **D-E,** aNSCs infected by lentivirus expressing sh-miR-137. Blue: DAPI nuclear staining. Green: GFP. **F.** Relative miRNA expression, calibrated to sh-Control lentivirus-treated cells, in proliferating aNSCs treated with a lentivirus expressing sh-miR-137. miRNA expression was tested in 2 independent experiments. Mean relative quantity with 95% CI is indicated.

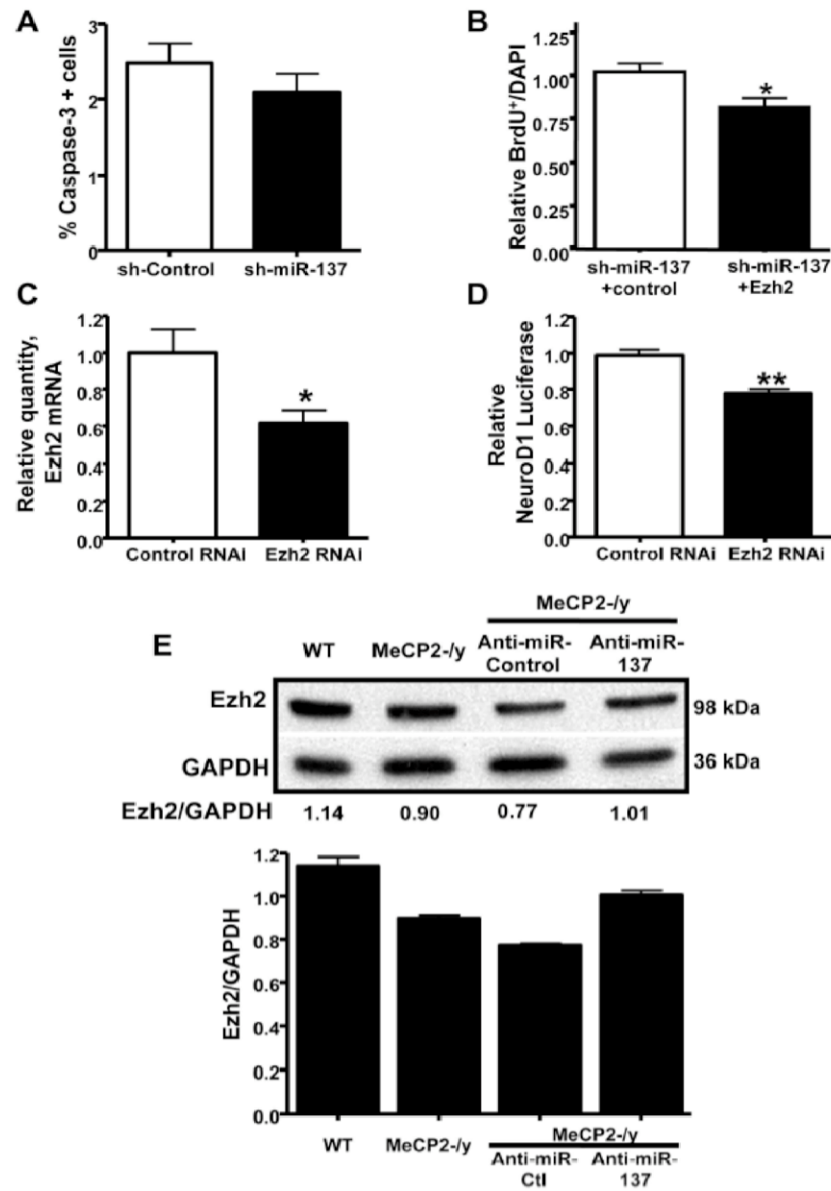


Figure S4. Verification of a functional interaction between miR-137 and Ezh2. **A.** Overexpression of miR-137 does not induce apoptosis in aNSCs. Proliferating aNSCs were treated with sh-Control or sh-miR-137 expressing lentivirus. Cells were immunostained for activated Caspase-3 as a marker of apoptosis. Quantitative analysis by stereology was used to determine the percentage of activated Caspase-3+ cells among GFP+ (lentiviral infected) cells ($p=0.3142$, unpaired t-test, $n=4$). **B.** Expression of Ezh2 could suppress increased proliferation of aNSCs caused by overexpression of miR-137. Cell proliferation was analyzed using BrdU pulse-labeling. Quantitative analysis by stereology was performed (* $p = 0.0364$, unpaired t-test, $n = 3$). **C&D.** Direct Ezh2 knockdown mimics sh-miR-137 treatment in aNSCs. **C.** Endogenous Ezh2 mRNA was targeted by an Ezh2 specific short-hairpin RNA (Ezh2 RNAi). Ezh2 mRNA was reduced 39% relative to cells treated with a control, non-specific short-hairpin RNA (Control RNAi), (Mean relative quantity with 95%CI). **D.** NeuroD1 promoter luciferase activity was reduced 23% in cells in which Ezh2 mRNA was reduced 39% relative to control treated cells ($p=0.0018$, unpaired t-test, $n=4$). **E.** Recovery of Ezh2 protein expression in *Mecp2-/-* aNSCs to levels similar in WT aNSCs using anti-miR-137. Western blot of Ezh2 in WT and *Mecp2-/-* aNSCs compared with *Mecp2-/-* aNSCs treated with either anti-miR-137 or a control anti-miR. Ezh2 levels are normalized to GAPDH expression ($n=3$, mean \pm SEM). Images are quantified with ImageJ software and are representative of multiple repeats.

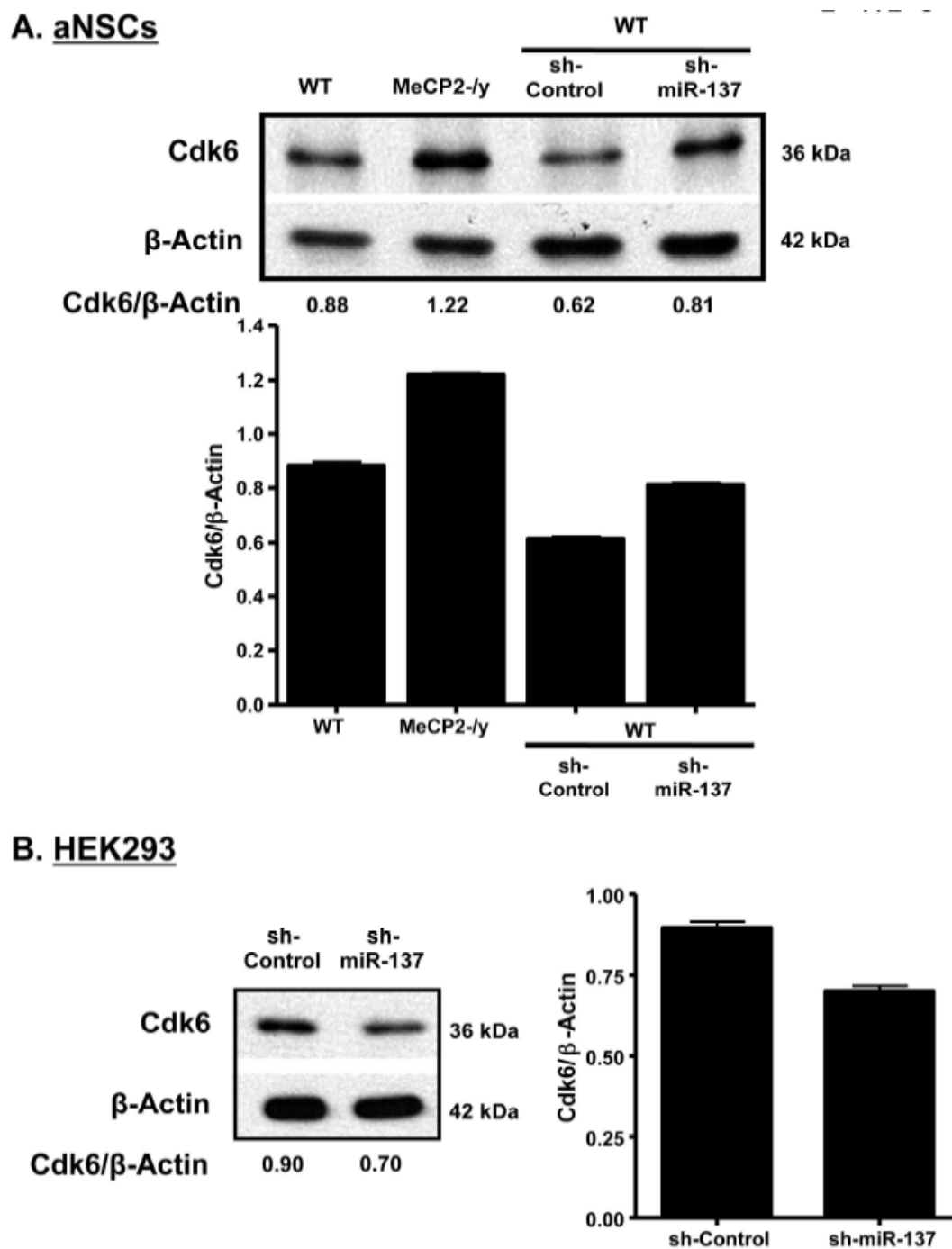


Figure S5. miR-137 has distinct effects on the expression of CDK6 in different cell types. A. Overexpression of miR-137 in WT aNSCs led to increased expression of CDK6 protein (n=3, mean \pm SEM). **B.** Overexpression of miR-137 in HEK293 cells repressed the expression of CDK6 protein (n=3, mean \pm SEM). Images are quantified with ImageJ software and are representative of multiple repeats.

Chapter 2 - Supplemental Table I

aNSC miRNA Profile

48-Plex Reverse Transcription Pool 1

Endogenous Control: miR-362

Sample	Detector	Avg Delta Ct	Delta Ct SD	RQ	RQ Min	RQ Max
MeCP2-/y	miR-10a	1.146	0.054	0.735	0.679	0.795
WT	miR-10a	0.701	0.055	1	0.922	1.084
MeCP2-/y	miR-124a	10.881	0.28	1.106	0.728	1.683
WT	miR-124a	11.027	0.235	1	0.703	1.422
MeCP2-/y	miR-125a	7.644	0.3	1.877	1.202	2.929
WT	miR-125a	8.553	0.214	1	0.729	1.371
MeCP2-/y	miR-141	9.216	0.153	0.64	0.51	0.803
WT	miR-141	8.572	0.126	1	0.829	1.206
MeCP2-/y	miR-15b	-0.092	0.056	0.95	0.875	1.031
WT	miR-15b	-0.166	0.037	1	0.947	1.056
MeCP2-/y	miR-181b	-1.445	0.046	1.26	1.178	1.349
WT	miR-181b	-1.112	0.037	1	0.946	1.057
MeCP2-/y	miR-181d	0.619	0.049	1.439	1.338	1.548
WT	miR-181d	1.145	0.04	1	0.942	1.061
MeCP2-/y	miR-197	8.921	0.343	0.34	0.204	0.566
WT	miR-197	7.365	0.113	1	0.845	1.183
MeCP2-/y	miR-199a	1.176	0.066	0.356	0.323	0.393
WT	miR-199a	-0.313	0.05	1	0.928	1.077
MeCP2-/y	miR-19a	1.057	0.049	0.997	0.927	1.073
WT	miR-19a	1.053	0.036	1	0.948	1.055
MeCP2-/y	miR-19b	1.54	0.056	0.601	0.553	0.653
WT	miR-19b	0.805	0.045	1	0.935	1.069
MeCP2-/y	miR-20b	-2.752	0.046	1.229	1.149	1.315
WT	miR-20b	-2.454	0.033	1	0.952	1.05
MeCP2-/y	miR-21	3.67	0.079	0.968	0.861	1.088
WT	miR-21	3.623	0.085	1	0.882	1.133
MeCP2-/y	miR-218	1.413	0.069	1.016	0.918	1.125
WT	miR-218	1.436	0.028	1	0.959	1.043
MeCP2-/y	miR-23bN	1.15	0.058	0.883	0.81	0.962
WT	miR-23bN	0.97	0.039	1	0.943	1.06
MeCP2-/y	miR-25	5.551	0.155	0.93	0.741	1.169
WT	miR-25	5.447	0.091	1	0.874	1.145
MeCP2-/y	miR-26b	1.982	0.057	0.654	0.601	0.712
WT	miR-26b	1.37	0.065	1	0.909	1.1
MeCP2-/y	miR-26bN	9.762	0.564	1.016	0.434	2.382
WT	miR-26bN	9.785	0.195	1	0.749	1.336
MeCP2-/y	miR-28	-2.664	0.044	0.868	0.813	0.926
WT	miR-28	-2.869	0.027	1	0.961	1.04
MeCP2-/y	miR-29a	-0.045	0.054	0.597	0.551	0.646
WT	miR-29a	-0.79	0.029	1	0.959	1.043
MeCP2-/y	miR-302a	11.334	0.129	0.759	0.624	0.922
WT	miR-302a	10.935	0.08	1	0.886	1.129
MeCP2-/y	miR-302a#	-0.175	0.056	1.01	0.929	1.098

WT	miR-302a#	-0.16	0.038	1	0.945	1.058
MeCP2- <i>ly</i>	miR-302c	11.483	0.073	0.694	0.622	0.774
WT	miR-302c	10.956	0.243	1	0.695	1.439
MeCP2- <i>ly</i>	miR-30a-3p	0.922	0.053	1.099	1.017	1.188
WT	miR-30a-3p	1.058	0.053	1	0.924	1.082
MeCP2- <i>ly</i>	miR-32	0.048	0.07	0.895	0.807	0.993
WT	miR-32	-0.111	0.028	1	0.959	1.043
MeCP2- <i>ly</i>	miR-320	-0.961	0.052	0.844	0.782	0.912
WT	miR-320	-1.205	0.037	1	0.947	1.056
MeCP2- <i>ly</i>	miR-330	-1.235	0.05	0.831	0.771	0.895
WT	miR-330	-1.503	0.031	1	0.955	1.048
MeCP2- <i>ly</i>	miR-337	3.966	0.086	0.897	0.791	1.019
WT	miR-337	3.809	0.074	1	0.897	1.115
MeCP2- <i>ly</i>	miR-345	0.985	0.051	0.54	0.501	0.582
WT	miR-345	0.095	0.038	1	0.946	1.057
MeCP2- <i>ly</i>	miR-34aN	7.473	0.409	0.387	0.21	0.714
WT	miR-34aN	6.103	0.4	1	0.552	1.811
MeCP2- <i>ly</i>	miR-34b	7.9	0.293	1.241	0.804	1.914
WT	miR-34b	8.212	0.333	1	0.611	1.637
MeCP2- <i>ly</i>	miR-380-5p	12.237	0.046	0.46	0.429	0.492
WT	miR-380-5p	11.115	0.27	1	0.668	1.497
MeCP2- <i>ly</i>	miR-99b	-2.198	0.044	0.781	0.732	0.833
WT	miR-99b	-2.555	0.031	1	0.956	1.046
MeCP2- <i>ly</i>	RNU6B	-0.358	0.053	1.024	0.945	1.11
WT	RNU6B	-0.324	0.026	1	0.961	1.04

48-Plex Reverse Transcription Pool 2

Endogenous Control: miR-142-5p

Sample	Detector	Avg Delta Ct	Delta Ct SD	RQ	RQ Min	RQ Max
MeCP2- <i>ly</i>	let-7d	4.778	0.101	0.951	0.82	1.104
WT	let-7d	4.706	0.115	1	0.843	1.186
MeCP2- <i>ly</i>	let-7e	-1.969	0.038	0.628	0.594	0.665
WT	let-7e	-2.639	0.051	1	0.928	1.078
MeCP2- <i>ly</i>	miR-101	11.379	0.048	1.165	1.085	1.25
WT	miR-101	11.599	0.107	1	0.853	1.173
MeCP2- <i>ly</i>	miR-108	5.155	0.211	1.256	0.919	1.716
WT	miR-108	5.484	0.234	1	0.708	1.413
MeCP2- <i>ly</i>	miR-122a	8.115	0.201	1.424	1.051	1.928
WT	miR-122a	8.625	0.413	1	0.541	1.848
MeCP2- <i>ly</i>	miR-126	-1.695	0.034	1.164	1.106	1.225
WT	miR-126	-1.476	0.051	1	0.927	1.079
MeCP2- <i>ly</i>	miR-126#	1.4	0.129	1.163	0.961	1.408
WT	miR-126#	1.618	0.088	1	0.879	1.138
MeCP2- <i>ly</i>	miR-127	0.365	0.132	0.695	0.571	0.844
WT	miR-127	-0.161	0.051	1	0.928	1.078
MeCP2- <i>ly</i>	miR-130aN	9.009	0.194	3.078	2.307	4.105
WT	miR-130aN	10.631	0.15	1	0.798	1.254
MeCP2- <i>ly</i>	miR-130b	6.514	0.121	2.051	1.716	2.451
WT	miR-130b	7.55	0.312	1	0.631	1.585
MeCP2- <i>ly</i>	miR-132	1.066	0.051	1.057	0.98	1.14
WT	miR-132	1.146	0.071	1	0.9	1.111

MeCP2- <i>ly</i>	miR-133a	7.258	0.27	1.338	0.898	1.994
WT	miR-133a	7.678	0.192	1	0.753	1.328
MeCP2- <i>ly</i>	miR-134	-0.603	0.033	1.092	1.04	1.147
WT	miR-134	-0.475	0.054	1	0.923	1.083
MeCP2- <i>ly</i>	miR-140	5.375	0.15	1.224	0.98	1.527
WT	miR-140	5.666	0.16	1	0.789	1.267
MeCP2- <i>ly</i>	miR-141	4.035	0.091	0.712	0.622	0.814
WT	miR-141	3.545	0.105	1	0.856	1.169
MeCP2- <i>ly</i>	miR-142-3p	3.517	0.073	1.062	0.954	1.183
WT	miR-142-3p	3.604	0.092	1	0.873	1.145
MeCP2- <i>ly</i>	miR-143	5.289	0.117	1.098	0.924	1.306
WT	miR-143	5.424	0.196	1	0.749	1.335
MeCP2- <i>ly</i>	miR-146b	0.708	0.047	1.15	1.073	1.233
WT	miR-146b	0.91	0.077	1	0.893	1.12
MeCP2- <i>ly</i>	miR-148b	7.439	0.207	1.094	0.806	1.486
WT	miR-148b	7.57	0.34	1	0.605	1.652
MeCP2- <i>ly</i>	miR-194	8.35	0.433	0.905	0.473	1.732
WT	miR-194	8.205	0.322	1	0.621	1.61
MeCP2- <i>ly</i>	miR-23b	1.172	0.063	0.897	0.818	0.985
WT	miR-23b	1.015	0.07	1	0.902	1.108
MeCP2- <i>ly</i>	miR-302b	-0.86	0.04	2.272	2.142	2.411
WT	miR-302b	0.324	0.057	1	0.919	1.088
MeCP2- <i>ly</i>	miR-30e-3p	5.224	0.178	0.591	0.454	0.769
WT	miR-30e-3p	4.464	0.185	1	0.76	1.317
MeCP2- <i>ly</i>	miR-326	-0.03	0.04	0.768	0.724	0.815
WT	miR-326	-0.411	0.051	1	0.928	1.078
MeCP2- <i>ly</i>	miR-33	8.07	0.325	1.261	0.778	2.045
WT	miR-33	8.404	0.135	1	0.82	1.22
MeCP2- <i>ly</i>	miR-342	7.298	0.313	2.297	1.443	3.657
WT	miR-342	8.498	0.386	1	0.563	1.776
MeCP2- <i>ly</i>	miR-34b	3.654	0.081	1.209	1.073	1.362
WT	miR-34b	3.927	0.112	1	0.847	1.18
MeCP2- <i>ly</i>	miR-374	7.056	0.084	1.051	0.927	1.193
WT	miR-374	7.129	0.176	1	0.771	1.297
MeCP2- <i>ly</i>	miR-377	11.415	0.235	0.98	0.693	1.388
WT	miR-377	11.386	0.161	1	0.788	1.269
MeCP2- <i>ly</i>	miR-381	2.584	0.059	0.887	0.812	0.968
WT	miR-381	2.41	0.08	1	0.888	1.126
MeCP2- <i>ly</i>	miR-383	0.818	0.035	1.06	1.006	1.117
WT	miR-383	0.903	0.076	1	0.894	1.118
MeCP2- <i>ly</i>	miR-423	2.168	0.092	1.705	1.489	1.954
WT	miR-423	2.938	0.094	1	0.871	1.149
MeCP2- <i>ly</i>	RNU6B	-0.582	0.04	0.943	0.887	1.003
WT	RNU6B	-0.667	0.066	1	0.904	1.106

48-Plex Reverse Transcription Pool 3

Endogenous Control: miR-181a

Sample	Detector	Avg Delta Ct	Delta Ct SD	RQ	RQ Min	RQ Max
MeCP2- <i>ly</i>	let-7g	-2.555	0.023	1.023	0.989	1.058
WT	let-7g	-2.522	0.046	1	0.935	1.07
MeCP2- <i>ly</i>	miR-1	7.981	0.224	1.041	0.742	1.46

WT	miR-1	8.039	0.127	1	0.828	1.208
MeCP2- <i>ly</i>	miR-106b	11.453	0.052	0.766	0.709	0.826
WT	miR-106b	11.068	0.055	1	0.921	1.085
MeCP2- <i>ly</i>	miR-147	10.927	0.072	0.85	0.764	0.946
WT	miR-147	10.692	0.097	1	0.867	1.154
MeCP2- <i>ly</i>	miR-153	4.204	0.05	1.213	1.127	1.306
WT	miR-153	4.483	0.062	1	0.913	1.095
MeCP2- <i>ly</i>	miR-154	9.908	0.075	1.223	1.092	1.371
WT	miR-154	10.199	0.05	1	0.929	1.076
MeCP2- <i>ly</i>	miR-154*	7.476	0.37	0.654	0.377	1.133
WT	miR-154*	6.863	0.092	1	0.871	1.148
MeCP2- <i>ly</i>	miR-155	9.338	0.168	0.693	0.539	0.892
WT	miR-155	8.809	0.382	1	0.566	1.765
MeCP2- <i>ly</i>	miR-16	6.276	0.134	0.938	0.77	1.144
WT	miR-16	6.184	0.267	1	0.673	1.487
MeCP2- <i>ly</i>	miR-17-3p	-1.054	0.023	0.759	0.734	0.784
WT	miR-17-3p	-1.453	0.043	1	0.938	1.066
MeCP2- <i>ly</i>	miR-17-5p	-0.97	0.025	1.144	1.102	1.186
WT	miR-17-5p	-0.776	0.045	1	0.935	1.069
MeCP2- <i>ly</i>	miR-181a	1.045	0.055	0.746	0.687	0.809
WT	miR-181a	0.621	0.049	1	0.93	1.075
MeCP2- <i>ly</i>	miR-181c	9.713	0.323	0.926	0.572	1.497
WT	miR-181c	9.601	0.163	1	0.786	1.272
MeCP2- <i>ly</i>	miR-183	-0.833	0.036	0.701	0.665	0.739
WT	miR-183	-1.346	0.05	1	0.928	1.077
MeCP2- <i>ly</i>	miR-184	2.744	0.236	0.921	0.649	1.309
WT	miR-184	2.626	0.163	1	0.784	1.275
MeCP2- <i>ly</i>	miR-189	9.753	0.226	0.867	0.618	1.216
WT	miR-189	9.547	0.136	1	0.816	1.225
MeCP2- <i>ly</i>	miR-191	11.257	0.069	1.102	0.996	1.22
WT	miR-191	11.397	0.28	1	0.66	1.516
MeCP2- <i>ly</i>	miR-195	9.776	0.021	0.878	0.851	0.906
WT	miR-195	9.588	0.061	1	0.914	1.094
MeCP2- <i>ly</i>	miR-196b	7.033	0.272	2.271	1.518	3.395
WT	miR-196b	8.216	0.155	1	0.794	1.259
MeCP2- <i>ly</i>	miR-199a*	8.625	0.506	1.061	0.503	2.24
WT	miR-199a*	8.71	0.039	1	0.943	1.06
MeCP2- <i>ly</i>	miR-199b	8.646	0.22	1.024	0.739	1.418
WT	miR-199b	8.68	0.059	1	0.916	1.092
MeCP2- <i>ly</i>	miR-199-s	10.996	0.094	0.269	0.234	0.31
WT	miR-199-s	9.103	0.265	1	0.674	1.484
MeCP2- <i>ly</i>	miR-200a	8.4	0.125	1.231	1.022	1.484
WT	miR-200a	8.7	0.046	1	0.934	1.071
MeCP2- <i>ly</i>	miR-200bN	2.292	0.046	0.687	0.642	0.736
WT	miR-200bN	1.75	0.066	1	0.907	1.102
MeCP2- <i>ly</i>	miR-200cN	8.942	0.022	0.606	0.586	0.626
WT	miR-200cN	8.218	0.044	1	0.937	1.067
MeCP2- <i>ly</i>	miR-203	11.128	0.028	0.797	0.765	0.832
WT	miR-203	10.802	0.11	1	0.851	1.176
MeCP2- <i>ly</i>	miR-208	2.998	0.077	0.68	0.607	0.761
WT	miR-208	2.441	0.073	1	0.897	1.115
MeCP2- <i>ly</i>	miR-210	9.531	0.267	0.748	0.503	1.113
WT	miR-210	9.113	0.371	1	0.574	1.742

MeCP2-ly	miR-211	7.674	0.103	0.788	0.677	0.918
WT	miR-211	7.331	0.117	1	0.841	1.189
MeCP2-ly	miR-214	9.161	0.281	1.905	1.272	2.851
WT	miR-214	10.09	0.258	1	0.69	1.449
MeCP2-ly	miR-217	2.446	0.085	0.578	0.51	0.656
WT	miR-217	1.656	0.07	1	0.902	1.109
MeCP2-ly	miR-23a	4.74	0.161	0.584	0.46	0.741
WT	miR-23a	3.963	0.135	1	0.819	1.221
MeCP2-ly	miR-34cN	7.764	0.064	1.006	0.914	1.108
WT	miR-34cN	7.773	0.07	1	0.902	1.109
MeCP2-ly	miR-380-3p	8.308	0.042	0.877	0.824	0.934
WT	miR-380-3p	8.118	0.062	1	0.912	1.097
MeCP2-ly	miR-433	-0.385	0.05	0.917	0.851	0.988
WT	miR-433	-0.51	0.043	1	0.938	1.066
MeCP2-ly	miR-449	9.195	0.02	0.821	0.797	0.846
WT	miR-449	8.911	0.04	1	0.942	1.061
MeCP2-ly	miR-452*	4.939	0.272	0.829	0.554	1.239
WT	miR-452*	4.668	0.172	1	0.775	1.29
MeCP2-ly	miR-7	1.857	0.069	1.055	0.953	1.168
WT	miR-7	1.934	0.077	1	0.893	1.12
MeCP2-ly	miR-99a	10.18	0.231	1.198	0.851	1.686
WT	miR-99a	10.441	0.041	1	0.94	1.063
MeCP2-ly	RNU6B	-0.063	0.029	0.735	0.703	0.767
WT	RNU6B	-0.508	0.056	1	0.918	1.089
MeCP2-ly	snoR-02	9.005	0.02	0.883	0.857	0.91
WT	snoR-02	8.825	0.039	1	0.944	1.06
MeCP2-ly	snoR-12	8.526	0.125	0.729	0.606	0.877
WT	snoR-12	8.069	0.14	1	0.813	1.23

48-Plex Reverse Transcription Pool 4

Endogenous Control: miR-26a

Sample	Detector	Avg Delta Ct	Delta Ct SD	RQ	RQ Min	RQ Max
MeCP2-ly	miR-100	3.523	0.027	1.016	0.977	1.057
WT	miR-100	3.546	0.015	1	0.978	1.023
MeCP2-ly	miR-105	11.006	0.149	0.608	0.488	0.759
WT	miR-105	10.289	0.231	1	0.71	1.408
MeCP2-ly	miR-106a	5.178	0.042	0.935	0.878	0.996
WT	miR-106a	5.082	0.035	1	0.95	1.053
MeCP2-ly	miR-107	8.506	0.209	1.056	0.773	1.441
WT	miR-107	8.584	0.135	1	0.819	1.221
MeCP2-ly	miR-124b	11.551	0.192	1.066	0.803	1.417
WT	miR-124b	11.644	0.085	1	0.881	1.135
MeCP2-ly	miR-125b	-0.896	0.029	0.616	0.59	0.643
WT	miR-125b	-1.595	0.016	1	0.976	1.024
MeCP2-ly	miR-135a	5.476	0.086	0.856	0.754	0.973
WT	miR-135a	5.252	0.052	1	0.926	1.08
MeCP2-ly	miR-146a	7.08	0.094	0.944	0.821	1.085
WT	miR-146a	6.997	0.093	1	0.871	1.148
MeCP2-ly	miR-150	9.881	0.249	0.478	0.33	0.691
WT	miR-150	8.815	0.18	1	0.763	1.31
MeCP2-ly	miR-152N	7.673	0.158	0.547	0.433	0.692

WT	miR-152N	6.803	0.096	1	0.868	1.152
MeCP2- <i>ly</i>	miR-181c	5.133	0.108	0.784	0.669	0.92
WT	miR-181c	4.783	0.045	1	0.935	1.069
MeCP2- <i>ly</i>	miR-182*	8.559	0.321	0.401	0.247	0.651
WT	miR-182*	7.24	0.216	1	0.724	1.381
MeCP2- <i>ly</i>	miR-186	5.166	0.042	1.015	0.955	1.08
WT	miR-186	5.188	0.026	1	0.962	1.039
MeCP2- <i>ly</i>	miR-190	9.262	0.201	1.028	0.764	1.384
WT	miR-190	9.302	0.267	1	0.672	1.488
MeCP2- <i>ly</i>	miR-192	8.273	0.075	1.081	0.967	1.208
WT	miR-192	8.385	0.197	1	0.746	1.341
MeCP2- <i>ly</i>	miR-20a	2.45	0.027	1.099	1.056	1.143
WT	miR-20a	2.586	0.034	1	0.951	1.052
MeCP2- <i>ly</i>	miR-222	5.608	0.037	0.383	0.362	0.404
WT	miR-222	4.222	0.027	1	0.961	1.041
MeCP2- <i>ly</i>	miR-223	10.949	0.258	0.832	0.565	1.226
WT	miR-223	10.685	0.265	1	0.676	1.479
MeCP2- <i>ly</i>	miR-26aN	4.035	0.027	0.728	0.7	0.758
WT	miR-26aN	3.577	0.017	1	0.974	1.026
MeCP2- <i>ly</i>	miR-27bN	5.123	0.167	0.8	0.625	1.025
WT	miR-27bN	4.802	0.139	1	0.814	1.228
MeCP2- <i>ly</i>	miR-296	3.796	0.327	1.606	0.988	2.61
WT	miR-296	4.479	0.02	1	0.971	1.03
MeCP2- <i>ly</i>	miR-29a	2.38	0.04	0.671	0.633	0.711
WT	miR-29a	1.804	0.05	1	0.929	1.076
MeCP2- <i>ly</i>	miR-29c	3.241	0.104	0.703	0.603	0.819
WT	miR-29c	2.732	0.034	1	0.951	1.051
MeCP2- <i>ly</i>	miR-302c#	12.221	0.078	0.956	0.852	1.072
WT	miR-302c#	12.155	0.073	1	0.897	1.114
MeCP2- <i>ly</i>	miR-302d	12.905	0.047	0.641	0.597	0.688
WT	miR-302d	12.263	0.29	1	0.648	1.543
MeCP2- <i>ly</i>	miR-30a-5p	3.849	0.035	1.25	1.187	1.317
WT	miR-30a-5p	4.171	0.017	1	0.975	1.025
MeCP2- <i>ly</i>	miR-30a-5pN	1.376	0.031	1.079	1.032	1.129
WT	miR-30a-5pN	1.486	0.031	1	0.955	1.047
MeCP2- <i>ly</i>	miR-30d	3.58	0.061	0.697	0.636	0.763
WT	miR-30d	3.059	0.061	1	0.914	1.094
MeCP2- <i>ly</i>	miR-321	4.332	0.102	0.822	0.706	0.956
WT	miR-321	4.049	0.032	1	0.954	1.049
MeCP2- <i>ly</i>	miR-324-5p	3.765	0.045	1.153	1.079	1.231
WT	miR-324-5p	3.97	0.067	1	0.906	1.104
MeCP2- <i>ly</i>	miR-339	6.773	0.185	0.606	0.461	0.796
WT	miR-339	6.051	0.129	1	0.826	1.21
MeCP2- <i>ly</i>	miR-346	11.433	0.153	0.928	0.738	1.167
WT	miR-346	11.326	0.146	1	0.807	1.24
MeCP2- <i>ly</i>	miR-34c	6.282	0.117	1.565	1.318	1.859
WT	miR-34c	6.929	0.197	1	0.748	1.337
MeCP2- <i>ly</i>	miR-361	5.062	0.107	0.713	0.608	0.835
WT	miR-361	4.573	0.06	1	0.915	1.093
MeCP2- <i>ly</i>	miR-371	11.828	0.028	1.095	1.05	1.142
WT	miR-371	11.959	0.088	1	0.877	1.14
MeCP2- <i>ly</i>	miR-378	7.412	0.172	2.889	2.241	3.726
WT	miR-378	8.943	0.154	1	0.797	1.255

MeCP2- <i>ly</i>	miR-379	10.985	0.341	2.837	1.708	4.712
WT	miR-379	12.489	0.215	1	0.725	1.38
MeCP2- <i>ly</i>	miR-92	0.42	0.042	0.894	0.84	0.95
WT	miR-92	0.258	0.029	1	0.958	1.044
MeCP2- <i>ly</i>	miR-92N	0.011	0.029	1.11	1.063	1.159
WT	miR-92N	0.162	0.022	1	0.967	1.034
MeCP2- <i>ly</i>	RNU6B	1.525	0.037	1.184	1.113	1.259
WT	RNU6B	1.769	0.027	1	0.96	1.042
MeCP2- <i>ly</i>	snoR-02	12.861	0.141	1.039	0.844	1.279
WT	snoR-02	12.916	0.086	1	0.88	1.136

48-Plex Reverse Transcription Pool 5

Endogenous Control: let-7b

Sample	Detector	Avg Delta Ct	Delta Ct SD	RQ	RQ Min	RQ Max
MeCP2- <i>ly</i>	miR-139	9.014	0.134	1.636	1.342	1.995
WT	miR-139	9.724	0.129	1	0.826	1.21
MeCP2- <i>ly</i>	miR-193b	13.433	0.613	1.759	0.703	4.405
WT	miR-193b	14.248	0.159	1	0.788	1.269
MeCP2- <i>ly</i>	miR-202	11.873	0.294	1.454	0.942	2.243
WT	miR-202	12.413	0.243	1	0.698	1.432
MeCP2- <i>ly</i>	miR-213	5.741	0.032	0.931	0.888	0.977
WT	miR-213	5.638	0.046	1	0.934	1.071
MeCP2- <i>ly</i>	miR-301	3.673	0.039	1.702	1.606	1.804
WT	miR-301	4.44	0.023	1	0.967	1.034
MeCP2- <i>ly</i>	miR-31	4.01	0.053	0.595	0.55	0.644
WT	miR-31	3.261	0.043	1	0.938	1.066
MeCP2- <i>ly</i>	miR-325N	9.879	0.167	1.587	1.24	2.032
WT	miR-325N	10.545	0.245	1	0.696	1.436
MeCP2- <i>ly</i>	miR-340	6.278	0.088	1.692	1.486	1.926
WT	miR-340	7.036	0.15	1	0.801	1.248
MeCP2- <i>ly</i>	miR-365	5.431	0.034	1.17	1.113	1.229
WT	miR-365	5.657	0.049	1	0.93	1.076
MeCP2- <i>ly</i>	miR-370	10.161	0.099	7.197	6.221	8.326
WT	miR-370	13.008	0.259	1	0.679	1.473
MeCP2- <i>ly</i>	miR-375	14.478	0.086	1.296	1.138	1.476
WT	miR-375	14.852	0.436	1	0.518	1.931
MeCP2- <i>ly</i>	miR-382	12.866	0.288	4.347	2.84	6.654
WT	miR-382	14.986	0.238	1	0.698	1.433
MeCP2- <i>ly</i>	miR-412	10.77	0.202	1.054	0.781	1.421
WT	miR-412	10.846	0.257	1	0.684	1.461
MeCP2- <i>ly</i>	miR-422b	8.939	0.259	1.102	0.751	1.616
WT	miR-422b	9.079	0.108	1	0.852	1.173
MeCP2- <i>ly</i>	miR-425	8.376	0.39	0.927	0.521	1.649
WT	miR-425	8.266	0.218	1	0.724	1.38
MeCP2- <i>ly</i>	miR-453	14.797	0.19	1.472	1.111	1.949
WT	miR-453	15.355	0.054	1	0.922	1.085
MeCP2- <i>ly</i>	miR-485-3p	12.412	0.283	1.451	0.953	2.211
WT	miR-485-3p	12.949	0.255	1	0.687	1.457
MeCP2- <i>ly</i>	miR-488	13.32	0.366	2.944	1.703	5.09
WT	miR-488	14.878	0.317	1	0.62	1.614
MeCP2- <i>ly</i>	miR-489	14.633	0.18	1.238	0.948	1.618

WT	miR-489	14.941	0.225	1	0.716	1.397
MeCP2- <i>ly</i>	miR-490	14.495	0.153	0.801	0.638	1.005
WT	miR-490	14.174	0.095	1	0.867	1.153
MeCP2- <i>ly</i>	miR-491	9.965	0.182	1.219	0.931	1.595
WT	miR-491	10.251	0.264	1	0.677	1.478
MeCP2- <i>ly</i>	miR-494	15.442	0.015	0.713	0.697	0.729
WT	miR-494	14.954	0.227	1	0.715	1.398
MeCP2- <i>ly</i>	miR-496	14.212	0.035	1.57	1.49	1.655
WT	miR-496	14.864	0.343	1	0.592	1.688
MeCP2- <i>ly</i>	RNU6B	3.026	0.02	1.139	1.106	1.173
WT	RNU6B	3.214	0.114	1	0.845	1.183

48-Plex Reverse Transcription Pool 6

Endogenous Control: let-7c

Sample	Detector	Avg Delta Ct	Delta Ct SD	RQ	RQ Max	RQ Min
WT	let-7i	5.952770417	0.944760939	1	1.899823931	0.5264
MeCP2- <i>ly</i>	let-7i	5.208754667	0.540065944	1.674831259	1.443193379	0.6929
WT	miR-522	9.292784622	0.340437609	1	1.260179161	0.7935
MeCP2- <i>ly</i>	miR-522	9.062044	0.707517803	1.173437191	1.617053541	0.6184
WT	RNU6B	3.209559111	0.706791586	1	1.616256032	0.6187
MeCP2- <i>ly</i>	RNU6B	2.679202556	0.340550167	1.4442861	1.260275516	0.7935

48-Plex Reverse Transcription Pool 7

Endogenous Control: miR-140*

Sample	Detector	Avg Delta Ct	Delta Ct SD	RQ	RQ Min	RQ Max
MeCP2- <i>ly</i>	miR-101	5.406	0.166	1.308	1.024	1.671
WT	miR-101	5.794	0.477	1	0.492	2.031
MeCP2- <i>ly</i>	miR-101b	3.662	0.139	2.248	1.831	2.761
WT	miR-101b	4.83	0.151	1	0.799	1.251
MeCP2- <i>ly</i>	miR-106a	-0.791	0.067	1.564	1.416	1.728
WT	miR-106a	-0.145	0.076	1	0.894	1.119
MeCP2- <i>ly</i>	miR-124a	3.75	0.163	1.867	1.468	2.374
WT	miR-124a	4.651	0.177	1	0.77	1.3
MeCP2- <i>ly</i>	miR-127	6.207	0.169	6.474	5.033	8.328
WT	miR-127	8.902	0.043	1	0.937	1.068
MeCP2- <i>ly</i>	miR-129-3p	0.6	0.086	0.612	0.539	0.694
WT	miR-129-3p	-0.109	0.05	1	0.929	1.076
MeCP2- <i>ly</i>	miR-129-5p	6.388	0.402	1.622	0.888	2.962
WT	miR-129-5p	7.086	0.279	1	0.658	1.52
MeCP2- <i>ly</i>	miR-140	-0.092	0.069	1.014	0.915	1.123
WT	miR-140	-0.072	0.067	1	0.906	1.104
MeCP2- <i>ly</i>	miR-151	1.005	0.085	0.974	0.859	1.105
WT	miR-151	0.967	0.07	1	0.902	1.109
MeCP2- <i>ly</i>	miR-17-3p	6.275	0.308	1.559	0.983	2.473
WT	miR-17-3p	6.916	0.173	1	0.772	1.295
MeCP2- <i>ly</i>	miR-187	1.454	0.15	3.941	3.16	4.915
WT	miR-187	3.433	0.375	1	0.575	1.739
MeCP2- <i>ly</i>	miR-192	6.61	0.156	0.955	0.758	1.203
WT	miR-192	6.544	0.096	1	0.867	1.153

MeCP2- <i>ly</i>	miR-203	7.856	0.103	0.613	0.525	0.716
WT	miR-203	7.151	0.149	1	0.8	1.249
MeCP2- <i>ly</i>	miR-204	7.028	0.456	5.234	2.659	10.302
WT	miR-204	9.416	0.115	1	0.843	1.187
MeCP2- <i>ly</i>	miR-207	9.438	0.144	0.93	0.751	1.152
WT	miR-207	9.334	0.076	1	0.893	1.119
MeCP2- <i>ly</i>	miR-211	2.608	0.124	0.743	0.618	0.893
WT	miR-211	2.179	0.073	1	0.897	1.114
MeCP2- <i>ly</i>	miR-221	-1.291	0.067	0.35	0.317	0.387
WT	miR-221	-2.805	0.046	1	0.934	1.07
MeCP2- <i>ly</i>	miR-293	7.708	0.329	1.696	1.044	2.756
WT	miR-293	8.47	0.124	1	0.829	1.206
MeCP2- <i>ly</i>	miR-30e*	-0.218	0.073	1.078	0.968	1.2
WT	miR-30e*	-0.11	0.077	1	0.892	1.121
MeCP2- <i>ly</i>	miR-31	-1.046	0.064	0.531	0.483	0.584
WT	miR-31	-1.958	0.046	1	0.934	1.071
MeCP2- <i>ly</i>	miR-322	1.401	0.103	1.107	0.951	1.289
WT	miR-322	1.548	0.083	1	0.885	1.13
MeCP2- <i>ly</i>	miR-324-5p	0.622	0.081	1.293	1.148	1.456
WT	miR-324-5p	0.993	0.125	1	0.831	1.203
MeCP2- <i>ly</i>	miR-325	5.713	0.158	0.581	0.459	0.735
WT	miR-325	4.929	0.223	1	0.717	1.396
MeCP2- <i>ly</i>	miR-326	5	0.121	1.079	0.903	1.291
WT	miR-326	5.11	0.124	1	0.832	1.202
MeCP2- <i>ly</i>	miR-337	8.915	0.123	1.121	0.935	1.344
WT	miR-337	9.079	0.11	1	0.848	1.179
MeCP2- <i>ly</i>	miR-9	-5.232	0.062	1.505	1.374	1.649
WT	miR-9	-4.642	0.037	1	0.947	1.056
MeCP2- <i>ly</i>	miR-93	-4.552	0.068	1.227	1.109	1.357
WT	miR-93	-4.257	0.038	1	0.946	1.057
MeCP2- <i>ly</i>	miR-99a	-1.958	0.068	0.833	0.753	0.921
WT	miR-99a	-2.222	0.057	1	0.92	1.087
MeCP2- <i>ly</i>	RNU6B	-2.215	0.062	0.934	0.852	1.024
WT	RNU6B	-2.313	0.041	1	0.941	1.062
MeCP2- <i>ly</i>	snoR-12	4.137	0.213	0.719	0.525	0.985
WT	snoR-12	3.66	0.087	1	0.88	1.137

48-Plex Reverse Transcription Pool 8

Endogenous Control: miR-30b

Sample	Detector	Avg Delta Ct	Delta Ct SD	RQ	RQ Min	RQ Max
MeCP2- <i>ly</i>	let-7a	1.92	0.031	1.248	1.192	1.307
WT	let-7a	2.24	0.029	1	0.958	1.044
MeCP2- <i>ly</i>	miR-129	9.74	0.262	0.483	0.327	0.713
WT	miR-129	8.689	0.256	1	0.683	1.463
MeCP2- <i>ly</i>	miR-133b	11.615	0.379	1.119	0.631	1.984
WT	miR-133b	11.777	0.203	1	0.738	1.356
MeCP2- <i>ly</i>	miR-137	9.397	0.147	4.639	3.726	5.776
WT	miR-137	11.611	0.254	1	0.686	1.458
MeCP2- <i>ly</i>	miR-151	9.016	0.26	0.893	0.609	1.31
WT	miR-151	8.852	0.204	1	0.739	1.353
MeCP2- <i>ly</i>	miR-187	3.263	0.058	2.162	1.983	2.357

WT	miR-187	4.375	0.106	1	0.855	1.17
MeCP2- <i>ly</i>	miR-18a	5.226	0.096	1.589	1.378	1.831
WT	miR-18a	5.894	0.104	1	0.857	1.167
MeCP2- <i>ly</i>	miR-193a	4.19	0.257	5.213	3.564	7.623
WT	miR-193a	6.572	0.391	1	0.559	1.789
MeCP2- <i>ly</i>	miR-212	5.014	0.095	0.859	0.747	0.988
WT	miR-212	4.795	0.046	1	0.934	1.071
MeCP2- <i>ly</i>	miR-219	10.468	0.207	1.767	1.296	2.407
WT	miR-219	11.289	0.214	1	0.725	1.378
MeCP2- <i>ly</i>	miR-22	5.932	0.104	0.75	0.643	0.875
WT	miR-22	5.517	0.091	1	0.874	1.145
MeCP2- <i>ly</i>	miR-27b	4.839	0.088	1.129	0.991	1.286
WT	miR-27b	5.014	0.131	1	0.824	1.214
MeCP2- <i>ly</i>	miR-29b	8.477	0.23	0.723	0.515	1.016
WT	miR-29b	8.01	0.173	1	0.774	1.292
MeCP2- <i>ly</i>	miR-30e-5p	6.357	0.089	1.137	0.996	1.297
WT	miR-30e-5p	6.542	0.059	1	0.917	1.091
MeCP2- <i>ly</i>	miR-331	2.74	0.031	1.004	0.959	1.051
WT	miR-331	2.746	0.032	1	0.954	1.048
MeCP2- <i>ly</i>	miR-422a	12.796	0.219	1.329	0.959	1.841
WT	miR-422a	13.206	0.116	1	0.842	1.188
MeCP2- <i>ly</i>	miR-424	12.145	0.339	1.498	0.902	2.488
WT	miR-424	12.728	0.091	1	0.873	1.145
MeCP2- <i>ly</i>	miR-450	13.21	0.327	0.765	0.466	1.254
WT	miR-450	12.823	0.049	1	0.929	1.077
MeCP2- <i>ly</i>	miR-452	12.891	0.054	1.088	1.004	1.179
WT	miR-452	13.012	0.12	1	0.836	1.196
MeCP2- <i>ly</i>	miR-497	7.871	0.191	1.652	1.245	2.191
WT	miR-497	8.595	0.23	1	0.712	1.404
MeCP2- <i>ly</i>	miR-502	12.507	0.391	1.09	0.604	1.969
WT	miR-502	12.632	0.141	1	0.807	1.239
MeCP2- <i>ly</i>	miR-518d	12.531	0.054	0.952	0.879	1.032
WT	miR-518d	12.46	0.03	1	0.956	1.046
MeCP2- <i>ly</i>	miR-520a	13.693	0.141	0.755	0.613	0.931
WT	miR-520a	13.288	0.16	1	0.788	1.269
MeCP2- <i>ly</i>	miR-9	-3.219	0.024	1.187	1.146	1.229
WT	miR-9	-2.973	0.026	1	0.963	1.039
MeCP2- <i>ly</i>	miR-9*	-0.74	0.054	1.332	1.23	1.443
WT	miR-9*	-0.327	0.047	1	0.933	1.071
MeCP2- <i>ly</i>	miR-93	-1.132	0.033	1.253	1.194	1.316
WT	miR-93	-0.807	0.029	1	0.959	1.043
MeCP2- <i>ly</i>	miR-98	4.315	0.054	1.42	1.31	1.538
WT	miR-98	4.82	0.105	1	0.857	1.167
MeCP2- <i>ly</i>	RNU6B	1.718	0.022	0.898	0.868	0.929
WT	RNU6B	1.562	0.029	1	0.958	1.044

Chapter 2 - Supplemental Table II

Candidate miR-137 target list:

EZH2
FMNL2
EPHA7
PPARBP
MIB1
CUL3
NCOA3
ATP1B1
SCRT1
LBX1
CREBBP
NRP1
JMJD2A
NCOA3
ADCY1
ERBB2IP
GRIA1
EGR2
DNAJB1
DUSP4

Chapter 3: MicroRNA miR-137 regulates neuronal maturation by targeting ubiquitin ligase Mind Bomb-1

Abstract

A critical step in brain development is neuronal maturation, which is regulated by complex mechanisms and dysregulation of this process is frequently found in neurodevelopmental disorders including RTT. MicroRNAs have been implicated in several steps of neuronal maturation including dendritic and axonal growth, spine development, and synaptogenesis. We demonstrate that one neuron-enriched microRNA, miR-137, has a significant role in regulating neuronal maturation. Overexpression of miR-137 inhibits neuronal dendritic morphogenesis, phenotypic maturation, and spine development both in brain and cultured primary neurons. On the other hand, a reduction in miR-137 had opposite effects. We further show that miR-137 targets the *Drosophila* Mind bomb 1 (Mib1) protein through the conserved target site located in the 3' untranslated region of *Mib1* mRNA. Mib1 is an ubiquitin ligase known to be important for neurodevelopment. We show that exogenously expressed Mib1 could partially rescue the phenotypes associated with miR-137 overexpression. These results demonstrate a novel miRNA-mediated mechanism involving miR-137 and Mib1 that function to regulate neuronal maturation and dendritic morphogenesis during neuronal development.

Introduction

To function properly, neurons have to integrate into appropriate neural networks and establish correct communication with other neurons. A critical step in development is neuronal maturation, which is characterized by dendritic and axonal growth, synaptogenesis, neuronal and synaptic pruning, and modulations of neurotransmitter sensitivities (Webb, Monk et al. 2001; Waites, Craig et al. 2005). The process of neuronal maturation is regulated by complex mechanisms that are still unclear, and deficits in this step are evident in many neurodevelopmental disorders (Fiala, Spacek et al. 2002).

MicroRNAs (miRNAs) are small non-coding RNAs that can modulate gene expression at the post-translational level by targeting messenger RNA (mRNA), which leads to either reduced translation efficiency or cleavage of the target mRNAs. miRNAs are known to be involved in many cellular processes, such as proliferation, differentiation, apoptosis, and metabolism (Carninci, Kasukawa et al. 2005; Chang and Mendell 2007; Gangaraju and Lin 2009; Liu and Zhao 2009). Despite the fact that 70% of detectable miRNAs are expressed in the brain, where half that number are either brain specific or enriched (Cao, Yeo et al. 2006) there have been few functional studies of miRNA in the nervous system. Evidence has shown that many miRNAs act locally at the neuronal dendritic spines (Lugli, Torvik et al. 2008; Smalheiser and Lugli 2009). Both miR-134 and miR-138 are known to regulate dendritic patterning and spine morphogenesis by regulating protein translation at

the synapse (Schratt, Tuebing et al. 2006; Fiore, Khudayberdiev et al. 2009; Siegel, Obernosterer et al. 2009). In addition, brain-specific miR-124 is localized at presynaptic terminal of *Aplysia* and regulates synaptic plasticity by regulating transcription factor CREB (Rajasethupathy, Fiumara et al. 2009). A neuronal activity-dependent miRNA, miR-132, is found to regulate dendritic development by targeting a Rho family GTPase-activating protein, p250GAP (Wayman, Davare et al. 2008). Therefore, the function of small regulatory RNAs could be an important mechanism regulating mammalian neurodevelopment.

In this study we show that a specific miRNA, miR-137, has a significant role in regulating neuronal maturation. We further establish that miR-137 regulates the translation of the mouse homolog of *Drosophila* Mind bomb 1 (Mib1), a ubiquitin ligase known to be important for neurogenesis and neurodevelopment (Itoh, Kim et al. 2003; Choe, Liao et al. 2007; Ossipova, Ezan et al. 2009). Finally, we show that exogenously expressed Mib1 can partially rescue the phenotypic deficits associated with miR-137 overexpression. These data suggest that functional interaction between miRNA and Mib1 plays an important modulatory role in neuronal development.

Results

Identification of miRNA enriched in neurons

To identify the lineage specific miRNAs that may regulate neuronal development and functions in postnatal hippocampus, we profiled mature miRNA expression in adult hippocampal neuroprogenitors (A94-NSCs) differentiated into either neuronal or astrocyte lineages compared to undifferentiated progenitors (Figure S1A,B). We then quantitatively identified miRNAs that were enriched specifically in the neuronal lineage relative to the astrocyte lineage (Figure 1A). Several miRNAs, particularly miR-185, 27b, 182, 137, 29b, 132 and 146, showed enrichment in neurons rather than astrocytes or undifferentiated NSCs. Among them, miR-137 has previously found to be enriched in synaptosomes isolated from rat forebrains (Siegel, Obernosterer et al. 2009; Smalheiser and Lugli 2009). We further confirmed that the expression levels of miR-137 increased during neuronal differentiation of A94-NSCs (Figure 1B) and that miR-137 expression is significantly higher in isolated primary neurons compared to aNSCs (Figure 1C). The enrichment of miR-137 in neuronal lineage suggests that it may have important functions in neuronal development and functions.

It has been shown that miR-137 is expressed in the brain and enriched at the synaptic compartment (Siegel, Obernosterer et al. 2009; Smalheiser and Lugli 2009). We reasoned that if miR-137 is a mediator of neurodevelopment and function, it should be expressed in neurons of the adult hippocampus, which is a region of the brain exhibiting significant plasticity and continuous production of new neurons. We therefore examined the cellular localization of miR-137 in the adult hippocampus. Hybridization with the miR-137-specific probe showed an

enrichment of miR-137 within the DG and molecular layer of the hippocampus compared to the miR-1, a miRNA that is expressed at low levels in CNS (Figure 1D, E). Together, these data and previous observations (Siegel, Obernosterer et al. 2009; Smalheiser and Lugli 2009) suggest that miR-137 may play functional roles in neurons, and possibly during the formation of connectivity between neurons in the hippocampus.

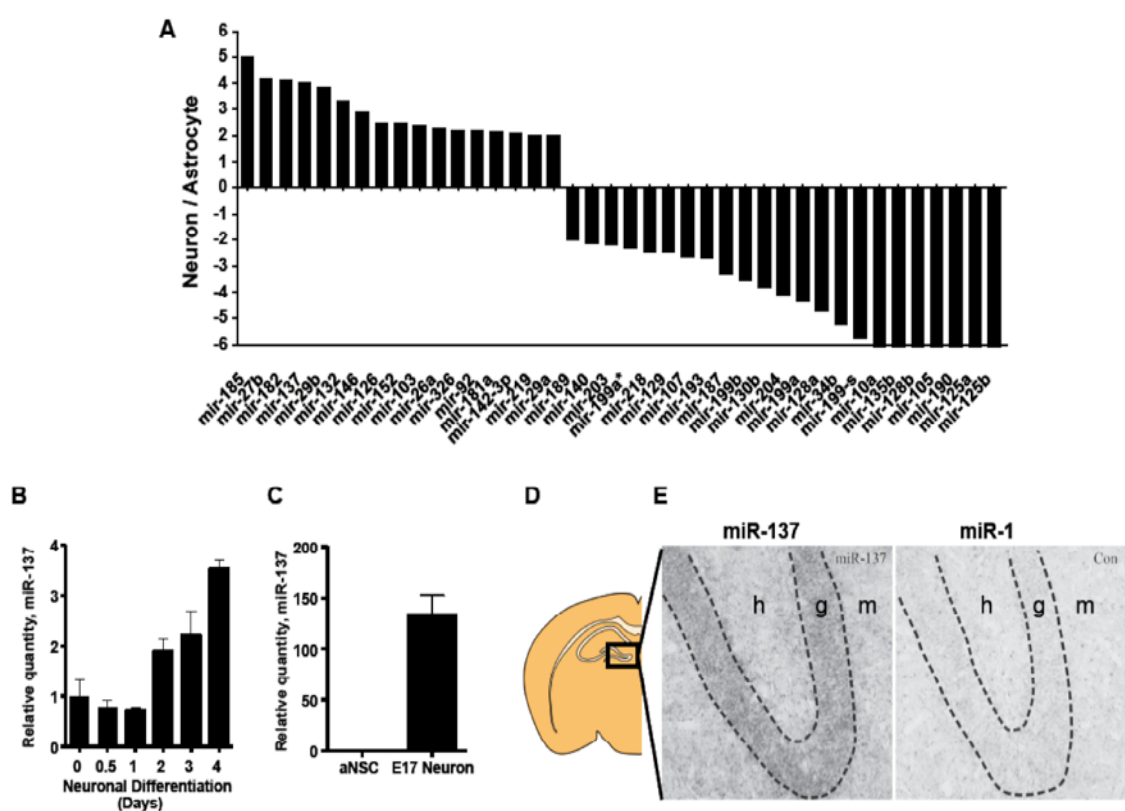


Figure 1. miR-137 is enriched in neurons and is expressed in the dentate gyrus and molecular layer of the hippocampus. **A.** A94-NSCs miRNA relative quantity expression ratios comparing cells differentiated according to a neuronal differentiation protocol to those differentiated according to an astrocyte differentiation protocol. **B.** Verification of increased miR-137 expression upon neuronal differentiation of A94-NSCs from 0-4 days. **C.** Enrichment of miR-137 in post-mitotic neurons isolated from E17 embryos relative to primary aNSCs. **D.** in situ hybridization of miR-137 showing expression within the granular (g) layer of the DG (h = hilus layer, m = molecular layer). miR-1 was used as a negative control.

miR-137 regulates dendritic development and phenotypic maturation of new neurons in vivo

miRNAs have been found to localize at the synapse and play an important role in dendritic patterning and spine morphogenesis (Schratt, Tuebing et al. 2006; Lugli, Torvik et al. 2008; Siegel, Obernosterer et al. 2009). To determine whether elevated miR-137 levels in neurons can affect neuronal maturation and dendritic morphogenesis, we overexpressed miR-137 in newborn cells of the adult DG using retrovirus-mediated gene delivery (Smrt, Eaves-Egenes et al. 2007). This method, referred to as the single-cell genetic approach (van Praag, Schinder et al. 2002; Song, Kempermann et al. 2005), makes use of recombinant retroviruses capable of infecting only dividing cells (Figure 2A). Due to the persistence of postnatal neurogenesis in the adult hippocampus, this method allows for delivery of the miR-137 transgene specifically to newborn cells in the DG and a detailed morphological and phenotypic analysis on these newly generated neurons in an otherwise normal brain (Song, Kempermann et al. 2005; Zhao, Teng et al. 2006; Smrt, Eaves-Egenes et al. 2007). Using stereotaxic microinjection surgery, retrovirus expressing both eGFP and short-hairpin miR-137 (sh-miR-137) was grafted into one hemisphere of the adult mouse DG, and a control retrovirus carrying nonspecific short-hairpin (sh-Control) and eGFP was injected into the contralateral hemisphere of the same animal (Figure 2A, B). At 4 weeks post-injection (4wpi), one cohort of injected animals was used to generate thick (300- μ m) sections, which preserves the dendritic arborization of eGFP-positive neurons and enables extensive

morphological analysis. Individual eGFP-expressing neurons in these sections were imaged using confocal microscopy. To precisely evaluate the dendritic complexity of eGFP+ neurons, eGFP+ dendritic arbors were reconstructed for image analysis using Neurolucida analysis software with image stack module (MicroBrightField, Inc.) (Figure 2C, D).

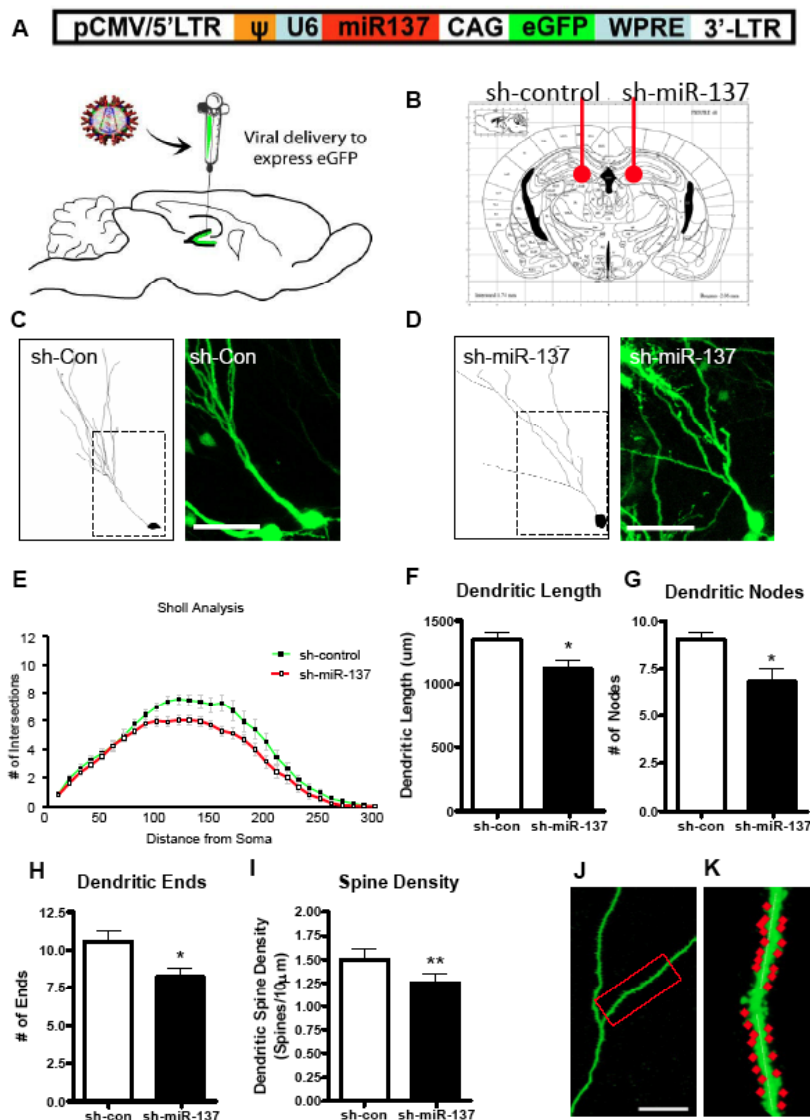


Figure 2. miR-137 regulates dendritic development and phenotypic maturation of new neurons in vivo. **A.** A schematic diagram showing the retroviral vector used for in vivo miR-137 expression. MiR-137 or control miR was expressed as a short hairpin under U6 RNA Polymerase III promoter while eGFP was expressed under a chicken β -actin (CAG) promoter. **B.** Schematic diagram showing that control virus (sh-Control) was injected into the left hemisphere, and retrovirus expressing miR-137 (sh-miR-137) was injected into the right hemisphere. **C-D.** Confocal z-stacks showing eGFP-expressing neurons at 4 weeks post-injection (4 wpi) with representative traces from both the control (**C**) and sh-miR-137 condition (**D**) (scale bar = 50 μ m). **E.** Neurons overexpressing sh-miR-137 show reduced dendritic complexity compared with controls, as determined by Scholl analysis. **F-H.** Neurons overexpressing sh-miR-137 show reduced dendritic length (**F**), number of nodes (branch points, **G**), and dendritic ends (**H**). **I.** Neurons overexpressing sh-miR-137 show reduced dendritic spine density. **J.** Confocal z-stacks showing eGFP-expressing dendrites (scalebar = 20 μ m). **K.** A representative dendritic segment used for spine density analysis (* = $p < 0.05$).

Since previous reports have indicated that miR-137 has no effect on dendritic spine volume (Siegel, Obernosterer et al. 2009), quantitative analysis using established parameters for assessing neuronal dendritic development were used (Zhao, Teng et al. 2006; Duan, Chang et al. 2007). Sholl analysis indicated that miR-137-overexpressing neurons exhibited significantly reduced dendritic complexity compared to sh-control-expressing neurons (Figure 2E, $F(1,65) = 8.78$, $p = 0.004$, multivariate analysis of variance). In addition, miR-137-overexpressing neurons exhibited significantly reduced average dendritic length ($n = 3$ animals, $p < 0.05$), number of nodes (branch points) ($n = 3$, $p < 0.05$), and number of dendritic endpoints ($n = 3$, $p < 0.05$) compared with young neurons expressing sh-Control (Figure 2F-H).

Dendritic spine density increases as neurons mature, making the spine density of DG neurons a good indicator of neuronal maturation (Ge, Goh et al. 2006; Zhao, Teng et al. 2006). Furthermore, reduced spine density is a common characteristic of abnormal synaptic development in a variety of neurological disorders such as Fragile-X and Rett syndrome (Fiala, Spacek et al. 2002; Smrt, Eaves-Egenes et al. 2007). Therefore another cohort of virus-injected animals was used to generate 40- μm thin sections for dendritic spine analysis. To determine whether overexpression of miR-137 leads to deficits in spine morphogenesis, the dendritic spine density of newborn GFP-expressing DG granule neurons was analyzed at 4 weeks post-injection, a time at which labeled new neurons are believed to exhibit the dendritic morphology of mature neurons (van Praag, Schinder et al. 2002; Ge, Goh et al. 2006;

Zhao, Teng et al. 2006). To maximize consistency, dendritic fragments 25-100 μ m from the cell body of each eGFP+ neuron were analyzed. Spine density was quantified by counting the number of spines protruding from the dendrite within each 10- μ m segment. Quantitative analysis showed that miR-137-overexpressing neurons exhibited a 17% reduction in dendritic spine density compared with sh-Control-expression neurons (n = 3, p < 0.01) (Figure 2I-K).

New neurons in the DG express development stage-specific markers that define their maturation (Figure 3A) (Ming and Song 2005; Zhao, Deng et al. 2008). Using immunocytochemistry for doublecortin (DCX, an immature neuronal marker) and neuronal nuclear antigen (NeuN, a mature neuronal marker) immunostaining, new neurons in the DG were categorized into 3 subpopulations: immature neurons (DCX+ only), transitioning neurons (DCX+ and NeuN+), and mature neurons (NeuN+) (Brown, Couillard-Despres et al. 2003; Smrt, Eaves-Egenes et al. 2007). We then determined whether new neurons overexpressing miR-137 had a developmental phenotype that could be measured by the expression of stage-specific markers. Thus, retrovirus-labeled newborn neurons were analyzed at 4 weeks post-injection, a time when most virus-labeled cells have differentiated into mature neurons. We found that miR-137-overexpressing cells differentiated into fewer neurons (either DCX+ and/or NeuN+/GFP+ cells) in general compared with sh-Control treated cells (Figure 3A-C). We then quantified the proportion of each type of neuron among total eGFP+ neurons. The results summarized in Figure 3D show that neurons overexpressing miR-137 displayed a significant difference in the

proportion of immature vs. mature neurons compared with neurons overexpressing sh-Control. Specifically, miR-137-overexpressing neurons had an 80% decrease in the proportion of mature neurons (NeuN+, $n = 3$, $p < 0.05$) compared to control.

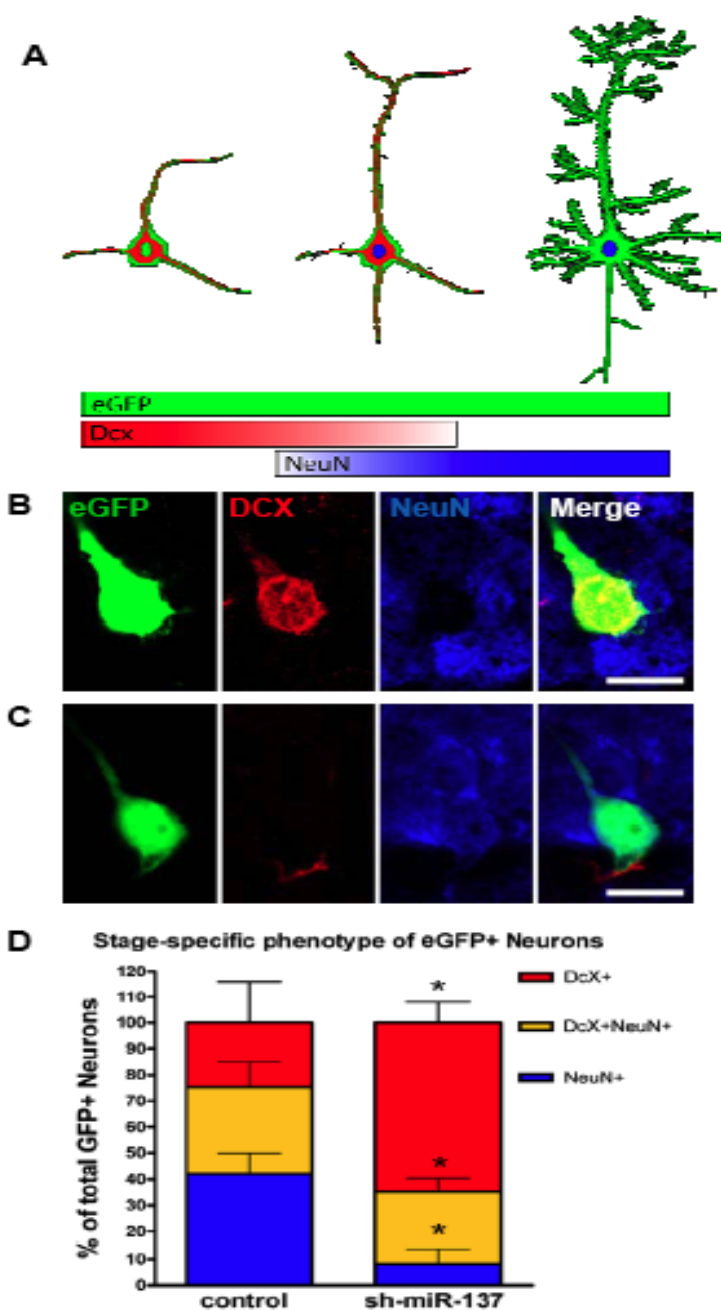


Figure 3. Overexpression of miR-137 leads to altered neuronal maturation of new neurons in vivo. **A.** Illustration showing the stage-specific neuronal markers that can be used to identify the maturation state of developing DG granule neurons. **B-C.** Confocal images showing representative eGFP-expressing neurons in the DG. **B.** A relatively immature eGFP neuron expressed DCX (immature marker) but not NeuN (mature neuron). **C.** A mature eGFP+ neuron expressed NeuN but not DCX. **D.** The miR-137-overexpressing neuron population had decreased proportions of NeuN+ only (blue) mature neurons and of DCX+/NeuN+ (yellow) transitioning neurons, but increased proportion of DCX+ only (red) immature neurons compared with control ($* = p < 0.05$).

Additionally, there was a 19% decrease in the proportion of transitioning neurons (NeuN+/DCX+, $n = 3$, $p > 0.05$) and a 62% increase in the proportion of immature neurons (DCX+, $n = 3$, $p = 0.05$) compared to control. Therefore, this indicates that elevated levels of miR-137 alter the sequential events leading to the development of a mature dentate granule neuron. Taken together, these *in vivo* data suggest that increased expression of miR-137 in newborn neurons results in decreased dendritic development.

miR-137 regulates neuronal dendritic development in vitro

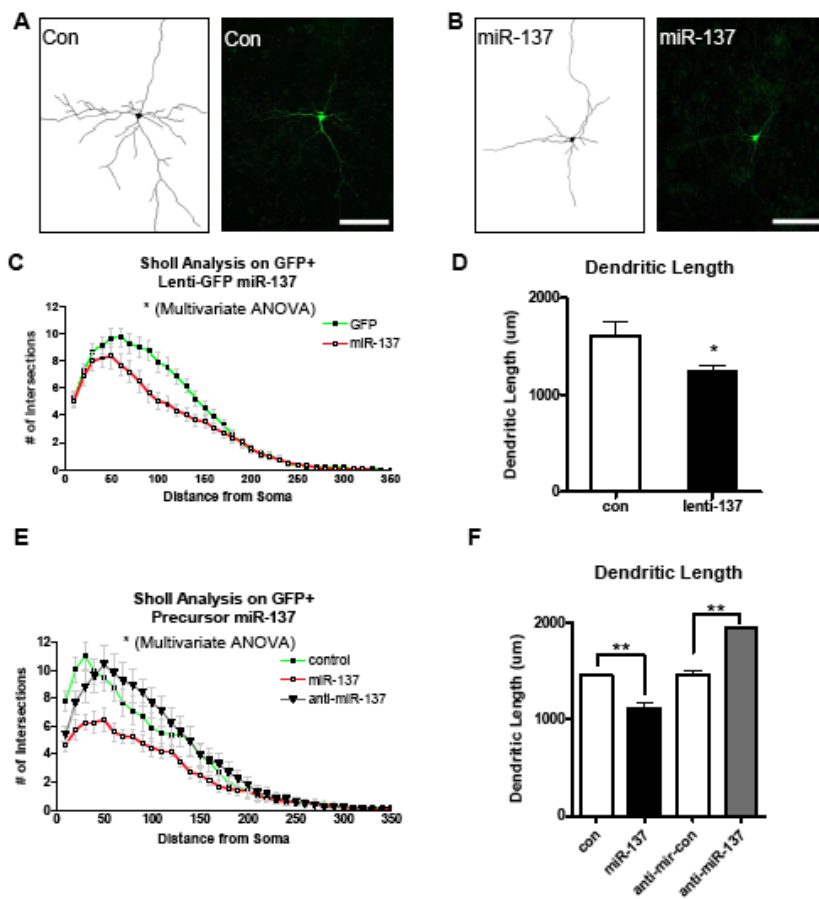
To investigate whether miR-137 overexpression affects neuronal maturation independent of its effect on the neuronal differentiation of neuroprogenitors, primary neurons were isolated and cultured for both gain-of-function and loss-of-function experiments. Hippocampal neurons serve as a good model for studying molecular mechanisms controlling dendritic and spine development, because they form elaborate dendritic trees, functional synapses, and they can respond to both chemical and electrical stimulation (Goslin and Banker 1989; Fletcher, Church et al. 1994; Okabe, Collin et al. 1998). Neurons were isolated from E17.5 mouse embryos and plated onto serum-free medium to limit astrocyte proliferation. To modulate miR-137 expression, miR-137 was expressed using two different gain-of-function assays. First, miR-137 was expressed as a short-hairpin RNA using a lentiviral vector coexpressing eGFP (Tsuda, Han et al. 2008). Second, synthetic double stranded miR-137 was cotransfected with an eGFP expression plasmid. Concurrently, loss-of-

function assays were performed by blocking endogenous miR-137 using 2'-O-methylated antisense oligonucleotides.

At 48 hours post-transfection, dsRNA-eGFP-expressing neurons were imaged, and the morphology of the soma, dendrites, and axons were manually traced and measured using Neurolucida (MicroBrightField, Inc.) image analysis software (Figure 4). Transfected eGFP+ neurons had clearly identifiable dendrites and axons. Axons were distinguished from dendrites by two characteristics: axons are the longest among all processes and have negative staining for MAP2, a somatodendritic marker (Jugloff, Jung et al. 2005). The morphology of cultured hippocampal neurons is not as uniform as developing neurons in the DG of the hippocampus, which may account for the variability observed in neuronal morphometry. However, the morphological differences between neurons expressing miR-137 and controls were apparent. Neurons transfected with plasmid expressing sh-miR-137 had a significantly reduced dendritic complexity ($F(1,52) = 5.15, p < 0.05$ multivariate analysis of variance) (Figure 4C) and 23% reduction in total dendritic length ($n = 3, p < 0.05$) (Figure 4D) compared with sh-control transfected neurons. Consistent with this result, neurons transfected with synthetic miR-137 also showed a 23% reduction in dendritic length and reduced dendritic length compared with control miR (miR-C) transfected neurons ($n = 3, p < 0.01$) (Figure 4F). On the other hand, neurons transfected with a specific inhibitor of miR-137 (anti-miR-137) had increased dendritic complexity ($F(2,51) = 3.58, p = 0.036$ multivariate analysis of variance) (Figure 4E) and a significant 25% increase in total dendritic length ($n = 3,$

$p < 0.01$) (Figure 4F) compared with anti-miR control (anti-C) transfected neurons. The total number of dendritic ends and nodes had a similar trend of a reduction in neurons transfected with miR-137 and an increase in anti-miR-137-transfected neurons; although these differences did not reach statistical significance. These loss-of-function and gain-of-function data in primary neurons further support our *in vivo* observation that high levels of miR-137 inhibit neuronal dendritic development.

Figure 4. miR-137 is important for dendritic development *in vitro*. A-B. E17 primary hippocampal neurons



were transfected with lentiviral vectors expressing either control miR (A) or miR-137 (B), as well as eGFP. Single eGFP-expressing neurons were shown next to their representative traces (scale bar = 50 μm; 20x/oil). C. Sholl analysis showing neurons overexpressing sh-miR-137 had reduced dendritic complexity compared with neurons overexpressing sh-Control. D. Neurons overexpressing sh-miR-137 had reduced total dendritic length compared with controls. E. Sholl analysis showing that neurons overexpressing miR-137 had reduced dendritic complexity compared with controls, whereas neurons transfected with a anti-miR-137 had opposite effect. F. Neurons overexpressing miR-137 had reduced total dendritic length compared with neurons overexpressing control miR. On the other hand, neurons

transfected with anti-miR-137 showed increased dendritic length compared to neurons transfected with control anti-miR. (*, $p < 0.05$, **, $p < 0.01$).

Expression of Mib1 rescues the miR-137-mediated reduction in dendritic complexity

To determine how miR-137 affects dendritic morphology during neuronal development, a bioinformatic approach was used to identify putative mRNA targets of miR-137. TargetScan 4.1, PicTar, and miRanda were referenced to compile a set of potential candidate targets (Lewis, Shih et al. 2003; John, Enright et al. 2004; Krek, Grun et al. 2005). Targets were then selected for further analyses based on 3 criteria: conservation, context score of target “seed sequences,” and known relevance to dendritic morphogenesis and neuronal development. Among the candidate miR-137 targets are Ezh2, EphA7, EphB2, Shank2, Snap23, and Mib1. Interestingly, Mib1, a mouse homolog of *Drosophila* Mind bomb 1 (Mib1), is an E3 ubiquitin ligase that has been directly implicated in dendritic development (Figure 5A) (Itoh, Kim et al. 2003). To test whether miR-137 could in fact target Mib1, we cloned the 3'-untranslated region (3'-UTR) of *Mib1* from mouse cDNA into a Renilla luciferase (R-luc) reporter construct (Figure 5B). This allows us to assess Mib1 protein translation through the *Mib1* 3'-UTR. The 3'-UTR R-luc construct along with a firefly luciferase (f-luc) control plasmid was cotransfected into cultured primary neurons. We found that overexpression of miR-137 suppressed over 50% of the R-luc activity in primary neurons at 48 hours post-transfection (n = 7, p < 0.001) (Figure 5C). On the other hand, transfected anti-miR-137 led to a 28% increase in R-luc activity compared with the antisense control (n = 3, p < 0.05) (Figure 5E). To further validate the interaction between miR-137 and its target *Mib1* 3'-UTR, we mutated the seed sequence of miR-137 located within the *Mib1*-3'-UTR reporter (Figure 5A,B). This mutation substantially alleviated the miR-137-mediated

suppression of luciferase activity, suggesting that the action of miR-137 is specific to the miR-137 seed region within the *Mib1*-3'-UTR ($n = 5$, $p < 0.001$) (Figure 5D).

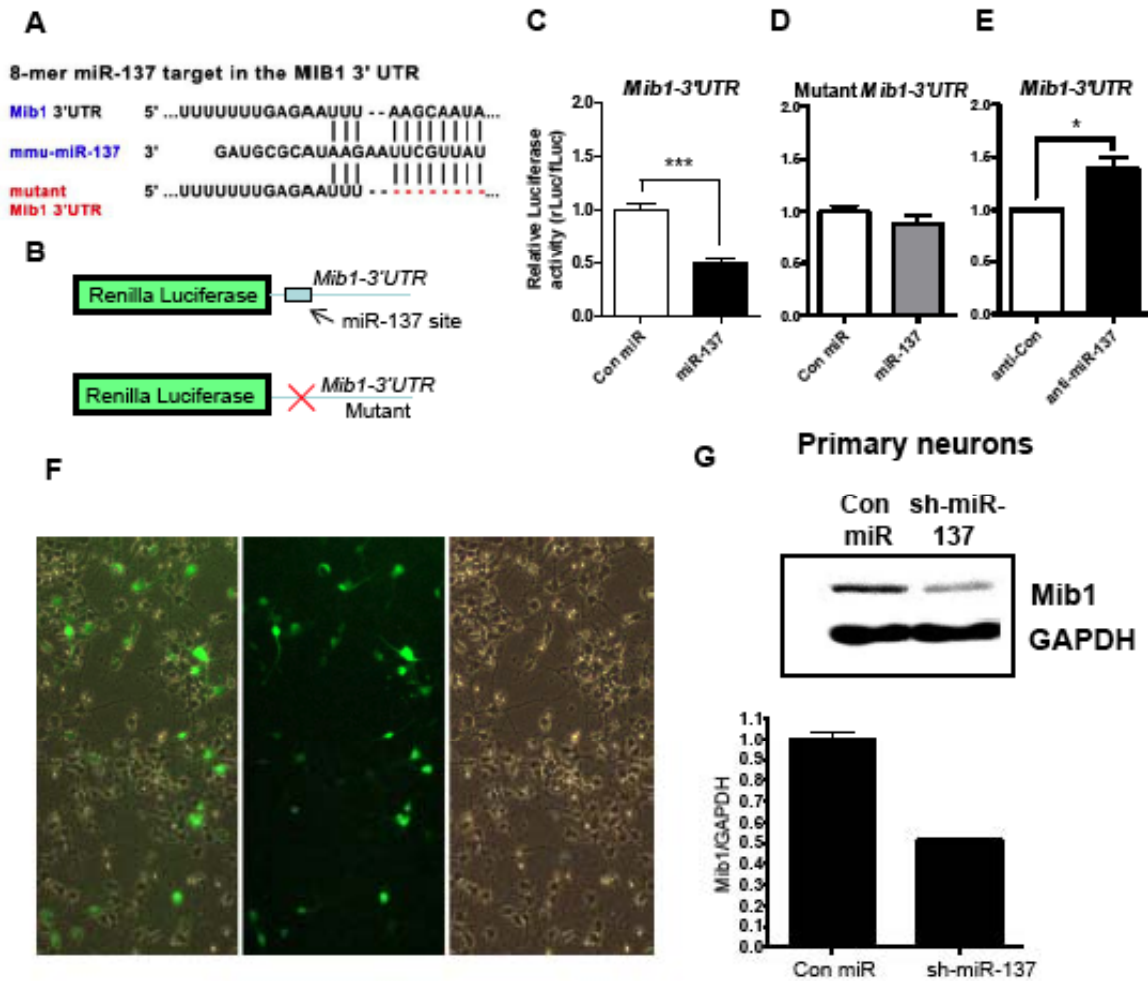


Figure 5. Mib1 is a functional target of miR-137. **A.** A miR-137 target site was found in the *Mib1* 3' untranslated region (3'UTR) as predicted by TargetScan software. The Mutant *Mib1* 3'UTR used in B-E with miR-137 site deleted is shown. **B.** Schematic diagram showing the predicted seed region where miR-137 is expected to bind the rLuc-*mib1* 3'-UTR (upper), and the mutated version lacking the binding site for miR-137. **C-E.** The result of miR-137 coexpression was calculated relative to the control. **C.** *Mib1*-3'-UTR-dependent expression of a Renilla luciferase reporter gene (R-luc) was suppressed by miR-137 over 50% in DIV6 primary neurons at 48 hours post-transfection ($n = 7$, $p < 0.001$). The 3'-UTR-dependent Renilla luciferase (rLuc) activities were normalized to control firefly luciferase (fLuc) activities in C-E. **D.** The mutant *Mib1*-3'-UTR alleviated the miR-137-mediated suppression of luciferase activity, suggesting that the action of miR-137 is specific to the miR-137 seed region within the *Mib1*-3'-UTR ($n = 5$, $p < 0.001$). **E.** *Mib1*-3'-UTR-dependent expression of rLuc was enhanced 28% by anti-miR-137 ($n = 3$, $p < 0.05$). **F.** 10x fluorescence and bright field images showing high infection efficiency of lentivirus expressing sh-miR-137 (also eGFP) in E17 primary cortical neurons. **G.** Primary neurons infected with lentivirus expressing sh-miR-137 had reduced Mib1 protein expression compared with control at 48 hours post-infection. (* = $p < 0.05$; *** = $p < 0.001$).

To investigate the effect of miR-137 on endogenous Mib1 expression in neurons, we used the same lentivirus expressing sh-miR-137 and eGFP to infect cultured primary neurons. Lentivirus transduction allows us to achieve relatively high expression efficiency in mouse primary neurons (Figure 5F). Neurons infected by lenti-miR-137 had a 10% decrease in endogenous Mib1 expression compared with sh-control virus-infected neurons ($n = 3$, $p < 0.05$) (Figure 5G). Taken together, these data suggest that miR-137 regulates the protein expression of Mib1 through the 3'-UTR of Mib1.

Targeting of Mib1 by miR-137 suggests that the reduction in dendritic complexity caused by overexpression of miR-137 might be rescued by restoring Mib1. Indeed, when neurons were cotransfected with Mib1 expression plasmid and a synthetic miR-137 dsRNA, Mib1 overexpression rescued the miR-137-mediated reduction both in dendritic length ($n = 4$, 14% difference between Mib1+miR137 and control, 31% difference between Mib1+miR137 and miR-137) (Figure 6A) and in dendritic complexity ($F(1,35) = 18.51$, $p < 0.001$) (Figure 6C). It was also noted that, as expected for a functional interaction between miR-137 and Mib1, overexpression of Mib1 alone led to significant increases in both dendritic length ($n = 4$, +39%, $p < 0.01$) and dendritic complexity ($F(1,36) = 23.00$, $p < 0.001$) compared with control vector-transfected neurons (Figure 6A,B). These data suggest that miR-137 regulates dendritic morphogenesis in developing neurons, at least in part, by translational regulation of Mib1 (Figure 6D).

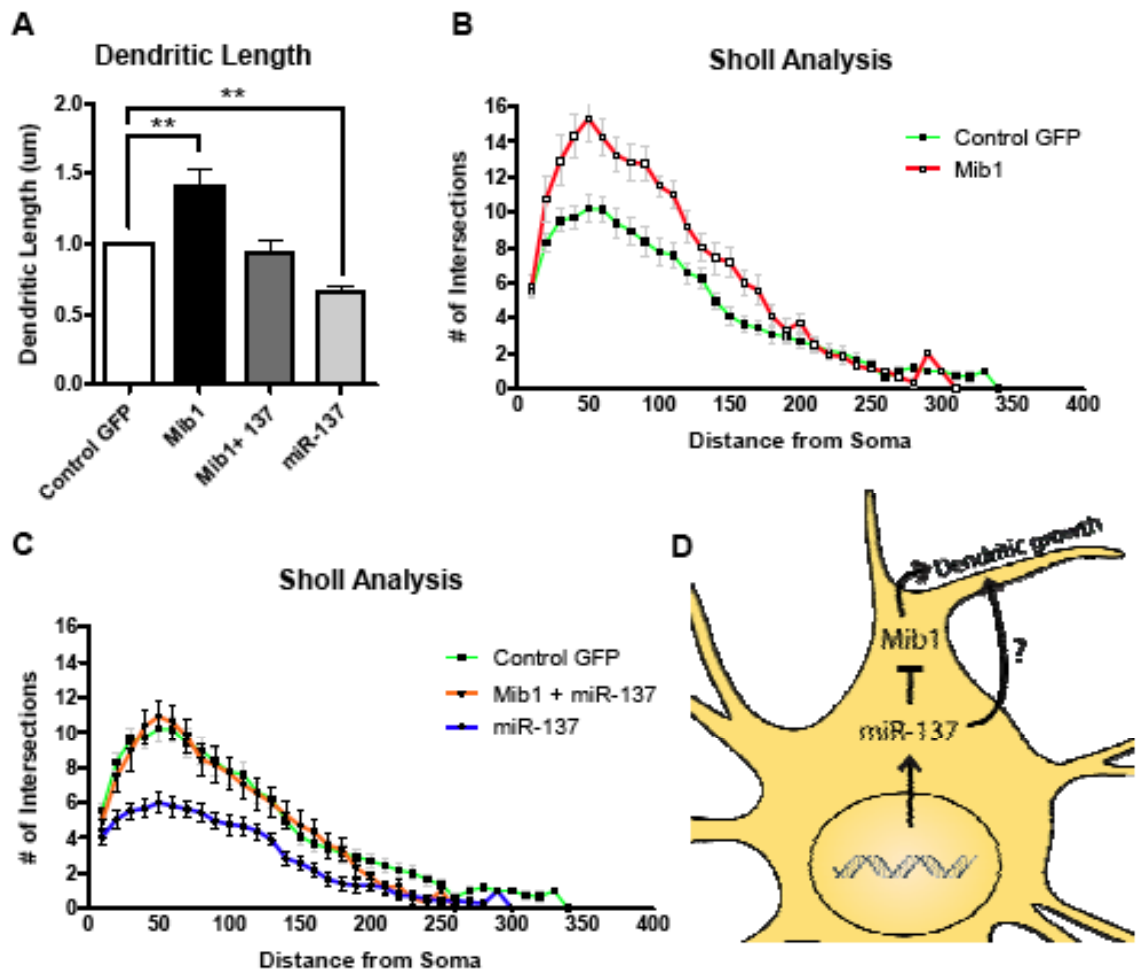


Figure 6. Mib-1 could rescue the neuronal maturation deficits associated with miR-137 overexpression *in vitro*. A,B. Overexpression of Mib1 could enhance the dendritic length (A) and complexity (B). C. Mib1 could rescue the miR-137-mediated reduction in dendritic length and complexity. (* = $p < 0.05$; ** = $p < 0.01$; *** = $p < 0.001$). D. Model illustrating that miR-137 regulates dendritic morphogenesis in developing neurons, at least in part, by translational regulation of Mib1.

Discussion

We have discovered a number of miRNAs that are enriched in NSCs differentiated into the neuronal lineage relative to either astrocyte lineage or undifferentiated NSCs. We demonstrated that one of these miRNAs, miR-137, has an important modulatory role in dendritic morphogenesis during neuronal development both *in vivo* and *in vitro*. We find that overexpression of miR-137 using the “single-cell

genetic approach” in newborn neurons of the adult hippocampus results in reduced dendritic complexity and spine density; however, since the single-cell genetic approach specifically targets proliferating cells prior to neuronal differentiation, we also demonstrated that overexpression of miR-137 has the same effect on post-mitotic cultured hippocampal neurons. Both overexpression and inhibition of miR-137 have significant but opposite effects on dendritic complexity, suggesting that a specific level of miR-137 expression is required for the normal dendritic development of hippocampal neurons.

The potential functions of miRNAs acting locally at the neuronal dendritic spines have only recently been studied (Smalheiser and Lugli 2009). As stated in the background, several miRNAs are found to be localized and functioning in dendrites and synapses. Among them, miR-132 and miR-137 are both found to be enriched in dendritic spines, but whereas miR-132 represses spine volume, miR-137 shows no effect on spine volume (Siegel, Obernosterer et al. 2009). Therefore it is likely that individual miRNAs at the synapse play specialized roles in dendritic morphogenesis and synaptic development. The most challenging step in determining the function of miRNA is to identify their downstream mRNA targets. It has been well demonstrated that each miRNA can have many potential mRNA targets based on bioinformatic software. However, only small number of predicted targets may be functional. In addition to Mib1, several additional miR-137 targets are strongly associated with neuronal development and synaptic function such as Ezh2, EphA7, EphB2, Shank2, and Snap23. We cannot exclude the possibility that miR-137 could

function by modulating the translation of multiple genes simultaneously. Further experiments in identifying additional miR-137 targets will provide more complete picture in miR-137 functions during neurodevelopment

Additionally, our ISH data (Figure 1) shows miR-137 expression is wide-spread in the DG suggesting that miR-137 may function in both developing and mature neurons. An interesting question to pursue is whether miR-137 could mediate neuronal activity-dependent dendritic development. One may speculate that miRNAs in the dendrite could participate in the regulation of local protein translation and modify synaptic plasticity at the synaptic compartment; however, the complete picture of how miRNAs and their dendritic target mRNAs regulate dendritic morphogenesis and synaptic development is still in its infancy and is a critical area of future neurodevelopmental studies.

Although there are many potential targets of miR-137 in neurons, we chose to follow ubiquitin ligase Mind bomb 1 (Mib1) because it too was previously shown to be enriched in the postsynaptic compartment by mass spectrometry (Choe, Liao et al. 2007; Sheng and Hoogenraad 2007). Loss of Mib1 leads to reduced lateral inhibition in Notch signaling, causing changes in the number of progenitors and altered neuronal differentiation during zebrafish CNS development (Itoh, Kim et al. 2003). Mib1 promotes ubiquitination and internalization of the Notch ligand Delta, leading to Notch pathway activation. In mammals, the function of Mib1 is not fully clear. In one study, Mib1 was found to activate the Notch pathway in embryonic

mice, and Mib1 mutant mice exhibit deficits in neurogenesis that resemble mice lacking Notch signaling components (Koo, Lim et al. 2005). Mib1 has also been shown to be phosphorylated by PAR-1 resulting in Mib1 degradation, and stimulation of neuronal differentiation in mammalian neuronal progenitors (Ossipova, Ezan et al. 2009). Similarly, Notch activation by Mib1-positive newborn neurons and intermediate progenitors in mice functions to ensure the maintenance of radial glial stemness during neurodevelopment (Yoon, Koo et al. 2008). However, the precise role of Mib1 in mammalian dendritic development is unknown. A recent study has shown that Mib1 inhibits dendritic development in cultured rat cortical neurons (Choe, Liao et al. 2007). Nevertheless the importance of Mib-1 in neuronal maturation is clearly demonstrated by both published literature and our data.

The possible roles of the E3 ubiquitin ligase Mib1 in neuronal maturation are intriguing. The ubiquitin pathway is best-characterized for its role in marking target proteins for specific proteolysis by proteasomes. However, the ubiquitin pathway may also be involved in regulating abundance of postsynaptic receptors (Burbea, Dreier et al. 2002). Neuronal deficiency of UBE3A, an ubiquitin protein ligase involved protein degradation, results in Angelman Syndrome, which is characterized by severe mental retardation. In a recent studies, the UBE3A was found to localize to the synapse and its deficiency results in abnormal dendritic and spine morphology (Dindot, Antalffy et al. 2008; Lu, Wang et al. 2009). Mib1 seems to be involved in protein trafficking rather than protein degradation (Itoh, Kim et al. 2003). It may modify post-synaptic receptors or other regulatory molecules at the

synapse and alter their intracellular localization, hence the dendritic patterning in developing and mature neurons. The fact that Mib1 can rescue the dendritic deficits associated with miR-137 overexpression further supports the positive effect of Mib1 in mammalian dendritic morphogenesis and its role as one of the downstream effectors of miR-137. Understanding this pathway may also shed light on the molecular mechanism underlying neurodevelopmental disorders with neuronal dendritic deficits.

Materials and Methods

Animals

Wildtype C57/B6 mice were used for in vivo and in vitro studies. For histological analyses, mice were euthanized by intraperitoneal injection of sodium pentobarbital. Mice were then perfused with saline followed by 4% PFA. Brains were dissected out, post-fixed overnight in 4% PFA, and then equilibrated in 30% sucrose. Forty-micrometer brain sections were generated using a sliding microtome and were stored in -20°C freezer as floating sections in 96-well plates filled with cryoprotectant solution (glycerol, ethylene glycol and 0.1 M phosphate buffer, pH 7.4, 1:1:2 by volume).

Isolation and differentiation of aNSCs.

Adult aNPCs used in this study were isolated from adult C57B/L6 male mice based on published methods (Zhao, Ueba et al. 2003). NSC differentiation was carried out using our established method (Barkho, Munoz et al. 2008; Tsuda, Han et al. 2008).

Relative quantification of mature miRNAs by Taqman miRNA real-time PCR

Mature miRNA expression was assayed using Applied Biosystems' TaqMan microRNA assays (miRNA Hu Panel, Early Access Kit PN4365381 or individual TaqMan miRNA assays) with individual reverse transcription and TaqMan microRNA real-time PCR according to protocols provided by the vendor (Lao, Xu et al. 2006). Briefly, 15 μ l reverse transcription reactions consisted of: 10ng total RNA isolated by TRIzol, 1X TaqMan miRNA Reverse Transcription Primer, 1.0 mM of each dNTP, 50.0 U MuLV Reverse Transcriptase, 1X Reverse Transcription Buffer, 0.25 U/ μ l RNase Inhibitor, and nuclease-free water. All reverse transcription reactions for profiling experiments were prepared in parallel using a Beckman Coulter Biomek FX automated pipettor. Reactions were incubated at 16°C for 30 min, 42°C for 30 min, and 85°C for 5 min. Individual TaqMan miRNA real-time PCR reactions for profiling experiments were performed on an Applied Biosystems 7900HT SDS in a 384-well format. For individual TaqMan miRNA assays experiments were performed on a Applied Biosystems 7500 Fast instrument, using the same conditions. PCR reactions were carried out in triplicate for each sample and each miRNA. 10 μ l PCR reactions consisted of 1X TaqMan Universal Master Mix, No AmpErase UNG, 1X TaqMan miRNA assay mix, 1.33 μ l cDNA, and nuclease-free water. All TaqMan PCR reactions for profiling experiments were prepared and aliquoted using a custom method on a Beckman Coulter Biomek FX automated pipettor. PCR reaction conditions were run under the Standard protocol without the 50°C incubation using version 2.3 of the SDS software, with reactions incubated at

95°C for 10 min, followed by 40 cycles of 95°C for 15 sec, and 60°C for 1 min. miRNA relative quantities (RQ) were determined using the $\Delta\Delta C_t$ method and either 18S rRNA (profiling experiments) or RNU6B (individual miRNA experiments) were used as an endogenous controls (Livak and Schmittgen 2001). 18S rRNA expression was assayed by real-time PCR of cDNA generated by standard SuperScriptIII random hexamer reverse transcription of 500ng total RNA isolated by TRIzol according to the manufacturer's protocols (Invitrogen). 10 μ l real-time PCR reactions were performed in triplicate and consisted of 1X SYBR Green Master Mix, 0.5 μ M forward and reverse primers (FW-5'- CGGCTACCACATCCAAGGAA, RV-5'- CCTGTATTGTTATTTTCGTCACTACCT), 1 μ l 1:10 diluted cDNA, and nuclease free water. All relative quantity (RQ) calculations were calibrated to undifferentiated A94 NSCs. RQ values and the associated error were determined using Applied Biosystems SDS v1.2 RQ manager or 7500 Fast System SDS Software v1.3.1 to calculate mean RQ and RQmin/max values based on a 95% confidence interval. Undifferentiated A94 NSCs were run in parallel with lineage specific differentiated A94 NSCs as paired samples. Data from the replicate experiments on undifferentiated A94 NSCs was then pooled and a single analysis of miRNA expression in each NSC lineage relative to undifferentiated NSCs was determined within the SDS v1.2 RQ manager to obtain the reported values.

miRNA In situ hybridization

Following transcardial perfusion, brain tissue was equilibrated in 30% sucrose, then embedded in OCT (Tissue Tek) and frozen in liquid nitrogen-cooled isopentane. 10

μm thick serial cryosections were cut in the sagittal plane on a Leica CM3050S cryomicrotome and stored at -20°C until hybridization could begin. In situ hybridization was carried out as outlined previously with a few modifications (Oberosterer, Martinez et al. 2007). Following tissue processing, slides were air-dried, then fixed in 4% PFA and washed in DEPC-treated PBS. Slides were then acetylated (590 ml DEPC water, 8ml triethanolamine, 1050 μl 37% HCl and 1.5 ml acetic anhydride), washed in PBS, treated with Proteinase K (5 $\mu\text{g}/\text{ml}$) and washed again. Slides were then prehybridized (50% formamide, 5X SSC, 5X Denhardt's, 200 $\mu\text{g}/\text{ml}$ yeast RNA, 500 $\mu\text{g}/\text{ml}$ salmon sperm DNA, 0.4g Roche blocking reagent and 1.75 ml DEPC water) for 4-8 hours at RT. For hybridization 0.1 μl of 25 μM DIG- or FITC-labeled LNA probe was added to 100 μL hybridization buffer (same as prehybridization buffer but with 500 μl 10% CHAPS, 100 μl 20% Tween and 1.15ml DEPC water) and applied to the tissue at 50-60C overnight ($\sim 20^{\circ}\text{C}$ below the predicted melting temperature (T_m) of probe:miRNA). Following hybridization, slides were washed in 5X and 0.2X SSC at 60C, followed by buffer B1 (0.1M Tris pH 7.5/0.15M NaCl) at RT. Sections were then blocked in 10% FCS in B1 and probed with anti-DIG/FITC-HRP antibodies as well as anti-synapsin and anti-neurofilament H. Following incubation in primary antibodies, slides were washed in B1 and then equilibrated in buffer B3 (0.1M Tris pH 9.5/0.1M NaCl/50 mm MgCl_2) for 10 minutes. Developer solution (100mg/ml NBT, 50 mg/ ml BCIP, 24 mg/ml levamisol and 10% Tween in B3) was then added to the tissue for ~ 4 hours RT. The reaction was stopped with washes in PBT, and sections were then probed with dye-coupled

secondary antibodies. Following final washing steps, slides were mounted in Aquamount and visualized using confocal microscopy.

Nucleic acid and expression constructs

Control shRNA (miR-C), miR-137, anti-miR-137, and anti-miR control (Anti-C) were purchased from GenePharma (Shanghai, China) or Ambion (AM17100, AM17110, AM17000, and AM17010, Austin, TX). mib1 expression plasmid was obtained from where (Jumin Peng mib-1 paper) Lentivirus-shControl was described previously (Barkho, Munoz et al. 2008; Li, Barkho et al. 2008). PCR based generation of the miR-137 shRNA driven by a U6 Pol III promoter was done as described in our publications (Barkho, Munoz et al. 2008; Li, Barkho et al. 2008) with the following PAGE purified long oligos:

shRNA	miR-137	(U6-miR-137-shRNA):	5'-
TATCGATAAAAAATTATTGCTTAAGAATACGCGTAGTCTCTTGAACACTACGCGTATTCT			
TAAGCAATAAAAAACAAGGCTTTTCTCCAAGGGA-3'			

Briefly, long oligo was used as reverse primers in combination with a common forward primer complementary to the 5' end of the U6 promoter (5'-AAAGTAACTAGTGGATCCGACGCCGCATCTC-3') to amplify the entire U6 promoter and shRNA in a single PCR product. Amplification was done using 20 ng of a previously generated U6-shRNA lentiviral construct (Tsuda, Han et al. 2008) with Applied Biosystems AmpliTaq Gold PCR (1X PCR buffer, 2.2 mM MgCl₂, 0.2 mM dNTP mix, 0.2 mM forward primer, 0.2 mM reverse primer, 1.75 U AmpliTaq Gold) at 95°C for 9 min, 40 cycles of 94°C for 1 min and 60°C for 1 min, followed by 60°C

for 10 min, and then storage at 4°C. We used 2 µl of PCR product in a TOPO TA cloning reaction with pCR2.1 vector and chemical transformation of TOP-10 competent cells (Invitrogen, K4500-01SC). U6-shRNA expression cassettes were removed from the TOPO vector and transferred to lentiviral and retroviral vectors by HpaI and ClaI restriction digestion followed by ligation. The lentiviral vectors expressing miR-137 or control shRNA were then verified by sequencing.

Neuronal culture

Hippocampal neurons were isolated from E17.5 fetal mice, and grown as described previously (Washbourne, Thompson et al. 2002; Tafoya, Mameli et al. 2006). Hippocampal neurons from wildtype E17.5 fetal mice were grown as dispersed mixed cell cultures, as established by the Wilson lab (Washbourne, Thompson et al. 2002). Briefly, hippocampi were micro-dissected in ice cold HBSS (Gibco). Hippocampi were then incubated in 0.05% trypsin-EDTA (Invitrogen, Carlsbad, CA) for 25 minutes at RT, then to Neurobasal A medium (Invitrogen) supplemented with 25 nM glutamate, 0.5 mM L- glutamine, and 1% antibiotics. Neurons were triturated with flame polished Pasteur pipettes and plated on poly-L-lysine/laminin coated 12 mm coverslips (3 coverslips/animal, ~150,000 cells/coverslip; BD biosciences Cat# 354087). After 4 DIV, glutamate was removed from the culture medium, and medium was changed every third day.

Transfection and of E17 hippocampal neurons

Hippocampal neurons were transfected on day 4 (DIV 4) as they are undergoing dendritic and axonal morphogenesis during this time. Transfection was performed as described (Tafoya, Mameli et al. 2006). Briefly, Lipofectamine 2000 (Invitrogen) was diluted in OptiMEM medium (GIBCO Invitrogen). 1 μ g of total DNA (or 50 μ m double stranded microRNA or single stand anti-microRNA) and 4 μ g of Lipofectamine 2000 reagent was used per coverslip. After incubation of transfection reagents at RT and gentle mixing, the reagent mix was applied to the cells in fresh Neurobasal A medium (Invitrogen) supplemented with 0.5 mM L-glutamine (no antibiotic), and the cultures were placed in a 37°C, 5% CO₂, humidified incubator. 48hours after transfection, the neurons were fixed and stained as described below. Transfection efficiencies were 1-2%.

3'-UTR dual luciferase assays of miR-137 target mRNA

3'-UTR sequences of candidate mRNAs were PCR amplified directly from proliferating aNSC first strand cDNA generated from 5 μ g TRIZOL-isolated total RNA using oligo-dT SuperScript III reverse transcription according to the manufacturer's protocol (Invitrogen, Cat. #1808-093). These primer sequences are available upon request. All primers were designed incorporating XhoI and NotI restriction sites and 4 bp of extra random sequence to aid in restricting digestion. XhoI- and NotI-digested PCR products were cloned into XhoI- and NotI-digested psiCHECK-2 dual luciferase vector (Promega, Cat# C8021) and were later transferred by XhoI/NotI double digestion and T4 DNA ligation into a pIS2 renilla luciferase vector modified with the addition of an XhoI restriction site and deletion of the SpeI restriction site.

miR-137 target site deletion was done using the QuickChange Site-Directed Mutagenesis Kit (Stratagene, Cat. #2000518) to delete UUCGUUAU. Briefly, E17 hippocampal neurons were cultured (as described above), and co-transfected by Lipofectamine 2000 with pIS2 renilla luciferase vector containing the MIB1 3'UTR, pIS0 firefly luciferase as a transfection control, and Control shRNA, miR-137, or anti-miR-137. All co-transfections used a total of 1 µg of plasmid DNA and 50ng of shRNA. Luciferase expression was detected using the Dual-Luciferase Reporter 1000 System (Promega, Cat# E1980) per the manufacturer's protocol. Briefly, 48 h after transfection, the cell culture medium was removed and cells were lysed with 20 µl of 1X passive lysis buffer at room temperature for 15 min. We then added 100 µl Luciferase Assay Buffer II and mixed briefly. Firefly luciferase (F-luc) activity was immediately read using a SpectraMax M2E (Molecular Devices Corp.). Next we added 100 µl Stop & Glo buffer with Stop & Glo substrate and mixed briefly. Renilla luciferase (R-luc) activity was immediately read. R-luc activity was normalized to F-luc activity to account for variation in transfection efficiencies, and miR-137-mediated knockdown of R-luc activity was calculated as the ratio of normalized R-luc activity in the U6-miR-137-shRNA treatments to normalized R-luc activity in the U6-neg-shRNA treatments. All luciferase readings were taken from 3-4 individual wells from each condition tested. Luciferase experiments were repeated at least three times. At 28-h post-transfection, hippocampal neurons were collected using cell lysis buffer from a Dual-Luciferase Reporter Assay System kit (Promega, #E1910). Luciferase activity was measured using a Veritas Microplate Luminometer

(Turner Biosystems) as described. The luciferase counts were then normalized to R-luc counts to obtain final promoter activities.

Construction of retroviral vector expressing miR-137 and in vivo retroviral grafting

Retroviral vector expressing both miR-137 and eGFP was engineered by deleting the original HpaI and ClaI sites in the CAG-EGFP vector (Zhao, Teng et al. 2006; Smrt, Eaves-Egenes et al. 2007) and inserting new HpaI and ClaI sites 5'-upstream from the CAG promoter. The U6-shRNA cassettes were then inserted between the HpaI and ClaI sites. Retrovirus production was performed as described previously (Zhao, Teng et al. 2006; Smrt, Eaves-Egenes et al. 2007). Briefly, retroviral transfer vector DNA and packaging plasmid DNA were cotransfected with the packaging plasmids pCMV-gag-pol and pCMV-Vsvg into HEK293T cells using the calcium phosphate method. The medium containing retrovirus was collected at 40, 64, and 88 h post-transfection, then pooled, filtered through a 0.2- μ m filter, and concentrated via ultracentrifugation at 19.4k rpm for 2 h at 20°C (Beckman SW27 Rotor). The virus was washed once with phosphate-buffered saline (PBS) and then resuspended in 150 μ l PBS. We routinely obtain greater than $0.5-1 \times 10^9$ infectious viral particles/ml.

In vivo retroviral grafting was performed as described (Zhao, Teng et al. 2006; Smrt, Eaves-Egenes et al. 2007). Briefly, 7- to 8-week-old C57B/L6 male mice were anesthetized with isofluorane, and virus (1.5 μ l with titer greater than $5 \times 10^5/\mu$ l) was injected stereotaxically into the dorsal ganglia (DG) using the following coordinates relative to bregma: anteroposterior, $-(1/2) \times d$ mm; lateral, ± 1.8 mm

(if $d > 1.6$) or otherwise ± 1.7 mm; ventral, -1.9 mm (from dura). For each mouse, the control siRNA virus was injected into the left DG, and the miR-137 virus was injected into the right DG. Four weeks after viral grafting, mice were deeply anesthetized with pentobarbital and perfused with saline followed by 4% PFA. Brains were dissected out, post-fixed overnight in 4% PFA, and then equilibrated in 30% sucrose. $320\mu\text{m}$ or $40\mu\text{m}$ brain sections were generated using a sliding microtome and were stored in a -20°C freezer as floating sections in 96-well plates filled with cryoprotectant solution (glycerol, ethylene glycol, and 0.2 M phosphate buffer, pH 7.4, 1:1:2 by volume).

Production of lentivirus and infection of E17 hippocampal neurons

We produced lentivirus as described previously (Barkho, Song et al. 2006; Barkho, Munoz et al. 2008; Tsuda, Han et al. 2008). Briefly, lentiviral transfer vector DNA and packaging plasmid DNA were transfected into cultured 293T cells using calcium phosphate methods. The medium containing lentivirus was collected at 40, 64, and 88 h post-transfection, then pooled, filtered through a $0.2\text{-}\mu\text{m}$ filter. To study the effects of miR-137 on development of dendrites in cultured neurons, 1:1 solution of virus containing supernatant and Neurobasal A medium (Invitrogen) supplemented with 25 nM glutamate, 0.5 mM L- glutamine, and 1% antibiotics was added to the neurons 1 day after plating. After 24 hours, the medium was replaced with fresh virus containing solution described above, and was incubated for an additional 24 hours. Infected neurons were collected in cell lysis buffer for western blot analysis.

Microscopy and morphological analysis

For cultured hippocampal neurons, DIV 6 cells were fixed in 4% paraformaldehyde (PFA) for 10 minutes. Immunostaining was performed as previously described (Zhao, Ueba et al. 2003; Smrt, Eaves-Egenes et al. 2007; Barkho, Munoz et al. 2008; Tsuda, Han et al. 2008). The primary antibody used was MAP2ab (mouse, 1:500, Sigma). The secondary antibody used was Cy3 (donkey anti-mouse, 1:500, Sigma). Low transfection efficiencies (1-2% neurons) permit imaging and quantification of single GFP expressing neurons. GFP expressing neurons were imaged with an Olympus BX51 upright microscope with 20x/oil immersion lens, a motorized stage, and digital camera. Dendritic traces were performed in real time using NeuroLucida (MicroBrightField, Inc.) image analysis software. Neurons were selected for quantification by expression of both GFP and microtubule associated protein (Map2a+b). Cells were excluded if the processes had excessive overlapping with adjacent GFP expressing neurons, the morphology was not intact, had excessive membrane varicosities, or displayed signs of a cell death such as compacted chromatin structure revealed by DAPI staining. Using the tracing software, dendrites, axons, and the cell body of single GFP+/Map2+ neurons were traced. Roughly 15-25 neurons per coverslip were traced. Data was extracted for Sholl analysis, total dendritic length, node number, dendritic end number, total axon length, and cell body area for each GFP+/Map2+ neuron. Each GFP+/Map2+ neuron has been observed to have a clearly identifiable axon, which is always many times longer than the other processes. The axon is identified using Map2 staining where

the only process not positive for Map2 is the axonal process (Jugloff, Jung et al. 2005).

Immunohistochemistry and confocal imaging analysis on floating brain sections were carried out as described (Smrt, Eaves-Egenes et al. 2007). Floating brain sections containing eGFP+ cells were selected for staining and matched by DG region. The primary antibodies used were chicken anti- GFP (Invitrogen, #A10262), mouse NeuN (Chemicon, MAB377), and rabbit anti-doublecortin (DCX, Cell Signaling, #4604). The secondary antibodies used were anti-chicken Alexa Fluor 488 (Invitrogen, #A11039), goat anti-mouse Alexa Fluor 647 (Invitrogen, #A21236), and goat anti-rabbit Alexa Fluor 568 (Invitrogen, #A11036).

For thick floating brain sections, GFP+ neurons were imaged on a LSM 510 confocal with a 20x/oil objective. Z-stacks of GFP+ dendrites were captured at 8 μ m intervals and the dendrites and the cell body of single GFP+ neurons were analyzed by NeuroLucida software (MicroBrightField, Inc.). Roughly 30-50 neurons per DG were traced. Data was extracted for Sholl analysis, total dendritic length, branch number, dendritic end number, and cell body area for each GFP+ neuron. Neurons were selected for analysis based on expression of GFP throughout the cell body and its processes. Cells were excluded if they exhibit excessive overlapping with adjacent GFP expressing neurons, their morphology is not intact, they have membrane varicosities, or they show signs of cell death such as compacted chromatin structure revealed by DAPI staining.

For dendritic spine density analyses, 1-in-3 floating brain sections containing eGFP+ cells (120 μm apart, approximately 8 brain sections) were used for immunohistological staining using a protocol described elsewhere. The primary antibody used for amplification of eGFP was rabbit anti-GFP (Invitrogen, Eugene, OR). Briefly, for spine quantification, a minimum of 12-15 images of dendritic fragments were taken at 25-100 μm from the cell body of each eGFP+ neuron using a confocal microscope with an oil immersion objective (100x; NA = 1.3; Zeiss). Z-stacks at 1 μm intervals were taken and merged for a maximum intensity projection. For quantification of dendritic spines, protrusions were counted along 10 μm long dendrite segments measured using Image-J software (NIH Image). The “dendritic spine density” result was calculated as number of spines per 10 μm length of dendrite. A minimum of 40 dendritic fragments (10- μm each) from a minimum of 4 eGFP+ neurons were quantified from each animal. At least 3 animals from each genotype were analyzed and the final results were compared using a Student’s t-test.

For quantification of stage-specific neuronal markers in the DG, 40- μm thick coronal tissue sections containing hippocampus were stained with antibodies against DCX (1:1000, goat, Santa Cruz), NeuN, and DAPI. This procedure was performed based on the published method (Brown, Couillard-Despres et al. 2003). The immunofluorescence signals were captured using a spinning disk confocal microscope (Nikon Eclipse TE2000-U, 40x oil, 1.2 NA; Nikon). Quantification was

done by a person who was blind to the genotypes of the mice. We then counted the proportion of eGFP+/DCX+, eGFP+/NeuN+, or eGFP+/NeuN+/DCX+ out of total eGFP+ cells. Z-stacks taken at 1- μ m intervals were examined using MetaMorph imaging software (Molecular Devices Inc., Sunnyvale, CA).

Western blot analysis

Protein samples were separated on SDS-PAGE gels and then transferred to PVDF membranes (Millipore). Membranes were processed following the ECL Western Blotting protocol (GE Healthcare, Cat #RPN2106). Anti-Mib1 (M20a, gift from Junmin Peng) were used as primary antibodies at a 1:1000 dilution. HRP-labeled secondary antibodies were obtained from Sigma (A0545). For loading controls, membranes were stripped and reprobed with the antibody against GAPDH (Ambion AM4300).

Statistical analysis

All statistical analyses were performed using unpaired, two-tailed, Student's t-test. The data bars and error bars indicate mean \pm standard error mean. (s.e.m). Sholl analysis was analyzed using a multivariate analysis of variance (MANOVA) using SPSS statistical software (SPSS version 17, SPSS Inc., Chicago, Ill, USA).

Supplementary Figures

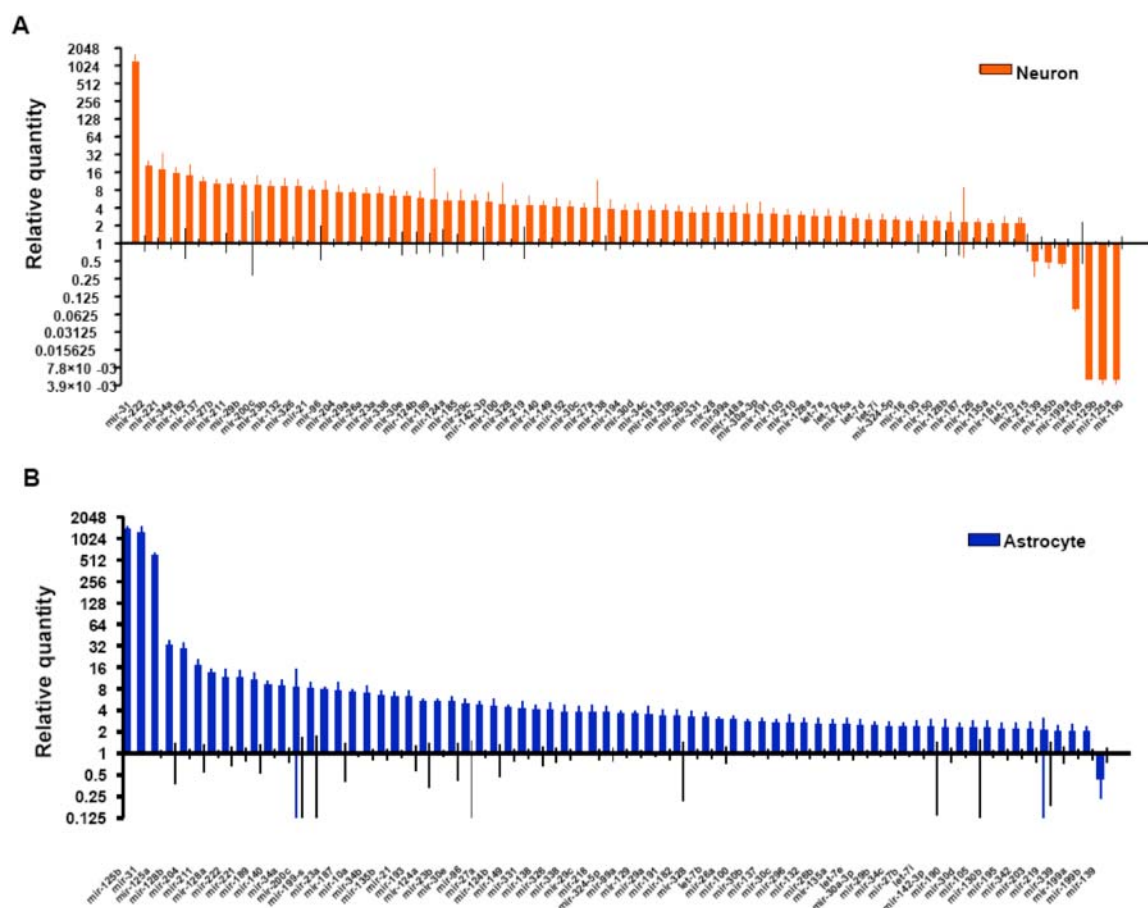


Figure S1. A94-NSC miRNA profiles **A.** miRNA expression profile for A94-NSCs treated according to a neuronal differentiation protocol. Relative quantity is calibrated to undifferentiated A94-NSC (n =3, mean with 95%CI). **B.** miRNA expression profile for A94-NSCs treated according to an astrocyte differentiation protocol. Relative quantity is calibrated to undifferentiated A94-NSC (n =3, mean with 95%CI).

Chapter 4: Identification of unannotated small noncoding RNA regulated by MeCP2 –Transcription start site associated RNAs reveal poised genes with altered expression in MeCP2-deficient neural stem cells

Abstract

Promoter proximal regulation of transcription reflects the poising of targeted genes for rapid responses to environmental cues. Such regulation is influenced by chromatin at transcription start sites (TSSs), implicating epigenetic processes in stimulus dependent transcription. Here the effect of MeCP2, an activity responsive epigenetic effector, on the expression of promoter proximal small RNA expression is assessed as a read out of promoter proximal transcription. 304 RefSeq transcripts exhibited differential small RNA expression at TSSs in MeCP2 deficient neural stem cells. Among these genes was *Pcdh10*, a protocadherin implicated in Autism-spectrum disorders that is also activity dependent in neurons. In MeCP2 deficient neural stem cells, increased TSS associated small expression at *Pcdh10* correlated with an equivalent increase in mRNA. A disproportionate increase in RNAPII occupancy relative to expression of *Pcdh10* in the absence of MeCP2 confirmed promoter proximal regulation of this gene. MeCP2 directly interacted near to the *Pcdh10* TSS and loss of MeCP2 correlated with an altered chromatin state that reflected *Pcdh10* expression. These results suggest an influence of MeCP2 on promoter proximal RNAPII activity at poised genes.

Introduction

Endogenous short RNAs associate with transcription start sites, RNA polymerase II presence, and histone modifications demarcating transcription in diverse eukaryotes (Nechaev, Fargo et al. ; Seila, Calabrese et al. 2008; Taft, Glazov et al. 2009). The production of these RNA has recently been linked to promoter proximal RNAPII stalling, a transcriptional regulatory process at many developmentally regulated and stimulus responsive genes. Rescue of stalled RNAPII near to transcription start sites involves cleavage of initiated transcripts by TFIIS, which subsequently rescues backtracked and arrested elongation complexes (Nechaev, Fargo et al.). Such cleavage by TFIIS predicts the generation of two RNA species that can be distinguished by specific end modifications and length. 3' to the TFIIS cleavage site would be a 5'phosphorylated RNA approximately the length which RNAPII backtracks (~18-20nt) (Taft, Kaplan et al. 2009). 5' to the TFIIS cleavage site would be a 7-methylguanosine (7mG) capped RNA whose length would be determined by the distance an elongating RNAPII travels prior to backtracking, minus the actual distance RNAPII backtracked, if at all. Indeed, both ~18nt 5'-phosphorylated RNAs and short 7mG-capped RNAs proximal to TSSs have been captured in small RNA sequencing experiments (Seila, Calabrese et al. 2008; Taft, Glazov et al. 2009). ~18 nt 5'-phosphorylated RNAs have been coined 'transcription initiation RNA' (tiRNA) and 'transcription start site associated RNA' (TSSa-RNA).

The overlapping proximity of stalled RNAPII and +1 nucleosomes has suggested a functional regulatory interaction between RNAPII and nucleosomes during the postinitiation step of transcription, a stage at which RNAPII activity is also intricately regulated (Mavrich, Jiang et al. 2008; Schones, Cui et al. 2008; Wang, Zang et al. 2008). +1 nucleosome positioning ~40nt downstream of TSSs in mammals thus predicts a peak of ~18nt 5' phosphorylated RNA to lie ~22nt downstream of TSSs. In fact, tiRNA and TSSa-RNA have been found to peak at approximately this distance downstream of TSSs (Seila, Calabrese et al. 2008; Taft, Glazov et al. 2009). TSSa-RNAs also exhibit a minor upstream antisense peak of expression around -170bp that is at least partially explained by the presence of widespread bidirectional transcription at active promoters. Here we have found that peaks of small RNA expression proximal to TSSs appear to be phased at nucleosome length intervals, directly suggesting that nucleosome occupancy does in fact influence promoter proximal small RNA expression.

We sought to assess an influence of chromatin based regulatory mechanisms on the production of promoter proximal small RNA by examining 5'-phosphorylated small RNAs in the presence or absence of the DNA methyl CpG binding protein 2 (MeCP2). MeCP2 has been linked to activity dependent transcriptional regulation in neurons through its association with multiple chromatin modifying complexes and transcription factors. At a subset of target genes, phosphorylation of MeCP2 upon membrane depolarization results in release of MeCP2 and altered mRNA expression (Chen, Chang et al. 2003; Martinowich, Hattori et al. 2003; Zhou, Hong et al. 2006;

Tao, Hu et al. 2009). Interestingly, MeCP2 has been reported as both an activator and repressor of transcription, consistent with a role in establishing and/or maintaining chromatin states that direct transcription (Chahrour, Jung et al. 2008). Such a role has recently been supported by observations indicating that MeCP2 is expressed at near histone octamer levels in neurons and globally influences the neuronal chromatin state (Skene, Illingworth et al.). Furthermore, human mutations in *MECP2* cause the majority of Rett Syndrome cases, suggesting a basis for activity dependent regulation of chromatin states and subsequent transcriptional responses in neurodevelopmental disease.

We hypothesized that MeCP2 may influence promoter proximal RNAPII activity through its widespread influence on chromatin states. By identifying specific TSSs at which promoter proximal 5'-phosphorylated small RNA expression was altered in the absence of MeCP2 we could distinguish putative MeCP2 targets that are more likely to invoke regulatory mechanisms associated with promoter proximal RNAPII stalling and exhibit developmental and/or stimulus responsiveness. Lastly, we find MeCP2 enriched proximally at particular genes producing small RNAs near TSSs, an indication that MeCP2 may directly influence expression of small RNA at TSSs and promoter proximal RNAPII activity. These results lend support to recent observations suggesting the involvement of activity dependent transcriptional regulation in neurodevelopmental disease and offer an alternative means by which to assess stimulus responsive genes in neural cell types.

Results

In total, >84.5 million adult neural stem cell (aNSC) 5'-phosphorylated small RNAs (14-30nt) were sequenced. This corresponded to ~42 million small RNA from both WT and *Mecp2*^{-/y} aNSCs, which served as a source of relatively homogenous enriched primary neural cells for assaying small RNA expression. This corresponded to >14.8 million reads which could be perfectly mapped to unique genomic locations (Table 1).

Summary of aNSC small RNA				
	WT	MeCP2 ^{-/y}	WT	MeCP2 ^{-/y}
Total reads	41676052	42864848		
3' Adapter Clipped	33877373 (81.3%)	34885522 (81.4%)		
	Unique		Total reads	
Collapsed/Unique	3900928	3515170	33877373	34885522
Aligned	307880	298171	7141408	7670651
miRNA	5092	4969	6462930	6911420
RepeatMasker	46649	50642	171375	190760
tRNA	20	30	31	53
snoRNA	2250	1733	63381	43820
Remaining	253869	240797	443691	524598

Table 1. Summary and annotation of aNSC small RNA obtained from WT and *Mecp2*^{-/y} aNSCs by SBS. Data are derived from combining two independent sequencing runs of separate biological replicates per genotype. Annotations were performed by sequentially removing known small noncoding RNAs, moving from top to bottom on the table (i.e. all miRNA were removed prior to identifying RepeatMasker associated small RNA and so on).

After the identification and removal of annotated noncoding RNAs (miRNA, Rmsk, tRNA, and snoRNA) sequences were most commonly 18nt in length (Fig 1 A&B), consistent with previous reports (Seila, Calabrese et al. 2008; Taft, Glazov et al.

2009). These sequences accounted for the second largest fraction of small RNA, besides annotated miRNA, and included 443,691 and 524,598 total reads in WT and *Mecp2*^{-y} aNSCs respectively.

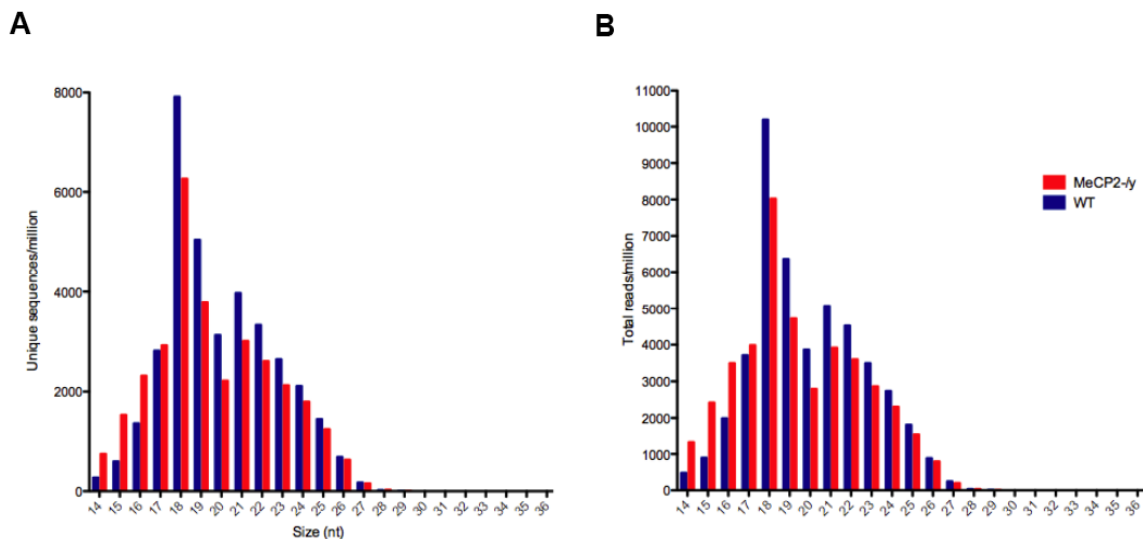


Figure 1. Size distributions of small RNA in WT and *Mecp2*^{-y} aNSCs. The “Remaining” small RNA from Table 1 were divided based on RNA length, indicating these sequences were most commonly 18nt. The total number of small RNA of a particular length was summed in each genotype and plotted based on the number of unique sequences (A) or total number of reads at each size (B).

Regions enriched for small RNA were characterized by comparing the distribution of small RNA around RefSeq TSSs to the distribution around random intergenic locations. A ~2kb region centered on TSSs was found to be significantly enriched for small RNA (Fig 2B). Small RNA near TSSs displayed a major peak 10-30nt downstream of TSSs in the sense orientation and a smaller antisense peak ~160-180nt upstream of TSSs (Fig 2A).

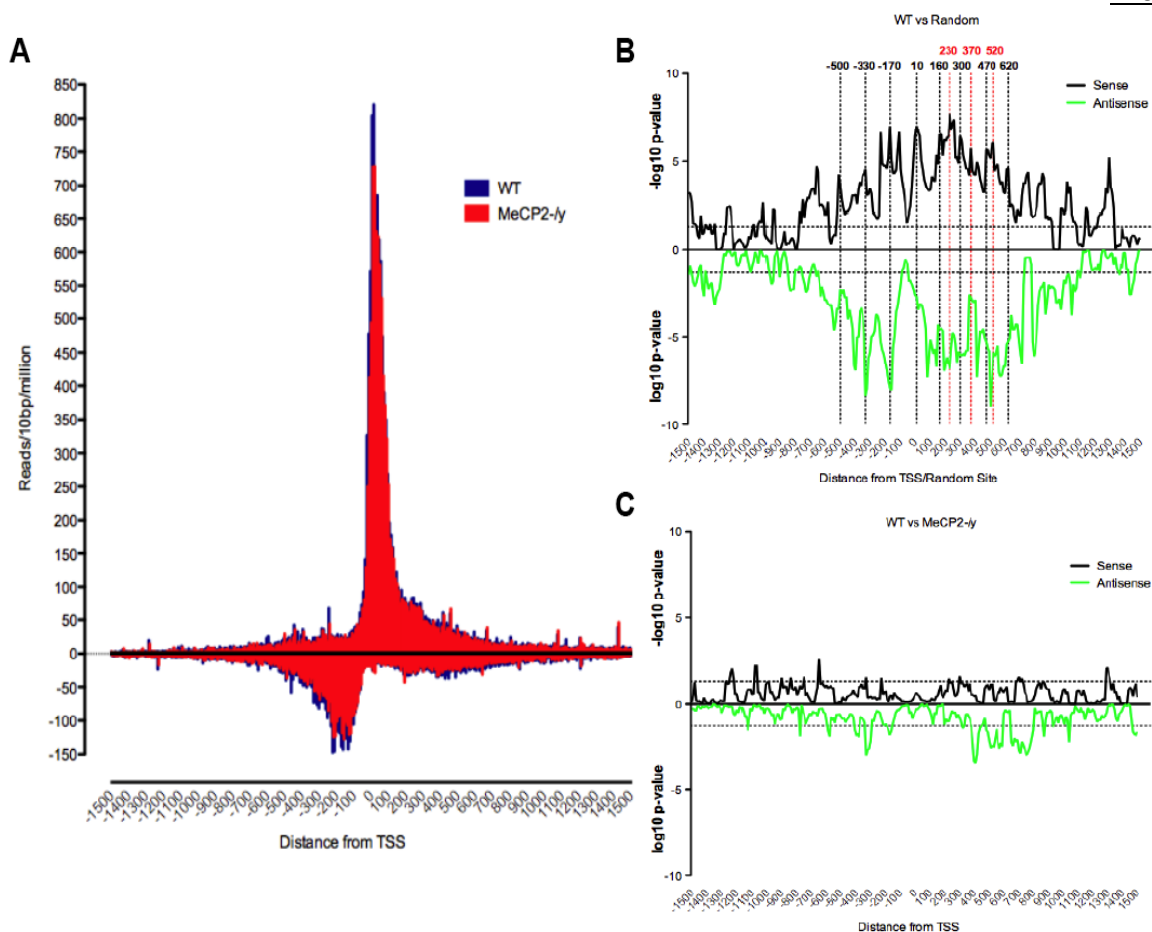


Figure 2. Association of unannotated small RNA with RefSeq TSSs. **A.** Unannotated small RNAs were mapped relative to RefSeq TSSs and the total number of small RNA 5' ends in 10bp bins centered on TSSs were summed. The read densities were then normalized based on the total number of aligned sequences in each genotype and plotted relative to RefSeq TSSs (positive x-axis values represent internal or downstream portions of RefSeq transcripts and negative numbers represent upstream portions of RefSeq transcripts). Reads are divided based on their orientation relative to the RefSeq transcript, where sense small RNA are give positive y-values and antisense RNA are give negative y-values. **B.** A ~2kb region, centered on RefSeq TSSs, was identified as significantly enriched for unannotated small RNA. A sliding window approach (50bp bins, 10bp slide) was used to calculate p-values (student's t-test) relative to randomly chosen genomic regions. $-\log_{10}$ or \log_{10} was used to convert p-values for sense and antisense small RNA, respectively. Horizontal dotted lines correspond to a p-value of 0.05. Vertical dotted lines depict p-values peaks that could be identified as spaced at distances approximately the length of DNA wrapped around 1 nucleosome (~150bp) **C.** Using the same sliding window approach to compare WT and *Mecp2*^{-/-} TSS associated small demonstrates there is no significant difference between genotypes.

Notably, many known stimulus responsive genes in neuronal cell types were found to produce significant numbers of small RNA close to TSSs including *c-Fos*, *Jun*, *c-Myc*, and *Homer1*, among others (Supp Figs 2-5). In light of the enrichment of small

RNA at known activity dependent genes such as these, we reasoned that we could identify additional loci that may be regulated by MeCP2 and promoter proximal RNAPII activity by identifying those genes differentially expressing small RNA in *Mecp2*^{-/y} aNSCs. This notion was supported by examination of known stimulus responsive MeCP2 targets such as *Bdnf*. We observed increased expression of small RNA proximal to the *Bdnf* promoter IV in *Mecp2*^{-/y} aNSCs (Supp Fig 6). These small RNA were directly downstream of a previously identified MeCP2 binding site that is critical for activity dependent regulation of *Bdnf* (Chen, Chang et al. 2003; Martinowich, Hattori et al. 2003; Hong, McCord et al. 2008). Interestingly, we observe an opposite effect on small RNA expression near upstream *Bdnf* promoters I-III. Here, small RNAs were increased in WT aNSCs compared to *Mecp2*^{-/y} aNSCs. These results are consistent with a repressive role for MeCP2 at the promoter IV, an activating effect at the upstream promoters I-III, and likely reflect the impact of MeCP2 on the overall chromatin state at *Bdnf*.

The composite distribution of all small RNA relative to all RefSeq TSSs combined indicated that there was not a significant difference in small RNA expression between genotypes (Fig 2A,C). This suggests that, although MeCP2 is likely to have a global effect on chromatin, it may influence promoter proximal small RNA expression only at specified loci rather than acting as a general effector of promoter proximal RNAPII activity in aNSCs (Fig 2C). However, as a general feature of the distribution surrounding TSSs, there was an apparent phasing of small RNA expression at nucleosome length intervals, particularly in the sense orientation (Fig

2B). This indicated an association between nucleosome positioning, and potentially histone modification, with small RNA expression close to TSSs.

The relationship between promoter proximal regulation of RNAPII, nucleosome, placement, and the expression of small RNA at TSSs suggested that the expression of these small RNA reflected genes that were poised for expression in response to an environmental stimulus. Therefore, in an effort to identify genes that may be both regulated by MeCP2 and poised for expression, those genes differentially expressing TSS associated small RNA in the absence of MeCP2 were found. In total, 14,222 RefSeq genes (54.9%) expressed a promoter proximal small RNA. 79.4% of small RNA producing genes did so in both genotypes (12,586 RefSeq genes in WT aNSCs and 12,923 RefSeq genes in *MeCP2*^{-/-} aNSCs). Overall expression of small RNA correlated very well ($r^2=0.84$) between genotypes, indicating consistency between libraries. However, a subset of 304 RefSeq transcripts exhibited differential promoter proximal small RNA expression in the absence of MeCP2 (Fig. 3, $p \leq 0.01$, Fisher's Exact, Bonferroni corrected, and Supp Table 1). These 304 genes represent putative targets of MeCP2 regulated by promoter proximal RNAPII activity that are likely to be stimulus responsive. Among the set of genes are multiple activity dependent genes in neurons that have further been implicated in autism spectrum disorders, including *Pcdh10*.

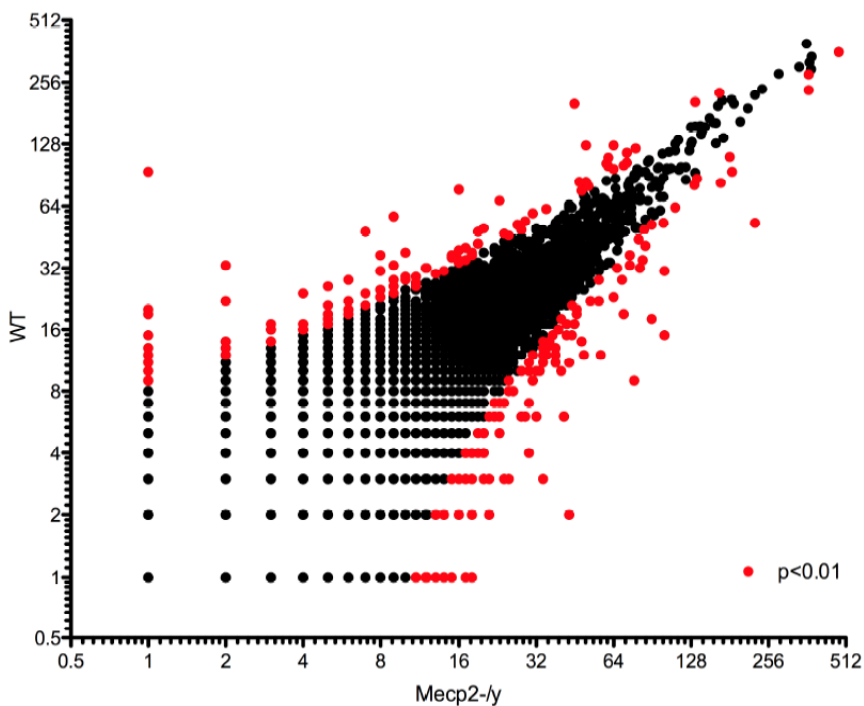


Figure 3. Differential expression analysis of TSS associated small RNA in WT and *Mecp2*-/*y* aNSCs. The total number of normalized reads mapping within 2kb of each RefSeq transcript were calculated and plotted against one another based on genotype. Each dot represents a single RefSeq transcript. Dots colored in red are those exhibiting differential expression at a p-value threshold of ≤ 0.01 (fisher's exact, bonferroni corrected, (Romualdi, Bortoluzzi et al. 2003)).

As an activity dependent gene expressing a relatively high number of TSS associated small RNA in aNSCs, *Pcdh10* served as candidate gene for assessing a potential MeCP2-mediated affect on the expression of promoter proximal small RNA. First, the expression *Pcdh10* mRNA was assayed by real-time quantitative PCR and was found to be increased in *Mecp2*-/*y* aNSCs proportionately to the increase in small RNA expression (Fig 4A,B). It was noted that directly upstream of the *Pcdh10* TSS there is a divergent, non-overlapping noncoding transcript. The expression of this long noncoding RNA was assayed using primers across two distinct exon junctions and was also significantly increased in the absence of MeCP2 (Fig 4 C-E). Interestingly, the upstream divergent noncoding RNA also appeared to express

promoter proximal small RNA disproportionately higher than the full-length transcript, albeit to a lesser extent as compared to the *Pcdh10* coding transcript (Fig 4). This may indicate that, while stalling of RNAPII regulates both transcripts, productive elongation of the entire transcript is only efficient for the sense, coding

Pcdh10 transcript.

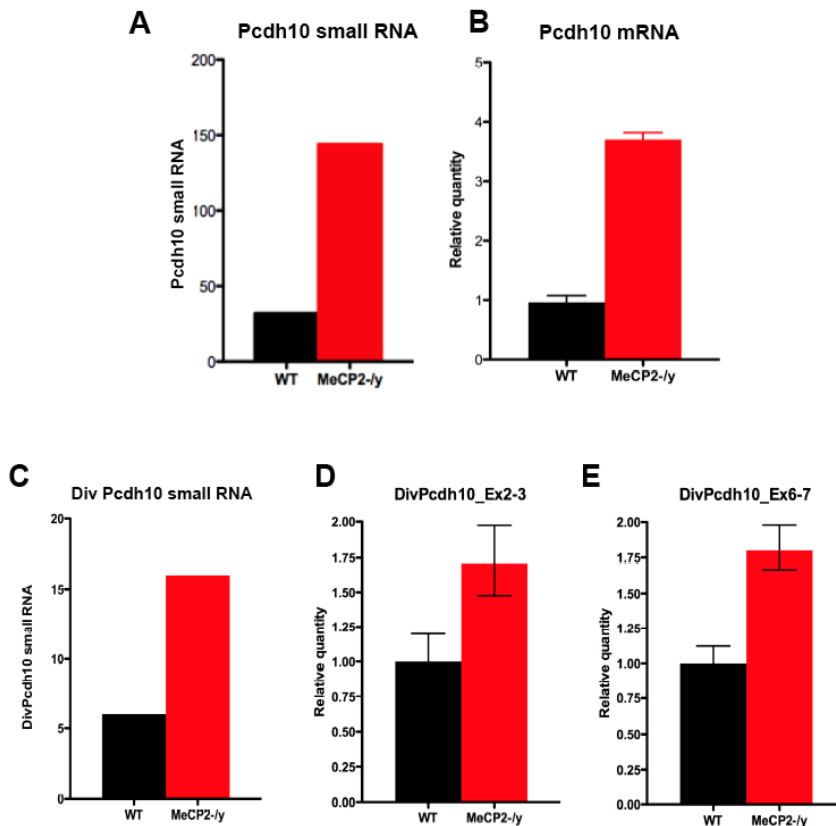


Figure 4. Expression of TSS associated small RNA and full-length transcripts at *Pcdh10* and *DivPcdh10*. A and C. The total number of small RNA associated with the TSSs of the *Pcdh10* and *DivPcdh10* transcripts in WT and *Mecp2*^{-/-} aNSCs are shown for comparison to the expression of the full-length transcripts. B, D, and E. Quantitative real-time PCR was used to determine the relative expression of the *Pcdh10* and *DivPcdh10* full length transcripts in WT and *Mecp2*^{-/-} aNSCs (n=4, mean ± 95%CI).

To begin to correlate the expression of promoter proximal small RNA and the associated full-length transcripts with RNAPII occupancy and chromatin state at *Pcdh10*, chromatin immunoprecipitation (ChIP) assays were performed. RNAPII was enriched 9.8-fold at the *Pcdh10* TSS in *Mecp2*^{-/-} aNSCs relative to WT aNSCs (Fig 5B), while the full length mRNA was increased only 3.9-fold (Fig. 4B). The 2.5-fold excess increase in RNAPII occupancy relative to the increase in *Pcdh10* mRNA

further suggests that the expression of *Pcdh10* is indeed regulated by promoter proximal RNAPII stalling.

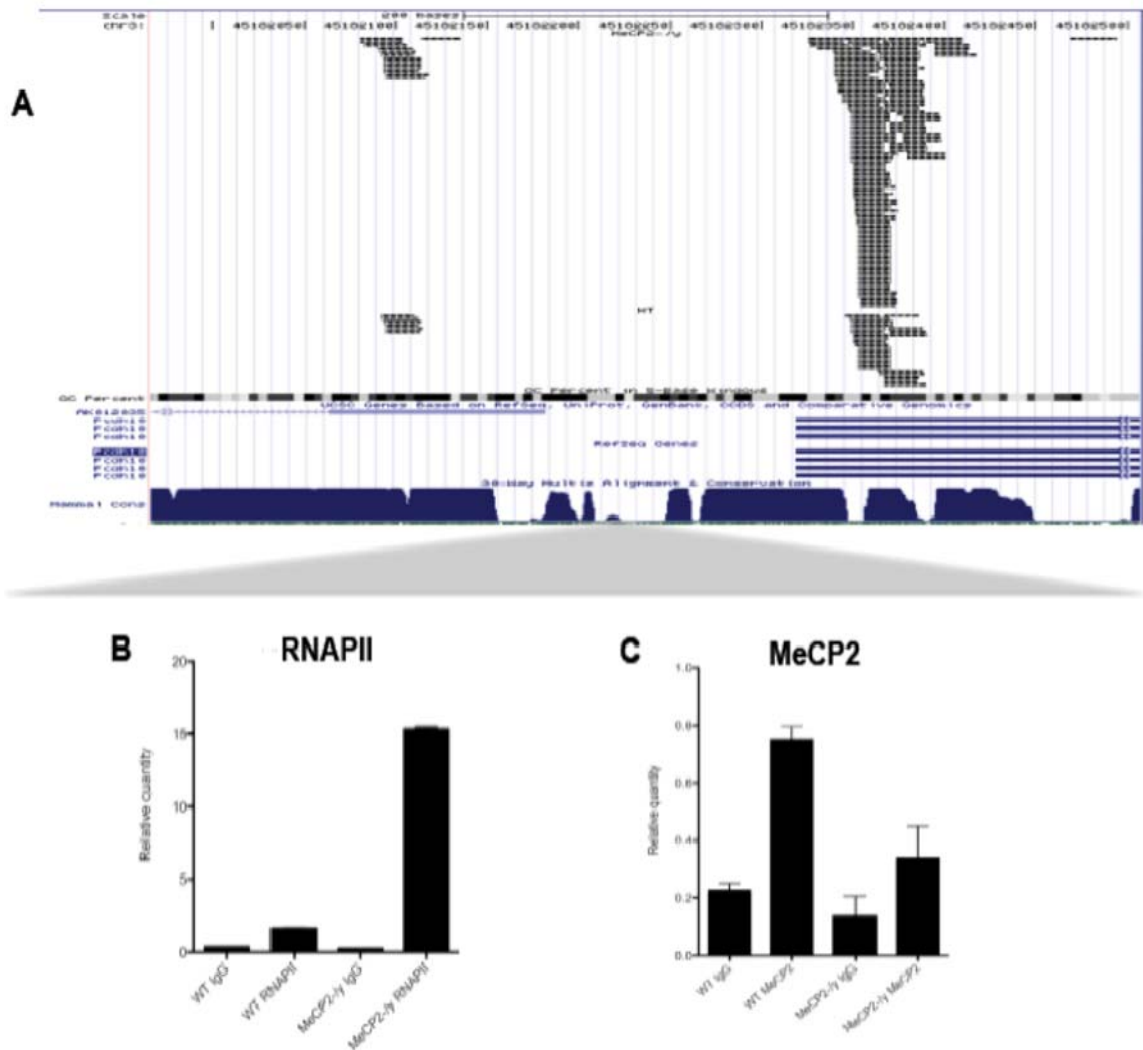


Figure 5. RNAPII occupancy and direct interaction of MeCP2 proximal to *Pcdh10*. **A.** A UCSC Genome Browser capture of the *Pcdh10* locus. The shaded triangle below indicates the region targeted by the primers used in the quantitative ChIP assays. **B.** Quantitative ChIP of RNAPII at *Pcdh10* in WT and *MeCP2*^{-/-} aNSCs. Normal Rabbit IgG was used as a non-specific control (n=3, mean ± SEM, * = p<0.05 for WT vs. *MeCP2*^{-/-} ChIPs). **C.** Quantitative ChIP of MeCP2 at *Pcdh10* in WT and *MeCP2*^{-/-} aNSCs. Normal Rabbit IgG was used as a non-specific control (n=3, mean ± SEM, * = p<0.05 for WT vs. *MeCP2*^{-/-} ChIPs).

The chromatin state of the *Pcdh10* TSS was also altered in a manner reflecting increased expression in the absence of MeCP2. H3-K4-TriMe, a mark generally associated with active TSSs, was enriched in *MeCP2*^{-/-} aNSCs when compared to WT

aNSCs (Supp Fig 1B). Furthermore, the transcriptionally active mark H3K9-Ac was enriched in MeCP2 deficient aNSCs (Supp Fig 1C), while H3-K27-TriMe, a repressive mark, was decreased (Supp Fig 1D). However, general H3 was unaltered (Supp Fig 1E). MeCP2 ChIP at the same location found ~3-fold increase in MeCP2 close to the *Pcdh10* TSS (Fig 5C), suggesting that *Pcdh10* is a direct target of MeCP2 in aNSCs. The proximity of MeCP2 and RNAPII indicates that MeCP2 may directly influence promoter proximal regulation of RNAPII activity at *Pcdh10* in aNSCs.

Discussion

A convergence of data has implicated MeCP2 in the activity dependent regulation of the neuronal chromatin state, which subsequently alters gene expression at specific loci. Here we use an SBS approach to profiling the expression of small noncoding RNA in aNSCs as a means of assessing promoter proximal RNAPII activity, a process known to regulate stimulus responsive genes in diverse eukaryotes. By directly comparing small RNA expression at TSSs in WT and *Mecp2*^{-/y} aNSCs 304 RefSeq genes with altered promoter proximal small RNA expression were identified. These genes represent putative stimulus responsive transcripts regulated by MeCP2 at which RNAPII is likely to be poised.

Among the 304 RefSeq transcripts, *Pcdh10* was identified as having been both reported as activity dependent in neurons and implicated in Autism spectrum disorders. A detailed analysis of the *Pcdh10* locus by RNAPII ChIP demonstrated a

disproportionate relationship between RNAPII occupancy and *Pcdh10* expression, where RNAPII was enriched 9.8-fold in *Mecp2*^{-/-} aNSCs while mRNA expression was increased only 3.9-fold. The 2.5-fold increase in RNAPII occupancy relative to mRNA expression is consistent with the notion that *Pcdh10* expression is indeed influenced by promoter proximal RNAPII activity. Furthermore, MeCP2 specific ChIP indicated a direct interaction between MeCP2 in the same region. This suggests that MeCP2 may directly influence the stimulus dependent transcription of *Pcdh10* through influencing promoter proximal RNAPII activity.

Interestingly, *Pcdh10* was implicated in Autism-spectrum disorders through an identity by a recent study which identified a >300kb deletion in a proximal downstream region that did not include the gene itself. The means by which such a proximal downstream deletion would affect expression of the upstream gene remained unclear. However, considering these results in the context of MeCP2 function, where MeCP2 may influence the general chromatin state in vicinity of *Pcdh10*, it may be reasonable to suggest that the proximal downstream deletion likewise affects the activity dependent regulation of *Pcdh10*. Such a deletion may alter the local chromatin state and thereby alter promoter proximal RNAPII activity.

Although 304 genes with altered TSS associated RNA were identified in MeCP2 deficient aNSCs, it remains possible that the full repertoire of genes regulated in such a manner is much larger. As promoter proximal regulation of RNAPII has been found to preferentially occur at genes responsive to environmental stimuli

(Guenther, Levine et al. 2007; Muse, Gilchrist et al. 2007; Zeitlinger, Stark et al. 2007; Adelman, Kennedy et al. 2009), the identification of such genes is dependent on the cellular environment. In the case of MeCP2 and RTT, there may in fact be a distinct set of genes that display altered promoter proximal RNAPII activity in response to distinct neuronal stimuli. Thus, upon particular neuronal signals there may be distinct sets of genes displaying altered expression in the absence of MeCP2. Based on the current dataset, those genes identified as enriched for promoter proximal small RNA, but not necessarily differentially expressing those small RNA in the absence of MeCP2, may serve as candidates for altered expression upon distinct cellular signals. This may at least partially explain previous observations indicating relatively modest changes in mRNA expression as well as conflicting data on specific genes in the absence of MeCP2.

Materials and Methods

Small RNA cloning and sequencing

Total RNA was isolated with TRIzol reagent (Invitrogen) and resuspended in Nuclease free water. 10ug was used to clone 5' phosphorylated/3'-hydroxylated small RNA according to the Illumina Small RNA Sample Prep protocol (version 1.4B). Small RNAs were size selected on a 15% PAGE-Urea gel and successively ligated to 5' and 3' adapters with T4 RNA ligase. Ligation products were size selected on PAGE-Urea gels after each successive ligation. RNAs were reverse transcribed with SuperScript II (Invitrogen) using a primer complementary to the

known 5' adapter sequence and then PCR amplified 15-17 cycles. PCR products were purified on a non-denaturing PAGE gel, quantified on an Agilent 2100 Bioanalyzer, and the subjected to cluster generation and 36-cycle single end sequencing at both 4 and 6pM concentrations on the Illumina GAIIx platform according to manufacturer's protocol (Part#1006080 Rev B. and Part#1005637 Rev A).

Sequence Preprocessing, Alignment, and Annotation

Raw sequence data was obtained by GERALD using the default settings provided by the Illumina Pipeline. Sequences were clipped of 3' adapter sequence using FASTX-Toolkit-0.0.7 fastx_clipper retaining only clipped sequences ≥ 14 nucleotides. A unique set of sequences was generated using fastx_collapser, where unique sequences and the number of times each was read were tracked. Unique sequences were aligned to NCBI Build 37 (mm9) mouse genomic sequence using Bowtie-0.10.1, retaining only full-length unique genomic matches for further analysis. Small RNAs were then annotated based on genomic location and unannotated small RNA were identified using a subtractive approach removing those sequences overlapping ≤ 1 bp of miRNA (miRBase Release 14), RepeatMasker (UCSC NCBI Build 37 mouse mm9 Assembly, Rmsk track), tRNA (tRNAScanSE), snoRNA (derived from those listed in RefSeq and liftOver of hg18 requiring $>95\%$ sequence identity) were considered as derived from the associated annotation and removed from further consideration. Of the remaining reads those that were sequenced >100 times were

tracked and removed from further consideration as previously described (Seila, Calabrese et al. 2008)

Regions enriched for small RNA were determined by first calculating the distance from a given small RNA 5' end to the closest RefSeq TSS. The total number of small RNA 5' ends in 10bp bins centered on RefSeq TSSs were then summed. Distributions were likewise generated for random genomic locations and RefSeq 3' ends.

Individual biological replicates produced nearly identical profiles relative to RefSeq TSSs, random genomic locations, and RefSeq 3' ends and were also consistent with previous reports. Additionally, there was an 83% overlap in RefSeq transcripts producing ≥ 1 small RNA when comparing independent experiments. Based on the consistency between small RNA libraries we combined biological replicates into a single dataset per genotype so as to maximize sequencing depth and increase the accuracy in downstream differential expression analysis. The distribution of small RNA around RefSeq TSSs was then compared to the distribution around random genomic locations using a sliding window approach to calculate the probability of a given genomic region being enriched for small RNA (student's t-test, 50bp windows, 10bp shift). A 2kb region, 1kb upstream and 1kb downstream, was defined as the region enriched for promoter proximal small RNA.

Differential small RNA expression analysis was performed by determining the total number of small RNA sequences with 5' ends mapping within 2kb of a RefSeq TSS,

the region found to be significantly enriched in small RNA relative to random genomic locations as described above, in each genotype. The significance of the difference in small RNA expression proximal to TSSs was determined using a Fisher's Exact Test with bonferroni correction, p-value threshold of $p \leq 0.01$ (Romualdi, Bortoluzzi et al. 2003).

Chromatin Immunoprecipitation (ChIP)

ChIP was performed according to a previously published method (Coffee, Zhang et al. 1999). Briefly, cells grown on 3 to 6 confluent 10-cm cell culture plates were fixed by 1% formaldehyde (Sigma-Aldrich) to culture medium for 10 min at room temperature. After washing with cold PBS, cells were collected with cold PBS, washed, and suspended in 1 ml cold cell lysis buffer (5 mM PIPES, pH 8.0, 85 mM KCl, 0.5% NP40, and 1X Complete Proteinase Inhibitor (Roche)), and incubated on ice for 5 min. Cell lysates were pelleted by centrifugation at 3000 rpm for 5 min, resuspended again in 1 ml of cold cell lysis buffer for 5 min on ice, and then repelleted to collect nuclei. Nuclei were lysed at room temperature with 500 μ l of nuclei lysis buffer (50 mM Tris pH 8.1, 10 mM EDTA, 1% SDS, and 1X Complete Protease Inhibitor). Nuclear lysates were sonicated using a Misonix 3000 Sonicator. The size of the sonicated chromatin (average size of ~500-600 bp) was verified by treating 5- μ l aliquots with 1 μ l 20 mg/ml proteinase A for 20 min at 50°C and running on a 1.5% agarose gel stained with ethidium bromide. For immunoprecipitation reactions we used 50 μ l of sonicated chromatin, precleared

with salmon sperm/tRNA-blocked protein A agarose for 60 min at 4°C in 950 µl IP dilution buffer (0.01% SDS, 1.1% Triton X-100, 1.2 mM EDTA, 20 mM Tris pH 8.1, 500 mM NaCl). Precleared chromatin was rotated at 4°C overnight with 10 µg of the appropriate antibody.

Antibodies: Normal rabbit IgG (Upstate, Cat# 12-370), rabbit polyclonal to MeCP2 (ChIP Grade, Abcam ab2828), Anti-trimethyl-Histone H3 (Lys4), clone MC315 (Millipore Cat.# 04-745), anti-acetyl-histone-H3 (Lys9) (Upstate, Cat. #07-352), Rabbit polyclonal to Histone H3 – ChIP Grade (Abcam, ab1791), Anti-trimethyl-Histone-H3 (Lys27) (Millipore, Cat#07-449), Anti-Pol II (H-224) (Santa Cruz sc-9001).

Antibodies were pulled down with 60-µl blocked protein A agarose beads for 1 h at 4°C with rotation. The beads were washed sequentially 2 times each in IP dilution buffer, TSE-500 solution (0.1% SDS, 1% Triton X-100, 2 mM EDTA, 20 mM Tris pH 8.1, 500 mM NaCl), freshly prepared Li/Cl wash solution (100 mM Tris pH 8.1, 300 mM LiCl, 1% NP40, 1% deoxycholic acid), and 1X TE for 10 min at 4°C. Protein-DNA complexes were eluted from the protein A agarose beads twice with 250 µl of IP elution buffer (50 mM NaHCO₃, 1% SDS) for 15 min at 37°C with rotation. Formaldehyde-induced protein-DNA crosslinking was heat reversed by incubating protein-DNA complex at 65°C overnight. DNA was purified using phenol:chloroform:isoamyl alcohol (25:25:1) isolations and precipitated with 2 volumes 100% ethanol and 10 µg linear acrylamide at -35°C overnight.

Immunoprecipitated and purified DNA fragments were resuspended in nuclease-free water, concentrations were determined by NanoDrop, and each sample was diluted to 1 ng/μl. We used 8 ng DNA in 20-μl SYBR Green real-time PCR reactions consisting of 1X Power SYBR Green Master Mix and 0.5 μM forward and reverse primers. Reactions were run on an Applied Biosystems SDS 7500 Fast Instrument using the Standard 7500 default cycling protocol and SDS 7500 Fast System Software version 1.3.1 without the 50°C incubation. Primer sequences were designed against a region directly between the *Pcdh10* and *DivPcdh10* transcripts using Applied Biosystems' Primer Express 3.0 software and were: FW-5'-TGAGCTTTCTGGTATCTTTGTTGCTA, RV-5'-CAGACCCAATGCCTCCTATCA.

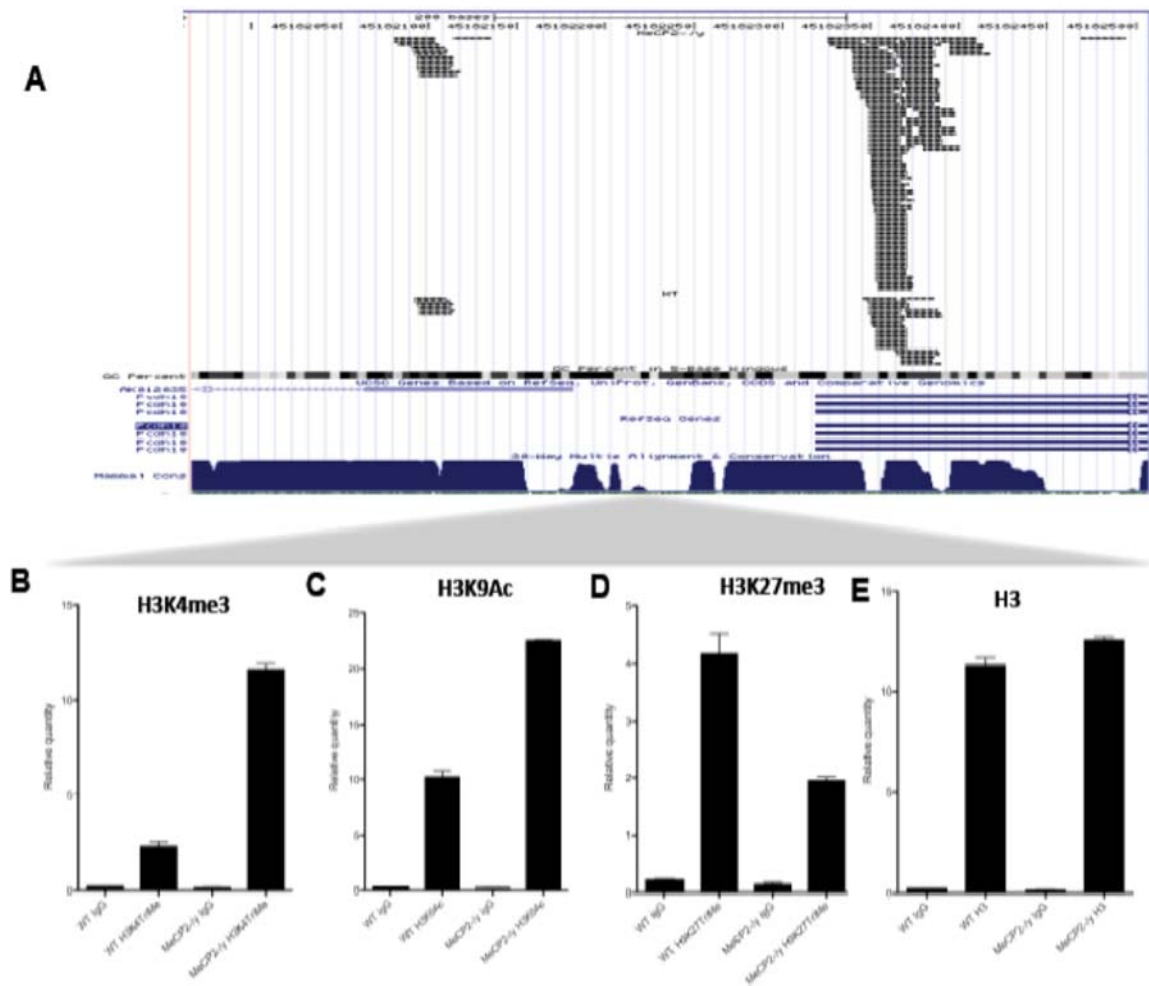
Absolute quantification was based upon standard curves generated from 4 10-fold dilutions ranging from 0.08-80 ng input DNA treated in parallel with immunoprecipitated DNA during reverse crosslinking and purification steps.

Absolute quantities were determined based upon input DNA-generated standard curves and reported directly for both specific and IgG nonspecific immunoprecipitations. All ChIP experiments were from 3 independent chromatin preparations, and all real-time PCR reactions were carried out in triplicate for each sample on each amplicon. Representative ChIP experiments are displayed. All primer sets we subjected to a dissociation curve analysis and produced single peaks on a derivative plot of raw fluorescence.

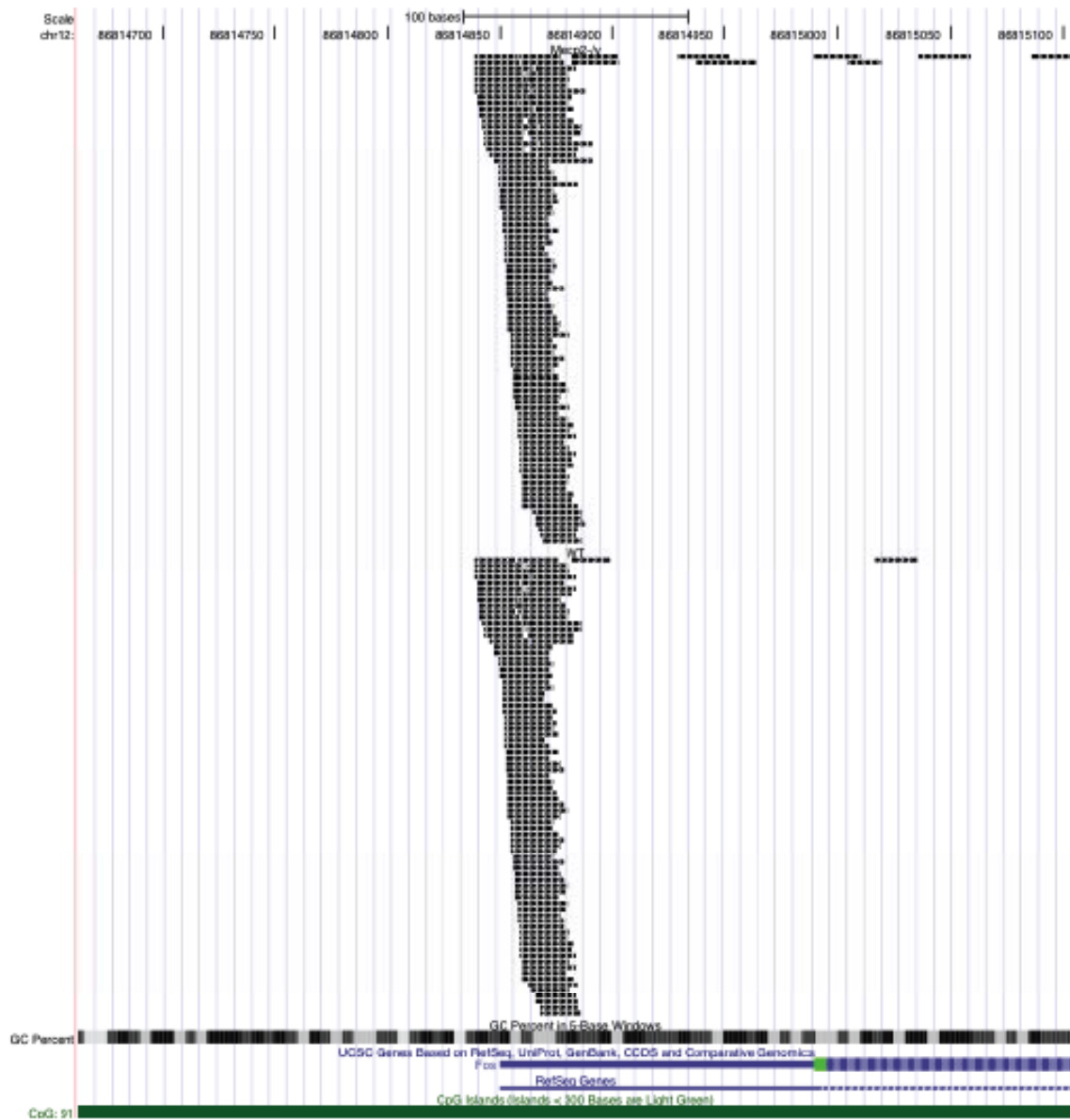
qRT-PCR

1 µg of total RNA isolated by TRIzol (Invitrogen, 15596-026) from WT and *Mecp2*^{-/-} aNSCs was reverse transcribed using random hexamers to generate first strand cDNA with SuperScript III (Invitrogen) according to the manufacturer's protocol. 8 µL 1:10 diluted cDNA was used directly in 20 µL SYBR Green real-time PCR reactions that consisted of 1X Power SYBR Green Master Mix, 0.5 µM forward and reverse primers, and nuclease-free water. 18S rRNA was used as an endogenous control for all samples, with 8 µL of cDNA diluted 1:100 in nuclease-free water used. Reactions were run on an Applied Biosystems SDS 7500 Fast Instrument using the Standard 7500 default cycling protocol and SDS 7500 Fast System Software version 1.3.1 without the 50°C incubation primers for *Pcdh10* mRNA, the divergent *Pcdh10* long noncoding RNA (*divPcdh10*) and 18S rRNA were designed using Applied Biosystems Primer Express 3.0 software and were: *Pcdh10*, FW-5'-CAGCAACCAGACATCATTTCCA, RV-5'-AGCTCTGCTCGCTGGTGTTC, *divPcdh10* (across junction of exons 2 and 3) FW-5'-TGATTCCTGCTGTCTACTCCTCTTG, RV-5'-TGGCAACTCCTCCTTCTCAGA, *divPcdh10* (across junction of exons 6 and 7), FW-5'-TCTTAGAGAATTATGGGCAGATGAAC, 18S rRNA, FW-5'-CGGCTACCACATCCAAGGAA, RV-5'-CCTGTATTGTTATTTTCGTCACCT. All real-time PCR reactions were performed in triplicate, and relative quantities were calculated using the $\Delta\Delta C_t$ method (95% confidence level) with calibration to WT samples. All primer sets were subjected to a dissociation curve analysis and produced single peaks on a derivative plot of raw fluorescence.

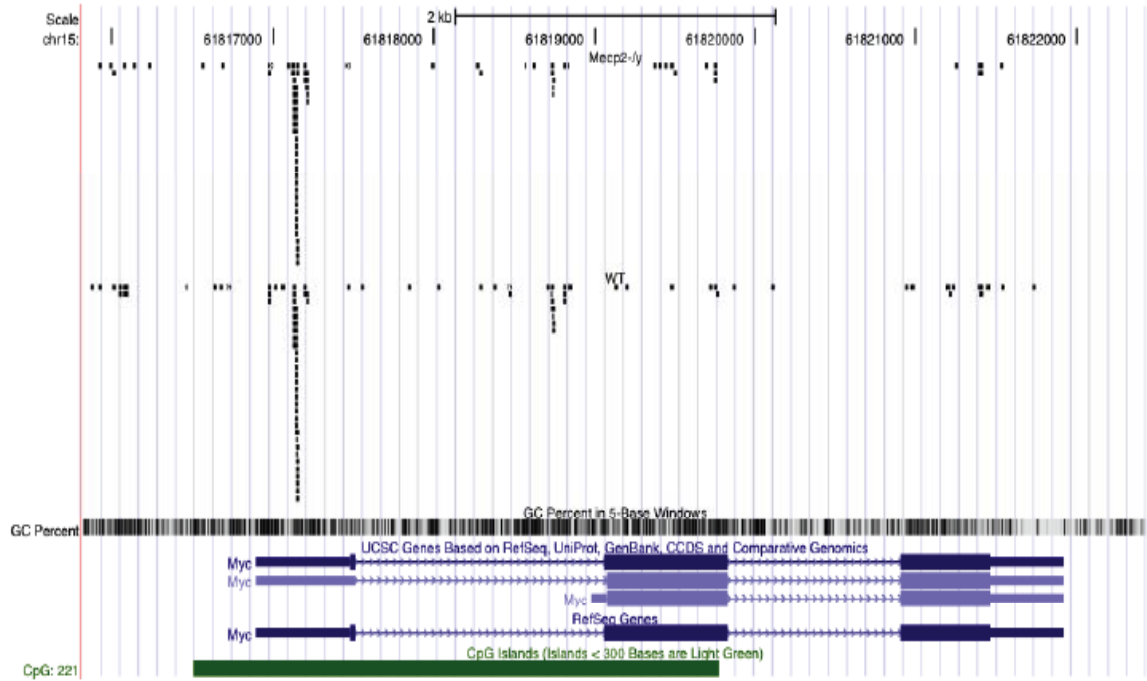
Supplemental Figures



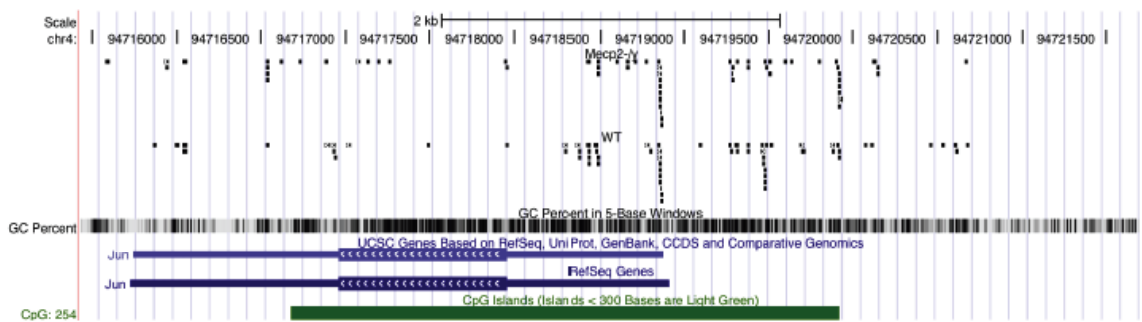
Supp Fig 1. The TSS associated chromatin state at *Pcdh10* in WT and *MeCP2*^{-/-} aNSCs. **A. A UCSC Genome Browser capture of the *Pcdh10* locus. The shaded triangle below indicates the region targeted by the primers used in the quantitative ChIP assays. **B.** Quantitative ChIP of H3K4me3 at *Pcdh10* in WT and *MeCP2*^{-/-} aNSCs. Normal Rabbit IgG was used as a non-specific control (n=3, mean ± SEM, * = p<0.05 for WT vs. *MeCP2*^{-/-} ChIPs). **C.** Quantitative ChIP of H3K9Ac at *Pcdh10* in WT and *MeCP2*^{-/-} aNSCs. Normal Rabbit IgG was used as a non-specific control (n=3, mean ± SEM, * = p<0.05 for WT vs. *MeCP2*^{-/-} ChIPs). **D.** Quantitative ChIP of H3K27me3 at *Pcdh10* in WT and *MeCP2*^{-/-} aNSCs. Normal Rabbit IgG was used as a non-specific control (n=3, mean ± SEM, * = p<0.05 for WT vs. *MeCP2*^{-/-} ChIPs). **E.** Quantitative ChIP of H3 at *Pcdh10* in WT and *MeCP2*^{-/-} aNSCs. Normal Rabbit IgG was used as a non-specific control (n=3, mean ± SEM).**



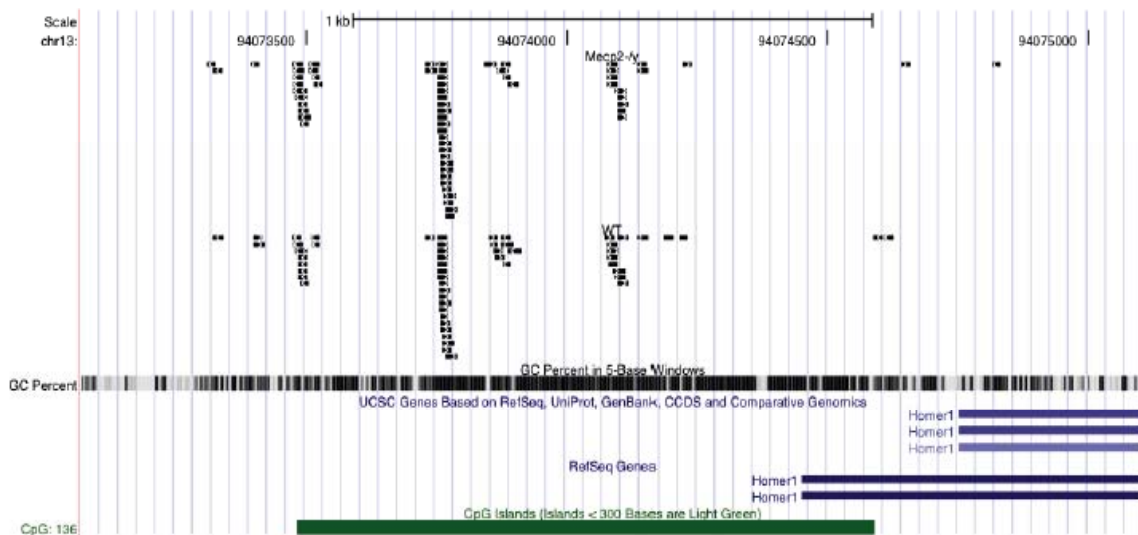
Supp Fig 2. TSS associated small RNA expression at *c-Fos* in WT and *MeCP2*^{-/y} aNSCs. A. A UCSC Genome Browser capture of the *c-Fos* locus. Individual ticks represent unique sequences.



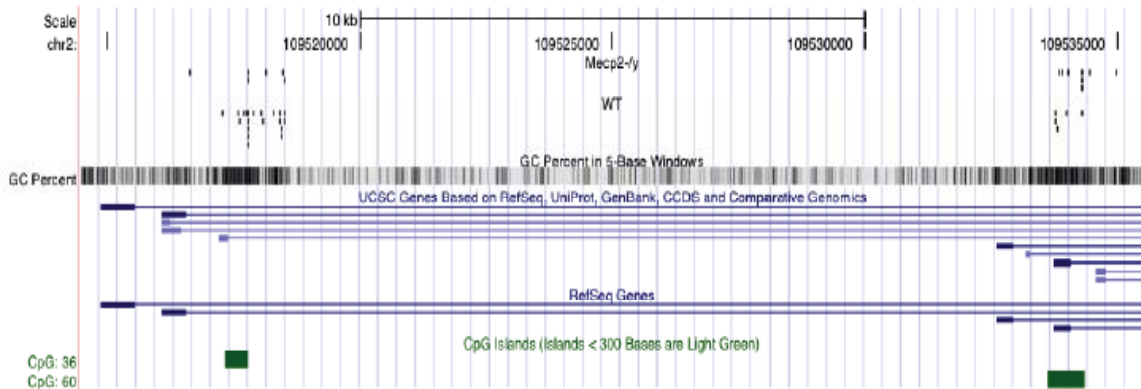
Supp Fig 3. TSS associated small RNA expression at *c-Myc* in WT and *MeCP2-/-* aNSCs. A. A UCSC Genome Browser capture of the *c-Myc* locus. Individual ticks represent unique sequences.



Supp Fig 4. TSS associated small RNA expression at *Jun* in WT and *MeCP2-/-* aNSCs. A. A UCSC Genome Browser capture of the *Jun* locus. Individual ticks represent unique sequences.



Supp Fig 5. TSS associated small RNA expression at *Homer1* in WT and *MeCP2*^{-/-y} aNSCs. A. A UCSC Genome Browser capture of the *Homer1* locus. Individual ticks represent unique sequences.



Supp Fig 6. TSS associated small RNA expression at *Bdnf* in WT and *MeCP2*^{-/-y} aNSCs. A. A UCSC Genome Browser capture of the *Bdnf* locus. Individual ticks represent unique sequences. Promoters I-III are more upstream or to the left of the screen capture and display more TSS associated small RNA in WT aNSCs (WT = 22 total, *MeCP2*^{-/-y} = 7 total). Promoter IV is more downstream or to the right of the screen capture and displays more TSS associated small RNA in the *MeCP2*^{-/-y} aNSCs (WT = 5 total, *MeCP2*^{-/-y} = 8 total).

Chapter 4 - Supplemental Table I

RefSeq ID	WT	Mecp2-/y	Fisher p-value	
NM_030692		227	53	0
NR_003513		101	15	0
NM_146194		101	31	0
NR_028480		90	18	0
NM_007591		77	9	0
NM_017382		70	19	0
NM_019738		57	12	0
NM_145986		50	126	0
NM_011043,N		45	201	0
NM_00111318		43	2	0
NM_207667		41	6	0
NM_00108109		34	3	0
NM_009323		24	0	0
NM_023063		23	68	0
NM_007599		16	77	0
NM_174849		9	57	0
NM_027090		7	48	0
NM_00100133		2	33	0
NM_029598		1	94	0
NM_00110244		0	113	0
NR_028537		185	94	0.000001
NM_153792		167	83	0.000001
NM_00108197		64	126	0.000001
NR_004445		367	234	0.000002
NM_145401		0	18	0.000002
NR_028128		49	12	0.000004
NM_008657		8	37	0.000004
NM_00111102		1	20	0.000007
NM_00111021		30	4	0.000008
NR_030702		133	205	0.000009
NM_011127,N		2	22	0.000013
NM_029008		1	19	0.000014
NM_054051		10	38	0.000017
NM_175127		81	32	0.000018
NM_00112294		43	11	0.000028
NM_134156		32	6	0.000031
NM_009573		25	3	0.000033
NM_011756		48	14	0.000034
NM_011543		64	23	0.000035
NM_172612		83	35	0.000042
NM_007569		61	110	0.000044
NR_028556		40	10	0.000047
NM_008952		24	3	0.000058
NM_153782		21	2	0.000075
NM_013454		4	24	0.000075

NM_025824	9	33	0.000083
NM_010361	5	26	0.000084
NM_010573	18	1	0.000085
NM_010276	18	1	0.000085
NM_033371	6	28	0.000089
NM_013494	69	28	0.000096
NR_030701	14	0	0.000131
NM_018784	29	6	0.000142
NM_144530	8	31	0.000145
NM_025312	17	1	0.000159
NM_133854	20	50	0.000165
NM_023773	19	48	0.000194
NM_009233	1	15	0.000196
NM_00104437	60	103	0.000211
NR_028526	165	227	0.000218
NM_009155	74	33	0.000218
NM_172867	30	7	0.000232
NM_00108128	28	6	0.000233
NM_016710	38	11	0.000263
NM_018782	21	3	0.000312
NM_145713	85	41	0.00033
NM_175246	72	116	0.00033
NM_008131	181	111	0.000337
NM_008241	0	11	0.000355
NM_024474	0	11	0.000355
NM_031165	44	15	0.000361
NR_028538	56	22	0.000375
NM_010828	47	84	0.00043
NM_00102542	18	2	0.000442
NM_00104248	78	122	0.000497
NM_007548	20	3	0.000544
NM_146036	20	3	0.000544
NM_175136	38	12	0.000547
NM_053269	15	1	0.000558
NR_030494	481	358	0.000611
NM_009627	100	53	0.000633
NM_007631	61	100	0.000656
NM_008092	0	10	0.000731
NM_028126	1	13	0.000734
NM_019479	42	15	0.000792
NM_028426	45	17	0.000846
NM_029556	11	0	0.00102
NM_010574	11	0	0.00102
NM_00103801	23	5	0.00103
NM_144799	14	1	0.001039
NM_025745	14	1	0.001039
NM_00108081	14	1	0.001039
NM_015774	16	39	0.00104
NM_175661	38	13	0.001073

NR_030703	111	63	0.001075
NM_00104255	33	10	0.00109
NM_00116363	3	17	0.001166
NM_172296	5	21	0.001216
NM_00113557	10	29	0.001227
NM_00111109	15	37	0.001238
NM_009524	31	9	0.001242
NM_008872	31	9	0.001242
NM_175089	17	40	0.001283
NM_016769	50	84	0.001298
NM_023735	12	32	0.001374
NM_152229	9	28	0.001406
NM_00108112	16	2	0.001411
NM_00111351	1	12	0.001413
NM_013692	31	59	0.001438
NM_009032	34	11	0.001443
NM_172893	0	9	0.001505
NM_207260	0	9	0.001505
NM_00103332	0	9	0.001505
NM_00116339	0	9	0.001505
NM_175483	52	22	0.001507
NR_027943	74	37	0.001602
NM_053177	18	3	0.00162
NM_146217	18	3	0.00162
NM_133858	66	32	0.001639
NM_177368	32	10	0.001667
NM_028232	20	4	0.001699
NM_00116356	20	4	0.001699
NM_00116018	20	4	0.001699
NM_025966	7	24	0.001749
NR_028541	46	19	0.00179
NM_009621	15	36	0.001835
NM_025582	2	14	0.001849
NM_146634	2	14	0.001849
NM_178648	35	12	0.001863
NM_021565	19	42	0.001876
NM_019713	19	42	0.001876
NM_009234	10	28	0.001908
NM_022012	6	22	0.001909
NM_177909	13	1	0.00193
NM_011658	10	0	0.002024
NM_00103993	10	0	0.002024
NM_022419	10	0	0.002024
NM_00116794	3	16	0.002058
NM_009044	3	16	0.002058
NM_00100419	3	16	0.002058
NM_010112	27	52	0.00226
NM_009537	27	52	0.00226
NR_027826	132	81	0.00247

NM_00110997	11	29	0.002479
NM_00116408	8	25	0.002492
NM_025318	8	25	0.002492
NM_025329	42	17	0.002519
NM_00112288	23	6	0.002582
NM_00108136	23	6	0.002582
NM_00110045	1	11	0.002706
NM_010142	1	11	0.002706
NM_026044	1	11	0.002706
NM_011644	1	11	0.002706
NM_178206	34	12	0.002769
NM_00101360	17	3	0.002773
NM_028450	17	3	0.002773
NM_153068	19	4	0.002828
NM_008609	29	54	0.002878
NM_172775	46	20	0.002977
NM_173737	35	62	0.003027
NM_145554	0	8	0.003099
NM_029947	0	8	0.003099
NM_007632	0	8	0.003099
NM_008418	0	8	0.003099
NM_153412	26	8	0.003318
NM_010736	2	13	0.003366
NM_009761	5	19	0.003382
NM_009226	9	26	0.003399
NM_007766	64	97	0.003416
NM_146024,N	35	13	0.003453
NM_145979	35	13	0.003453
NM_007897	12	1	0.003573
NM_178683	12	1	0.003573
NM_028099	12	1	0.003573
NM_025862	12	1	0.003573
NM_024184	4	17	0.003573
NR_028091	24	7	0.003711
NM_027162	24	7	0.003711
NM_027485	30	10	0.00382
NM_173775	80	44	0.003888
NM_00116829	9	0	0.00402
NM_008057	24	47	0.004045
NM_198702	22	6	0.004097
NM_019766	22	6	0.004097
NM_025947	36	14	0.004228
NM_00111348	36	14	0.004228
NM_011777	39	16	0.004269
NM_00102531	90	52	0.004274
NR_028552	90	52	0.004274
NM_172865	14	2	0.00441
NM_00103911	14	2	0.00441
NM_025987	20	5	0.004439

NM_007426	20	5	0.004439
NM_00108122	20	5	0.004439
NM_026041	18	38	0.004619
NR_030442	18	4	0.004676
NM_173437	18	4	0.004676
NM_029734	18	4	0.004676
NM_022997	16	3	0.004714
NM_025518	16	35	0.004731
NM_019740	51	80	0.004969
NM_009237	51	80	0.004969
NM_021372	6	20	0.005023
NM_024461	6	20	0.005023
NM_177290	34	13	0.005031
NM_008487	34	13	0.005031
NM_007682	25	8	0.00508
NM_029482	37	15	0.005095
NM_027296	1	10	0.005157
NM_029019	1	10	0.005157
NM_027184	48	76	0.005181
NM_177856	5	18	0.005571
NM_013745	5	18	0.005571
NM_031185	5	18	0.005571
NM_145369	5	18	0.005571
NM_007764	11	27	0.00567
NM_153534	11	27	0.00567
NM_009787	23	7	0.005757
NM_025911	23	7	0.005757
NM_008708	13	30	0.00577
NM_153407	135	87	0.005773
NM_175201	4	16	0.006027
NR_015549,NI	4	16	0.006027
NM_00108121	4	16	0.006027
NM_009456	4	16	0.006027
NM_015786	56	28	0.006047
NM_00103337	8	23	0.006076
NM_025630	8	23	0.006076
NM_138748	8	23	0.006076
NM_146074	2	12	0.006083
NM_145415	2	12	0.006083
NM_011828	2	12	0.006083
NM_030229	2	12	0.006083
NM_199016	3	14	0.006266
NM_146251	3	14	0.006266
NM_025877	3	14	0.006266
NM_026203	3	14	0.006266
NM_027259	3	14	0.006266
NM_00116603	3	14	0.006266
NR_030715	0	7	0.006381
NM_028755	0	7	0.006381

NM_198031	0	7	0.006381
NM_029628	0	7	0.006381
NM_00116315	0	7	0.006381
NM_00103489	0	7	0.006381
NM_020578	0	7	0.006381
NR_030526	0	7	0.006381
NM_029999	72	104	0.006451
NM_134151	21	6	0.006453
NR_028544	367	279	0.006506
NM_009801	18	37	0.006543
NM_021549	11	1	0.006583
NM_033580	11	1	0.006583
NM_012055	11	1	0.006583
NM_178711	11	1	0.006583
NM_00107763	11	1	0.006583
NM_175126	16	34	0.006792
NM_174874	14	31	0.006954
NM_00100395	7	21	0.007022
NM_008343	84	49	0.007045
NM_026765	19	5	0.00712
NM_008937	30	11	0.007134
NM_00104259	70	101	0.007222
NM_011185	17	4	0.007671
NM_177192	17	4	0.007671
NM_00101336	17	4	0.007671
NM_010712	13	2	0.007723
NM_053109	13	2	0.007723
NM_00101375	17	35	0.00795
NM_178670	15	3	0.007955
NM_028140	15	3	0.007955
NM_133937	9	24	0.007967
NM_183221	8	0	0.00799
NM_008856	8	0	0.00799
NM_019425	8	0	0.00799
NM_011424	8	0	0.00799
NM_177462	8	0	0.00799
NM_00110044	6	19	0.008044
NM_00104242	6	19	0.008044
NM_153423	40	18	0.008248
NM_178668	11	26	0.008469
NM_178203	28	10	0.008498
NM_007437	28	10	0.008498
NM_028388	25	46	0.008518
NM_021547	28	49	0.008607
NM_00100850	34	14	0.008702
NM_00108111	31	12	0.008714
NM_00100406	22	7	0.008859
NM_00104335	22	7	0.008859
NM_016910	22	7	0.008859

NM_027353	44	21	0.008992
NM_007414	5	17	0.009095
NM_019965	5	17	0.009095
NM_008838	5	17	0.009095
NM_027060,N	1	9	0.009766
NR_027953	1	9	0.009766
NR_029811	1	9	0.009766
NM_133767	1	9	0.009766
NM_144921	1	9	0.009766
NM_138676	1	9	0.009766
NM_00108135	1	9	0.009766
NM_012018	1	9	0.009766
NM_019919	1	9	0.009766
NM_011145	25	9	0.009975

Chapter 5 - Discussion and Future Directions

A central issue toward understanding the molecular etiology of RTT has remained determining the means by which mutations in *MECP2* are translated into altered chromatin function and transcriptional output. Here I have worked toward identifying the transcripts displaying altered expression in MeCP2 deficient aNSCs, focusing specifically on the in depth characterization of small noncoding RNA expression and function. The diverse regulatory functions exhibited by such small noncoding RNA, including miRNA, at many different steps of gene expression suggest the importance of understanding the contribution of these molecules to RTT.

Initially, a focused approach using real-time quantitative PCR miRNA expression profiling identified a subset of miRNA with altered expression in MeCP2-deficient aNSCs. At a threshold of 2.5-fold change in the absence of MeCP2, four miRNA exhibited decreased expression while three miRNA displayed increased expression. Although this work establishes a relatively small number of miRNA as differentially expressed at a threshold of 2.5-fold in *Mecp2*^{-/-} aNSCs, the inclusive set of miRNA with quantitatively defined changes in expression are reported in Chapter 2, Supplemental Table I. Certainly, this represents the complexity with which MeCP2 may influence gene expression in general. Moving forward, it will be important to not only consider the effects that the misexpression of the individual miRNA identified here have, but to also consider the combinatorial and/or synergistic

effects that simultaneous misexpression of multiple miRNA may have. The sheer complexity of such a question will likely make it critical to work within the context of well-established phenotypes caused by specific *Mecp2* mutations. This will ultimately allow for the accurate assessment of phenotypic modification by the miRNA described here.

The complexity in the output generated by altered miRNA mediated gene regulation in the absence of MeCP2 is further confounded by the nature of miRNA function itself. The ability of a single miRNA to simultaneously target multiple mRNAs on the basis of as little as 6-8 nucleotides of complementarity indicates that the ultimate output on gene expression is far beyond the miR-137/*Ezh2* interaction described here. However, the thorough identification of miRNA targets and the ultimate effects that misexpression may have on mRNA output, in terms of protein expression, remains technically difficult. Making use of increasingly sensitive methods of protein detection and translation may make such a problem more approachable.

Nonetheless, taking an approach focused on miR-137 has proven useful. One particularly intriguing observation stemming from the focused analysis on the function of miR-137 was the unexpected means by which miR-137 influenced aNSC proliferation and differentiation. Based on the fact that miR-137 normally increases upon aNSC differentiation, it was expected that overexpression of miR-137 would reduce aNSC proliferation and induce differentiation. In fact, just the opposite was observed here. However, a previous publication (Silber, Lim et al. 2008) indicated

that miR-137 did in fact inhibit proliferation of glioblastoma multiforme cells and induce differentiation of brain tumor cells. The effect of miR-137 in these systems was explained through miR-137 mediated suppression of CDK6. Here, it is shown that upon overexpression of miR-137 in primary aNSCs, Cdk6 protein expression is actually increased. Likewise, in *Mecp2*-/*y* aNSCs, which also display increased miR-137 expression, we find that Cdk6 expression is also increased. Yet, when miR-137 is overexpressed in HEK293T cells, CDK6 expression could be suppressed. These observations appear to highlight the subtleties with which miRNA may fine tune gene expression in different cell types. Furthermore, these results stress the importance of identifying targets of miR-137 in distinct cell types.

As a first step to understanding the potentially diverse functions of miR-137 in distinct neurodevelopmental contexts, the effect of miR-137 overexpression on the development and maturation of newborn neurons was assessed in Chapter 3. Using rat HCN-A94 aNSCs, which could be differentiated toward both astrocyte and neuronal lineages, it was found that miR-137 was among those miRNA most enriched in neurons relative to astrocytes. This was consistent with data in Chapter 2 indicating that in primary aNSCs miR-137 expression increased upon neuronal differentiation. Together with published data demonstrating the enrichment of miR-137 in synaptoneuroosomes (Siegel, Obernosterer et al. 2009), these data suggested that in addition to influencing aNSC proliferation and differentiation miR-137 may also play important roles in more mature neurons.

Interestingly, at later stages of neuronal differentiation *in vivo*, miR-137 was found to reduce the maturation and dendritic complexity of newborn neurons. These phenotypes displayed upon overexpression of miR-137 were consistent with those previously observed in *Mecp2* mutant mice (Smrt, Eaves-Egenes et al. 2007), indicating that overexpression of miR-137 in *Mecp2* mutant mice may in fact result in immature neurons with reduced dendritic complexity. These results again highlight the importance of considering the subtle effects of miRNA mediated gene regulation in distinct cell types and will be important to consider in moving forward with experiments addressing the role of miRNA in RTT.

Taking a focused approach based specifically on miRNA expression profiling identified a number of miRNA with altered expression in the absence of MeCP2 and emphasized the complexity that such alterations may have on gene regulation in general. As part of Chapter 4, I sought to more thoroughly assess the expression of small noncoding RNA in aNSCs, and worked toward identifying previously unannotated small noncoding RNA whose expression was altered in MeCP2 deficient aNSCs. To do this a combination of SBS and bioinformatic sequence annotation was used to quantify small noncoding RNA in both WT and *Mecp2*^{-/-} aNSCs. After annotation of the small RNA sequences a particular class of previously unannotated small RNA, ~18nt in length, was identified. These RNAs were found to associate specifically with RefSeq TSSs. These data were consistent with reports from multiple groups working in diverse eukaryotes and indicated that the expression of such small RNA was the result of promoter proximal RNAPII activity

in conjunction with nucleosome placement at TSSs (Seila, Calabrese et al. 2008; Seila, Core et al. 2009; Taft, Glazov et al. 2009; Taft, Kaplan et al. 2009).

Findings that the regulation of promoter proximal RNAPII (postinitiation) occurs preferentially at stimulus and/or developmentally regulated genes suggested the possibility that MeCP2 could influence the expression of promoter proximal small RNA, since it too is known to regulate activity dependent transcription in neurons. On this basis, RefSeq transcripts displaying differential promoter proximal small RNA expression in *Mecp2*^{-/-} aNSCs were identified such that MeCP2 targets regulated in a stimulus dependent manner could be found. In total, 304 RefSeq transcripts were identified as having altered small RNA expression near to TSSs.

Among these genes, *Pcdh10*, was previously reported as associated with Autism-spectrum disorders as well as being activity dependent in neurons. The relative increase in RNAPII occupancy as compared to mRNA expression, indicated that *Pcdh10* was in fact regulated by promoter proximal RNAPII stalling. Furthermore, the direct interaction of MeCP2, which also correlated with an altered chromatin state, indicated that MeCP2 may directly influence promoter proximal RNAPII activity. This suggests that one mechanism by which MeCP2 may regulate expression of targeted genes in an activity dependent manner is by influencing genes with poised RNAPII. Thus, the absence of MeCP2 may ultimately result in the widespread alteration of transcriptional responses to environmental stimuli, rather than continually altering basal transcription genome wide. This effect might be

exacerbated in neurons, which both express high levels of MeCP2 and receive constant and varied extracellular signals.

In summary, these findings demonstrate the misexpression of specific types small noncoding RNA in MeCP2 deficient aNSCs, a previously unappreciated level of gene regulation in the context of Rett Syndrome. Furthermore, the MeCP2 mediated regulation of miRNAs and transcription start site associated RNAs revealed diversity in the types of gene regulatory pathways that may contribute to the pathogenesis of Rett Syndrome.

References

- Abel, T. and R. S. Zukin (2008). "Epigenetic targets of HDAC inhibition in neurodegenerative and psychiatric disorders." Curr Opin Pharmacol **8**(1): 57-64.
- Adelman, K., M. A. Kennedy, et al. (2009). "Immediate mediators of the inflammatory response are poised for gene activation through RNA polymerase II stalling." Proc Natl Acad Sci U S A **106**(43): 18207-12.
- Altman, J. and G. D. Das (1965). "Autoradiographic and histological evidence of postnatal hippocampal neurogenesis in rats." J Comp Neurol **124**(3): 319-35.
- Altman, J. and G. D. Das (1967). "Postnatal neurogenesis in the guinea-pig." Nature **214**(93): 1098-101.
- Amir, R. E., I. B. Van den Veyver, et al. (1999). "Rett syndrome is caused by mutations in X-linked MECP2, encoding methyl-CpG-binding protein 2." Nat Genet **23**(2): 185-8.
- Asaka, Y., D. G. Jugloff, et al. (2006). "Hippocampal synaptic plasticity is impaired in the Mecp2-null mouse model of Rett syndrome." Neurobiol Dis **21**(1): 217-27.
- Avilion, A. A., S. K. Nicolis, et al. (2003). "Multipotent cell lineages in early mouse development depend on SOX2 function." Genes Dev **17**(1): 126-40.
- Ballas, N., C. Grunseich, et al. (2005). "REST and its corepressors mediate plasticity of neuronal gene chromatin throughout neurogenesis." Cell **121**(4): 645-57.
- Ballas, N., D. T. Lioy, et al. (2009). "Non-cell autonomous influence of MeCP2-deficient glia on neuronal dendritic morphology." Nat Neurosci **12**(3): 311-7.
- Balmer, D., J. Goldstine, et al. (2003). "Elevated methyl-CpG-binding protein 2 expression is acquired during postnatal human brain development and is correlated with alternative polyadenylation." J Mol Med **81**(1): 61-8.
- Barbarotto, E., T. D. Schmittgen, et al. (2008). "MicroRNAs and cancer: profile, profile, profile." Int J Cancer **122**(5): 969-77.
- Barkho, B. Z., A. E. Munoz, et al. (2008). "Endogenous matrix metalloproteinase (MMP)-3 and MMP-9 promote the differentiation and migration of adult neural progenitor cells in response to chemokines." Stem Cells **26**(12): 3139-49.
- Barkho, B. Z., H. Song, et al. (2006). "Identification of astrocyte-expressed factors that modulate neural stem/progenitor cell differentiation." Stem Cells Dev **15**(3): 407-21.
- Bartel, D. P. (2004). "MicroRNAs: genomics, biogenesis, mechanism, and function." Cell **116**(2): 281-97.
- Bernstein, B. E., A. Meissner, et al. (2007). "The mammalian epigenome." Cell **128**(4): 669-81.
- Bernstein, E., S. Y. Kim, et al. (2003). "Dicer is essential for mouse development." Nat Genet **35**(3): 215-7.

- Bienvenu, T. and J. Chelly (2006). "Molecular genetics of Rett syndrome: when DNA methylation goes unrecognized." *Nat Rev Genet* **7**(6): 415-26.
- Bird, A. (2002). "DNA methylation patterns and epigenetic memory." *Genes Dev* **16**(1): 6-21.
- Birney, E., J. A. Stamatoyannopoulos, et al. (2007). "Identification and analysis of functional elements in 1% of the human genome by the ENCODE pilot project." *Nature* **447**(7146): 799-816.
- Boyer, L. A., T. I. Lee, et al. (2005). "Core transcriptional regulatory circuitry in human embryonic stem cells." *Cell* **122**(6): 947-56.
- Boyer, L. A., K. Plath, et al. (2006). "Polycomb complexes repress developmental regulators in murine embryonic stem cells." *Nature* **441**(7091): 349-53.
- Brown, J. P., S. Couillard-Despres, et al. (2003). "Transient expression of doublecortin during adult neurogenesis." *J Comp Neurol* **467**(1): 1-10.
- Burbea, M., L. Dreier, et al. (2002). "Ubiquitin and AP180 regulate the abundance of GLR-1 glutamate receptors at postsynaptic elements in *C. elegans*." *Neuron* **35**(1): 107-20.
- Bylund, M., E. Andersson, et al. (2003). "Vertebrate neurogenesis is counteracted by Sox1-3 activity." *Nat Neurosci* **6**(11): 1162-8.
- Cameron, H. A., C. S. Woolley, et al. (1993). "Differentiation of newly born neurons and glia in the dentate gyrus of the adult rat." *Neuroscience* **56**(2): 337-44.
- Cao, R. and Y. Zhang (2004). "The functions of E(Z)/EZH2-mediated methylation of lysine 27 in histone H3." *Curr Opin Genet Dev* **14**(2): 155-64.
- Cao, X., G. Yeo, et al. (2006). "Noncoding RNAs in the mammalian central nervous system." *Annu Rev Neurosci* **29**: 77-103.
- Carninci, P., T. Kasukawa, et al. (2005). "The transcriptional landscape of the mammalian genome." *Science* **309**(5740): 1559-63.
- Caviness, V. S., Jr. (1973). "Time of neuron origin in the hippocampus and dentate gyrus of normal and reeler mutant mice: an autoradiographic analysis." *J Comp Neurol* **151**(2): 113-20.
- Chahrour, M., S. Y. Jung, et al. (2008). "MeCP2, a key contributor to neurological disease, activates and represses transcription." *Science* **320**(5880): 1224-9.
- Chahrour, M. and H. Y. Zoghbi (2007). "The story of Rett syndrome: from clinic to neurobiology." *Neuron* **56**(3): 422-37.
- Chang, T. C. and J. T. Mendell (2007). "microRNAs in vertebrate physiology and human disease." *Annu Rev Genomics Hum Genet* **8**: 215-39.
- Chen, R. Z., S. Akbarian, et al. (2001). "Deficiency of methyl-CpG binding protein-2 in CNS neurons results in a Rett-like phenotype in mice." *Nat Genet* **27**(3): 327-31.
- Chen, W. G., Q. Chang, et al. (2003). "Derepression of BDNF transcription involves calcium-dependent phosphorylation of MeCP2." *Science* **302**(5646): 885-9.
- Cheng, L. C., M. Tavazoie, et al. (2005). "Stem cells: from epigenetics to microRNAs." *Neuron* **46**(3): 363-7.
- Choe, E. A., L. Liao, et al. (2007). "Neuronal morphogenesis is regulated by the interplay between cyclin-dependent kinase 5 and the ubiquitin ligase mind bomb 1." *J Neurosci* **27**(35): 9503-12.

- Coffee, B., F. Zhang, et al. (1999). "Acetylated histones are associated with FMR1 in normal but not fragile X-syndrome cells." Nat Genet **22**(1): 98-101.
- Cohen, D. R., V. Matarazzo, et al. (2003). "Expression of MeCP2 in olfactory receptor neurons is developmentally regulated and occurs before synaptogenesis." Mol Cell Neurosci **22**(4): 417-29.
- Conaco, C., S. Otto, et al. (2006). "Reciprocal actions of REST and a microRNA promote neuronal identity." Proc Natl Acad Sci U S A **103**(7): 2422-7.
- De Haan, G. and A. Gerrits (2007). "Epigenetic control of hematopoietic stem cell aging the case of Ezh2." Ann N Y Acad Sci **1106**: 233-9.
- Dindot, S. V., B. A. Antalffy, et al. (2008). "The Angelman syndrome ubiquitin ligase localizes to the synapse and nucleus, and maternal deficiency results in abnormal dendritic spine morphology." Hum Mol Genet **17**(1): 111-8.
- Dragich, J. M., Y. H. Kim, et al. (2007). "Differential distribution of the MeCP2 splice variants in the postnatal mouse brain." J Comp Neurol **501**(4): 526-42.
- Du, T. and P. D. Zamore (2005). "microPrimer: the biogenesis and function of microRNA." Development **132**(21): 4645-52.
- Duan, X., J. H. Chang, et al. (2007). "Disrupted-In-Schizophrenia 1 regulates integration of newly generated neurons in the adult brain." Cell **130**(6): 1146-58.
- Egger, G., G. Liang, et al. (2004). "Epigenetics in human disease and prospects for epigenetic therapy." Nature **429**(6990): 457-63.
- Ellis, P., B. M. Fagan, et al. (2004). "SOX2, a persistent marker for multipotential neural stem cells derived from embryonic stem cells, the embryo or the adult." Dev Neurosci **26**(2-4): 148-65.
- Ezhkova, E., H. A. Pasolli, et al. (2009). "Ezh2 orchestrates gene expression for the stepwise differentiation of tissue-specific stem cells." Cell **136**(6): 1122-35.
- Ferri, A. L., M. Cavallaro, et al. (2004). "Sox2 deficiency causes neurodegeneration and impaired neurogenesis in the adult mouse brain." Development **131**(15): 3805-19.
- Fiala, J. C., J. Spacek, et al. (2002). "Dendritic spine pathology: cause or consequence of neurological disorders?" Brain Res Brain Res Rev **39**(1): 29-54.
- Fiore, R., S. Khudayberdiev, et al. (2009). "Mef2-mediated transcription of the miR379-410 cluster regulates activity-dependent dendritogenesis by fine-tuning Pumilio2 protein levels." EMBO J **28**(6): 697-710.
- Fletcher, E. J., J. Church, et al. (1994). "Haloperidol blocks voltage-activated Ca²⁺ channels in hippocampal neurones." Eur J Pharmacol **267**(2): 249-52.
- Friez, M. J., J. R. Jones, et al. (2006). "Recurrent infections, hypotonia, and mental retardation caused by duplication of MECP2 and adjacent region in Xq28." Pediatrics **118**(6): e1687-95.
- Gage, F. H. (2000). "Mammalian neural stem cells." Science **287**(5457): 1433-8.
- Gangaraju, V. K. and H. Lin (2009). "MicroRNAs: key regulators of stem cells." Nat Rev Mol Cell Biol **10**(2): 116-25.
- Ge, S., E. L. Goh, et al. (2006). "GABA regulates synaptic integration of newly generated neurons in the adult brain." Nature **439**(7076): 589-93.

- Goslin, K. and G. Banker (1989). "Experimental observations on the development of polarity by hippocampal neurons in culture." J Cell Biol **108**(4): 1507-16.
- Gould, E., P. Tanapat, et al. (1998). "Proliferation of granule cell precursors in the dentate gyrus of adult monkeys is diminished by stress." Proc Natl Acad Sci U S A **95**(6): 3168-71.
- Graham, V., J. Khudyakov, et al. (2003). "SOX2 functions to maintain neural progenitor identity." Neuron **39**(5): 749-65.
- Grivna, S. T., B. Pyhtila, et al. (2006). "MIWI associates with translational machinery and PIWI-interacting RNAs (piRNAs) in regulating spermatogenesis." Proc Natl Acad Sci U S A **103**(36): 13415-20.
- Gueneau, G., A. Privat, et al. (1982). "Subgranular zone of the dentate gyrus of young rabbits as a secondary matrix. A high-resolution autoradiographic study." Dev Neurosci **5**(4): 345-58.
- Guenther, M. G., S. S. Levine, et al. (2007). "A chromatin landmark and transcription initiation at most promoters in human cells." Cell **130**(1): 77-88.
- Guy, J., J. Gan, et al. (2007). "Reversal of neurological defects in a mouse model of Rett syndrome." Science **315**(5815): 1143-7.
- Guy, J., B. Hendrich, et al. (2001). "A mouse *Mecp2*-null mutation causes neurological symptoms that mimic Rett syndrome." Nat Genet **27**(3): 322-6.
- Hendrich, B. and A. Bird (1998). "Identification and characterization of a family of mammalian methyl-CpG binding proteins." Mol Cell Biol **18**(11): 6538-47.
- Hong, E. J., A. E. McCord, et al. (2008). "A biological function for the neuronal activity-dependent component of *Bdnf* transcription in the development of cortical inhibition." Neuron **60**(4): 610-24.
- Hsieh, J. and F. H. Gage (2004). "Epigenetic control of neural stem cell fate." Curr Opin Genet Dev **14**(5): 461-9.
- Itoh, M., C. H. Kim, et al. (2003). "Mind bomb is a ubiquitin ligase that is essential for efficient activation of Notch signaling by Delta." Dev Cell **4**(1): 67-82.
- Ivey, K. N., A. Muth, et al. (2008). "MicroRNA regulation of cell lineages in mouse and human embryonic stem cells." Cell Stem Cell **2**(3): 219-29.
- Jaenisch, R. and R. Young (2008). "Stem cells, the molecular circuitry of pluripotency and nuclear reprogramming." Cell **132**(4): 567-82.
- Jay, C., J. Nemunaitis, et al. (2007). "miRNA profiling for diagnosis and prognosis of human cancer." DNA Cell Biol **26**(5): 293-300.
- Jin, P., D. C. Zarnescu, et al. (2004). "Biochemical and genetic interaction between the fragile X mental retardation protein and the microRNA pathway." Nat Neurosci **7**(2): 113-7.
- John, B., A. J. Enright, et al. (2004). "Human MicroRNA targets." PLoS Biol **2**(11): e363.
- Jones, P. L., G. J. Veenstra, et al. (1998). "Methylated DNA and MeCP2 recruit histone deacetylase to repress transcription." Nat Genet **19**(2): 187-91.
- Jugloff, D. G., B. P. Jung, et al. (2005). "Increased dendritic complexity and axonal length in cultured mouse cortical neurons overexpressing methyl-CpG-binding protein MeCP2." Neurobiol Dis **19**(1-2): 18-27.

- Kaludov, N. K. and A. P. Wolffe (2000). "MeCP2 driven transcriptional repression in vitro: selectivity for methylated DNA, action at a distance and contacts with the basal transcription machinery." Nucleic Acids Res **28**(9): 1921-8.
- Kaplan, M. S. and D. H. Bell (1984). "Mitotic neuroblasts in the 9-day-old and 11-month-old rodent hippocampus." J Neurosci **4**(6): 1429-41.
- Kaplan, M. S. and J. W. Hinds (1977). "Neurogenesis in the adult rat: electron microscopic analysis of light radioautographs." Science **197**(4308): 1092-4.
- Kapranov, P., J. Cheng, et al. (2007). "RNA maps reveal new RNA classes and a possible function for pervasive transcription." Science **316**(5830): 1484-8.
- Kimura, H. and K. Shiota (2003). "Methyl-CpG-binding protein, MeCP2, is a target molecule for maintenance DNA methyltransferase, Dnmt1." J Biol Chem **278**(7): 4806-12.
- Kishi, N. and J. D. Macklis (2004). "MECP2 is progressively expressed in post-migratory neurons and is involved in neuronal maturation rather than cell fate decisions." Mol Cell Neurosci **27**(3): 306-21.
- Klein, M. E., D. T. Liroy, et al. (2007). "Homeostatic regulation of MeCP2 expression by a CREB-induced microRNA." Nat Neurosci **10**(12): 1513-4.
- Kokura, K., S. C. Kaul, et al. (2001). "The Ski protein family is required for MeCP2-mediated transcriptional repression." J Biol Chem **276**(36): 34115-21.
- Koo, B. K., H. S. Lim, et al. (2005). "Mind bomb 1 is essential for generating functional Notch ligands to activate Notch." Development **132**(15): 3459-70.
- Kozaki, K., I. Imoto, et al. (2008). "Exploration of tumor-suppressive microRNAs silenced by DNA hypermethylation in oral cancer." Cancer Res **68**(7): 2094-105.
- Krek, A., D. Grun, et al. (2005). "Combinatorial microRNA target predictions." Nat Genet **37**(5): 495-500.
- Kriaucionis, S. and A. Bird (2004). "The major form of MeCP2 has a novel N-terminus generated by alternative splicing." Nucleic Acids Res **32**(5): 1818-23.
- Kuhn, H. G., H. Dickinson-Anson, et al. (1996). "Neurogenesis in the dentate gyrus of the adult rat: age-related decrease of neuronal progenitor proliferation." J Neurosci **16**(6): 2027-33.
- Lao, K., N. L. Xu, et al. (2006). "Multiplexing RT-PCR for the detection of multiple miRNA species in small samples." Biochem Biophys Res Commun **343**(1): 85-9.
- Larsen, F., G. Gundersen, et al. (1992). "CpG islands as gene markers in the human genome." Genomics **13**(4): 1095-107.
- LaSalle, J. M. (2007). "The odyssey of MeCP2 and parental imprinting." Epigenetics **2**(1): 5-10.
- Lee, E. R., F. E. Murdoch, et al. (2007). "High histone acetylation and decreased polycomb repressive complex 2 member levels regulate gene specific transcriptional changes during early embryonic stem cell differentiation induced by retinoic acid." Stem Cells **25**(9): 2191-9.

- Lee, R. C., R. L. Feinbaum, et al. (1993). "The *C. elegans* heterochronic gene *lin-4* encodes small RNAs with antisense complementarity to *lin-14*." Cell **75**(5): 843-54.
- Lee, T. I., R. G. Jenner, et al. (2006). "Control of developmental regulators by Polycomb in human embryonic stem cells." Cell **125**(2): 301-13.
- Lewis, B. P., I. H. Shih, et al. (2003). "Prediction of mammalian microRNA targets." Cell **115**(7): 787-98.
- Lewis, J. D., R. R. Meehan, et al. (1992). "Purification, sequence, and cellular localization of a novel chromosomal protein that binds to methylated DNA." Cell **69**(6): 905-14.
- Li, X., B. Z. Barkho, et al. (2008). "Epigenetic regulation of the stem cell mitogen *Fgf-2* by *Mbd1* in adult neural stem/progenitor cells." J Biol Chem **283**(41): 27644-52.
- Li, X., B. Z. Barkho, et al. (2008). "Epigenetic regulation of the stem cell mitogen *FGF-2* by *mbd1* in adult neural stem/progenitor cells." J Biol Chem (in press).
- Lim, D. A., Y. C. Huang, et al. (2009). "Chromatin remodelling factor *Mll1* is essential for neurogenesis from postnatal neural stem cells." Nature **458**(7237): 529-33.
- Liu, C. and X. Zhao (2009). "MicroRNAs in Adult and Embryonic Neurogenesis." Neuromolecular Med.
- Livak, K. J. and T. D. Schmittgen (2001). "Analysis of relative gene expression data using real-time quantitative PCR and the $2^{-\Delta\Delta C(T)}$ Method." Methods **25**(4): 402-8.
- Lu, Y., F. Wang, et al. (2009). "The *Drosophila* homologue of the Angelman syndrome ubiquitin ligase regulates the formation of terminal dendritic branches." Hum Mol Genet **18**(3): 454-62.
- Lugli, G., V. I. Torvik, et al. (2008). "Expression of microRNAs and their precursors in synaptic fractions of adult mouse forebrain." J Neurochem **106**(2): 650-61.
- Lugtenberg, D., A. P. de Brouwer, et al. (2006). "Chromosomal copy number changes in patients with non-syndromic X linked mental retardation detected by array CGH." J Med Genet **43**(4): 362-70.
- Ma, D. K., M. H. Jang, et al. (2009). "Neuronal activity-induced *Gadd45b* promotes epigenetic DNA demethylation and adult neurogenesis." Science **323**(5917): 1074-7.
- Martinowich, K., D. Hattori, et al. (2003). "DNA methylation-related chromatin remodeling in activity-dependent *BDNF* gene regulation." Science **302**(5646): 890-3.
- Mavrich, T. N., C. Jiang, et al. (2008). "Nucleosome organization in the *Drosophila* genome." Nature **453**(7193): 358-62.
- Meins, M., J. Lehmann, et al. (2005). "Submicroscopic duplication in *Xq28* causes increased expression of the *MECP2* gene in a boy with severe mental retardation and features of Rett syndrome." J Med Genet **42**(2): e12.
- Ming, G. L. and H. Song (2005). "Adult neurogenesis in the mammalian central nervous system." Annu Rev Neurosci **28**: 223-50.

- Mnatzakanian, G. N., H. Lohi, et al. (2004). "A previously unidentified MECP2 open reading frame defines a new protein isoform relevant to Rett syndrome." Nat Genet **36**(4): 339-41.
- Moretti, P. and H. Y. Zoghbi (2006). "MeCP2 dysfunction in Rett syndrome and related disorders." Curr Opin Genet Dev **16**(3): 276-81.
- Muse, G. W., D. A. Gilchrist, et al. (2007). "RNA polymerase is poised for activation across the genome." Nat Genet **39**(12): 1507-11.
- Nan, X., F. J. Campoy, et al. (1997). "MeCP2 is a transcriptional repressor with abundant binding sites in genomic chromatin." Cell **88**(4): 471-81.
- Nan, X., J. Hou, et al. (2007). "Interaction between chromatin proteins MECP2 and ATRX is disrupted by mutations that cause inherited mental retardation." Proc Natl Acad Sci U S A **104**(8): 2709-14.
- Nan, X., H. H. Ng, et al. (1998). "Transcriptional repression by the methyl-CpG-binding protein MeCP2 involves a histone deacetylase complex." Nature **393**(6683): 386-9.
- Nechaev, S., D. C. Fargo, et al. "Global analysis of short RNAs reveals widespread promoter-proximal stalling and arrest of Pol II in *Drosophila*." Science **327**(5963): 335-8.
- Nomura, T., M. Kimura, et al. (2008). "MeCP2-dependent repression of an imprinted miR-184 released by depolarization." Hum Mol Genet **17**(8): 1192-9.
- O'Carroll, D., S. Erhardt, et al. (2001). "The polycomb-group gene *Ezh2* is required for early mouse development." Mol Cell Biol **21**(13): 4330-6.
- Obernosterer, G., J. Martinez, et al. (2007). "Locked nucleic acid-based in situ detection of microRNAs in mouse tissue sections." Nat Protoc **2**(6): 1508-14.
- Okabe, S., C. Collin, et al. (1998). "Hippocampal synaptic plasticity in mice overexpressing an embryonic subunit of the NMDA receptor." J Neurosci **18**(11): 4177-88.
- Ossipova, O., J. Ezan, et al. (2009). "PAR-1 phosphorylates Mind bomb to promote vertebrate neurogenesis." Dev Cell **17**(2): 222-33.
- Paddison, P. J., A. A. Caudy, et al. (2002). "Short hairpin RNAs (shRNAs) induce sequence-specific silencing in mammalian cells." Genes Dev **16**(8): 948-58.
- Pelka, G. J., C. M. Watson, et al. (2006). "Mecp2 deficiency is associated with learning and cognitive deficits and altered gene activity in the hippocampal region of mice." Brain **129**(Pt 4): 887-98.
- Rajasethupathy, P., F. Fiumara, et al. (2009). "Characterization of small RNAs in aplysia reveals a role for miR-124 in constraining synaptic plasticity through CREB." Neuron **63**(6): 803-17.
- Reinhart, B. J., F. J. Slack, et al. (2000). "The 21-nucleotide let-7 RNA regulates developmental timing in *Caenorhabditis elegans*." Nature **403**(6772): 901-6.
- Romualdi, C., S. Bortoluzzi, et al. (2003). "IDEG6: a web tool for detection of differentially expressed genes in multiple tag sampling experiments." Physiol Genomics **12**(2): 159-62.
- Schones, D. E., K. Cui, et al. (2008). "Dynamic regulation of nucleosome positioning in the human genome." Cell **132**(5): 887-98.

- Schratt, G. M., F. Tuebing, et al. (2006). "A brain-specific microRNA regulates dendritic spine development." *Nature* **439**(7074): 283-9.
- Seila, A. C., J. M. Calabrese, et al. (2008). "Divergent transcription from active promoters." *Science* **322**(5909): 1849-51.
- Seila, A. C., L. J. Core, et al. (2009). "Divergent transcription: a new feature of active promoters." *Cell Cycle* **8**(16): 2557-64.
- Shahbazian, M., J. Young, et al. (2002). "Mice with truncated MeCP2 recapitulate many Rett syndrome features and display hyperacetylation of histone H3." *Neuron* **35**(2): 243-54.
- Shahbazian, M. D., B. Antalffy, et al. (2002). "Insight into Rett syndrome: MeCP2 levels display tissue- and cell-specific differences and correlate with neuronal maturation." *Hum Mol Genet* **11**(2): 115-24.
- Shahbazian, M. D. and H. Y. Zoghbi (2002). "Rett syndrome and MeCP2: linking epigenetics and neuronal function." *Am J Hum Genet* **71**(6): 1259-72.
- Shen, X., Y. Liu, et al. (2008). "EZH1 mediates methylation on histone H3 lysine 27 and complements EZH2 in maintaining stem cell identity and executing pluripotency." *Mol Cell* **32**(4): 491-502.
- Sheng, M. and C. C. Hoogenraad (2007). "The postsynaptic architecture of excitatory synapses: a more quantitative view." *Annu Rev Biochem* **76**: 823-47.
- Sher, F., R. Rossler, et al. (2008). "Differentiation of neural stem cells into oligodendrocytes: involvement of the polycomb group protein Ezh2." *Stem Cells* **26**(11): 2875-83.
- Shiraki, T., S. Kondo, et al. (2003). "Cap analysis gene expression for high-throughput analysis of transcriptional starting point and identification of promoter usage." *Proc Natl Acad Sci U S A* **100**(26): 15776-81.
- Shors, T. J., G. Miesegaes, et al. (2001). "Neurogenesis in the adult is involved in the formation of trace memories." *Nature* **410**(6826): 372-6.
- Siegel, G., G. Obernosterer, et al. (2009). "A functional screen implicates microRNA-138-dependent regulation of the depalmitoylation enzyme APT1 in dendritic spine morphogenesis." *Nat Cell Biol* **11**(6): 705-16.
- Silber, J., D. A. Lim, et al. (2008). "miR-124 and miR-137 inhibit proliferation of glioblastoma multiforme cells and induce differentiation of brain tumor stem cells." *BMC Med* **6**: 14.
- Skene, P. J., R. S. Illingworth, et al. "Neuronal MeCP2 is expressed at near histone-octamer levels and globally alters the chromatin state." *Mol Cell* **37**(4): 457-68.
- Smalheiser, N. R. and G. Lugli (2009). "microRNA regulation of synaptic plasticity." *Neuromolecular Med* **11**(3): 133-40.
- Smrt, R. D., J. Eaves-Egenes, et al. (2007). "Mecp2 deficiency leads to delayed maturation and altered gene expression in hippocampal neurons." *Neurobiol Dis*.
- Smrt, R. D., J. Eaves-Egenes, et al. (2007). "Mecp2 deficiency leads to delayed maturation and altered gene expression in hippocampal neurons." *Neurobiol Dis* **27**(1): 77-89.

- Snyder, J. S., N. S. Hong, et al. (2005). "A role for adult neurogenesis in spatial long-term memory." *Neuroscience* **130**(4): 843-52.
- Song, H., G. Kempermann, et al. (2005). "New neurons in the adult mammalian brain: synaptogenesis and functional integration." *J Neurosci* **25**(45): 10366-8.
- Stanfield, B. B. and J. E. Trice (1988). "Evidence that granule cells generated in the dentate gyrus of adult rats extend axonal projections." *Exp Brain Res* **72**(2): 399-406.
- Suh, H., A. Consiglio, et al. (2007). "In Vivo Fate Analysis Reveals the Multipotent and Self-Renewal Capacities of Sox2(+) Neural Stem Cells in the Adult Hippocampus." *Cell Stem Cell* **1**(5): 515-528.
- Tafoya, L. C., M. Mameli, et al. (2006). "Expression and function of SNAP-25 as a universal SNARE component in GABAergic neurons." *J Neurosci* **26**(30): 7826-38.
- Taft, R. J., E. A. Glazov, et al. (2009). "Tiny RNAs associated with transcription start sites in animals." *Nat Genet* **41**(5): 572-8.
- Taft, R. J., C. D. Kaplan, et al. (2009). "Evolution, biogenesis and function of promoter-associated RNAs." *Cell Cycle* **8**(15): 2332-8.
- Tang, X., D. L. Falls, et al. (2007). "Antigen-retrieval procedure for bromodeoxyuridine immunolabeling with concurrent labeling of nuclear DNA and antigens damaged by HCl pretreatment." *J Neurosci* **27**(22): 5837-44.
- Tao, J., K. Hu, et al. (2009). "Phosphorylation of MeCP2 at Serine 80 regulates its chromatin association and neurological function." *Proc Natl Acad Sci U S A* **106**(12): 4882-7.
- Taranova, O. V., S. T. Magness, et al. (2006). "SOX2 is a dose-dependent regulator of retinal neural progenitor competence." *Genes Dev* **20**(9): 1187-202.
- Tsuda, H., S. M. Han, et al. (2008). "The amyotrophic lateral sclerosis 8 protein VAPB is cleaved, secreted, and acts as a ligand for Eph receptors." *Cell* **133**(6): 963-77.
- Van Esch, H., M. Bauters, et al. (2005). "Duplication of the MECP2 region is a frequent cause of severe mental retardation and progressive neurological symptoms in males." *Am J Hum Genet* **77**(3): 442-53.
- van Praag, H., A. F. Schinder, et al. (2002). "Functional neurogenesis in the adult hippocampus." *Nature* **415**(6875): 1030-4.
- van Praag, H., A. F. Schinder, et al. (2002). "Functional neurogenesis in the adult hippocampus." *Nature* **415**(6875): 1030-4.
- Waites, C. L., A. M. Craig, et al. (2005). "Mechanisms of vertebrate synaptogenesis." *Annu Rev Neurosci* **28**: 251-74.
- Wang, Y., R. Medvid, et al. (2007). "DGCR8 is essential for microRNA biogenesis and silencing of embryonic stem cell self-renewal." *Nat Genet* **39**(3): 380-5.
- Wang, Z., C. Zang, et al. (2008). "Combinatorial patterns of histone acetylations and methylations in the human genome." *Nat Genet* **40**(7): 897-903.
- Washbourne, P., P. M. Thompson, et al. (2002). "Genetic ablation of the t-SNARE SNAP-25 distinguishes mechanisms of neuroexocytosis." *Nat Neurosci* **5**(1): 19-26.

- Wayman, G. A., M. Davare, et al. (2008). "An activity-regulated microRNA controls dendritic plasticity by down-regulating p250GAP." Proc Natl Acad Sci U S A **105**(26): 9093-8.
- Webb, S. J., C. S. Monk, et al. (2001). "Mechanisms of postnatal neurobiological development: implications for human development." Dev Neuropsychol **19**(2): 147-71.
- Weber, M., J. J. Davies, et al. (2005). "Chromosome-wide and promoter-specific analyses identify sites of differential DNA methylation in normal and transformed human cells." Nat Genet **37**(8): 853-62.
- Yekta, S., I. H. Shih, et al. (2004). "MicroRNA-directed cleavage of HOXB8 mRNA." Science **304**(5670): 594-6.
- Yi, R., M. N. Poy, et al. (2008). "A skin microRNA promotes differentiation by repressing 'stemness'." Nature **452**(7184): 225-9.
- Yoon, K. J., B. K. Koo, et al. (2008). "Mind bomb 1-expressing intermediate progenitors generate notch signaling to maintain radial glial cells." Neuron **58**(4): 519-31.
- Zappone, M. V., R. Galli, et al. (2000). "Sox2 regulatory sequences direct expression of a (beta)-geo transgene to telencephalic neural stem cells and precursors of the mouse embryo, revealing regionalization of gene expression in CNS stem cells." Development **127**(11): 2367-82.
- Zeitlinger, J., A. Stark, et al. (2007). "RNA polymerase stalling at developmental control genes in the *Drosophila melanogaster* embryo." Nat Genet **39**(12): 1512-6.
- Zhao, C., W. Deng, et al. (2008). "Mechanisms and functional implications of adult neurogenesis." Cell **132**(4): 645-60.
- Zhao, C., E. M. Teng, et al. (2006). "Distinct morphological stages of dentate granule neuron maturation in the adult mouse hippocampus." J Neurosci **26**(1): 3-11.
- Zhao, X., T. Ueba, et al. (2003). "Mice lacking methyl-CpG binding protein 1 have deficits in adult neurogenesis and hippocampal function." Proc Natl Acad Sci U S A **100**(11): 6777-82.
- Zhou, Z., E. J. Hong, et al. (2006). "Brain-specific phosphorylation of MeCP2 regulates activity-dependent Bdnf transcription, dendritic growth, and spine maturation." Neuron **52**(2): 255-69.